②

AD-A212 977

NAVAL POSTGRADUATE SCHOOL
Monterey, California

THESIS

WIRE GRID MODELING OF THE
LINEAR TAPERED SLOT ANTENNA

by

Daniel K. Miller

June 1989

Thesis Advisor: Ramakrishna Janaswamy

Security Classification of this page

REPORT DOCUMENTATION PAGE

1a Report Security Classification Unclassified			1b Restrictive Markings			
2a Security Classification Authority			3 Distribution Availability of Report			
2b Declassification/Downgrading Schedule			Approved for public release; distribution is unlimited			
4 Performing Organization Report Number(s)			5 Monitoring Organization Report Number(s)			
6a Name of Performing Organization Naval Postgraduate School		6b Office Symbol *(If Applicable)* 62	7a Name of Monitoring Organization Naval Postgraduate School			
6c Address *(city, state, and ZIP code)* Monterey, CA 93943-5000			7b Address *(city, state, and ZIP code)* Monterey, CA 93943-5000			
8a Name of Funding/Sponsoring Organization		8b Office Symbol *(If Applicable)*	9 Procurement Instrument Identification Number			
8c Address *(city, state, and ZIP code)*			10 Source of Funding Numbers			
			Program Element Number	Project No	Task No	Work Unit Accession No

11 Title *(Include Security Classification)* WIRE GRID MODELING OF THE LINEAR TAPERED SLOT ANTENNA

12 Personal Author(s) MILLER, Daniel K.

13a Type of Report Master's Thesis	13b Time Covered From To	14 Date of Report *(year, month,day)* June 1989	15 Page Count 90

16 Supplementary Notation The views expressed in this thesis are those of the author and do not reflect the official policy or position of the Department of Defense or the U.S. Government.

17 Cosati Codes			18 Subject Terms *(continue on reverse if necessary and identify by block number)*
Field	Group	Subgroup	LTSA; Flare Angle; Substrate; Antenna; Plannar Antenna; Radiation Pattern; Method of Moments; The Linearly Tapered Slot Antenna

19 Abstract *(continue on reverse if necessary and identify by block number)*

The Linearly Tapered Slot Antenna (LTSA) has been the subject of considerable study and experimentation. Accurate theoretical models based on the Method of Moments (MOM) have been developed to study the radiation characteristics of this antenna. However, these models are limited due to the great amount of Central Processing Unit (CPU) time required to obtain the solution. Employing the Numerical Electromagnetics Code (NEC) an accurate wire-grid model of the LTSA is developed here in order to reduce the CPU time needed to obtain the solution. Numerical results are presented for the radiation pattern and compared with experimental results of the actual planar structure to validate the model and optimize the wire-grid. Once the model has been optimized, effects of variable design parameters on radiation pattern are studied. Conclusions are made regarding optimum designs for the LTSA.

20 Distribution/Availability of Abstract [X] unclassified/unlimited [ ] same as report [ ] DTIC users	21 Abstract Security Classification Unclassified	
22a Name of Responsible Individual JANASWAMY, R.	22b Telephone *(Include Area code)* 408-646-3217	22c Office Symbol 62JS

DD FORM 1473, 84 MAR   83 APR edition may be used until exhausted   security classification of this page
All other editions are obsolete   Unclassified

**Wire Grid Modeling of the
Linearly Tapered Slot Antenna**

by

Daniel K. Miller
Captain, United States Marine Corps
B.S., United States Naval Academy, 1982

Submitted in partial fulfillment of the
requirements for the degree of

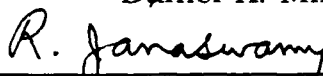MASTER OF SCIENCE IN ELECTRICAL ENGINEERING

from the

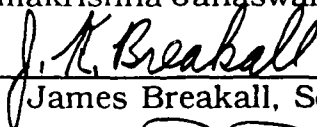NAVAL POSTGRADUATE SCHOOL
June 1989

Author: _____
Daniel K. Miller

Approved by: _____
Ramakrishna Janaswamy, Thesis Advisor

_____
James Breakall, Second Reader

_____
John P. Powers, Chairman, Department of
Electrical and Computer Engineering

_____
Gordon E. Schacher
Dean of Science and Engineering

ii

ABSTRACT

The Linearly Tapered Slot Antenna (LTSA) has been the subject of considerable study and experimentation. Accurate theoretical models based on the Method of Moments (MOM) have been developed to study the radiation characteristics of this antenna. However, these models are limited due to the great amount of Central Processing Unit (CPU) time required to obtain the solution. Employing the Numerical Electromagnetics Code (NEC), an accurate wire-grid model of the LTSA is developed here in order to reduce the CPU time needed to obtain the solution. Numerical results are presented for the radiation pattern and compared with experimental results of the actual planar structure to validate the model and optimize the wire-grid. Once the model has been optimized, effects of variable design parameters on radiation patterns are studied. Conclusions are made regarding optimum designs for the LTSA.

iii

TABLE OF CONTENTS

iv

v

I. INTRODUCTION

The Linearly Tapered Slot Antenna (LTSA) is an integrated planar antenna consisting of a thin film of metal with or without dielectric substrate on one side of the film. The slot is very narrow toward one end and then tapered so that a traveling wave propagating near the slot gradually radiates in the endfire direction. The narrow end is coupled to devices such as mixer diodes. The antenna was first introduced by Prasad and Mahapatra (1979) and is suitable for many integrated circuit applications, near-millimeter imaging, and phased arrays. It belongs to a category of endfire tapered slot antennas which also include exponentially tapered (Vivaldi) and constant width (CWSA) antennas. It also has a moderately high (10-17 dB) directivity for a given cross section by virtue of its traveling-wave nature [Ref. 1]. This type of antenna finds applications in the fields of satellite communication, remote sensing, and radio astronomy to name a few. Some of the major advantages of the integrated planar antenna are that it does not require a large number of metallic waveguide feeds, it is small, and it is lightweight. Reducing the cost and weight factors on antennas such as those employed on satellites solves a number of problems of the previously employed methods and leads to further gains in the technology.

To maximize the value of integrated circuit techniques, the construction of the antenna should be one of planar geometry. This is

1

feasible due to the fact that the LTSA on a planar dielectric substrate produces a symmetric beam (in the E- and H-planes) despite its planar geometry [Ref. 1]. To take full advantage of this, effects of parameters such as length, total height, flare angle, dielectric thickness, and dielectric constant of the substrate on the radiation characteristics need to be explored. For experiments done with the LTSA, comparisons are made against well known "standard" traveling wave antennas. The characteristics most often considered are beamwidth, beam shape, beam efficiency, and directivity. The LTSA construction and physical antenna variables are illustrated in Figure 1.1.

Work in recent years by Janaswamy [Ref. 2] and Kelly [Ref. 3] has led to the use of accurate theoretical models in the design of the LTSA. Previous study and usage of the LTSA had been based on empirical designs, and, although the work of Janaswamy and Kelly provided a more efficient approach to design, the Central Processing Unit (CPU) time required to obtain the results was a principal limitation. This thesis presents the analysis of the radiation pattern of a wire-grid model of the LTSA which accurately approximates the results found by Janaswamy, while significantly reducing the CPU time required to obtain the solution.

Since the technique used in this research is the Method of Moments (MOM) of a wire-grid representation of the LTSA utilizing the Numerical Electromagnetics Code (NEC), a general review of MOM and wire-grid modeling and a brief overview of NEC
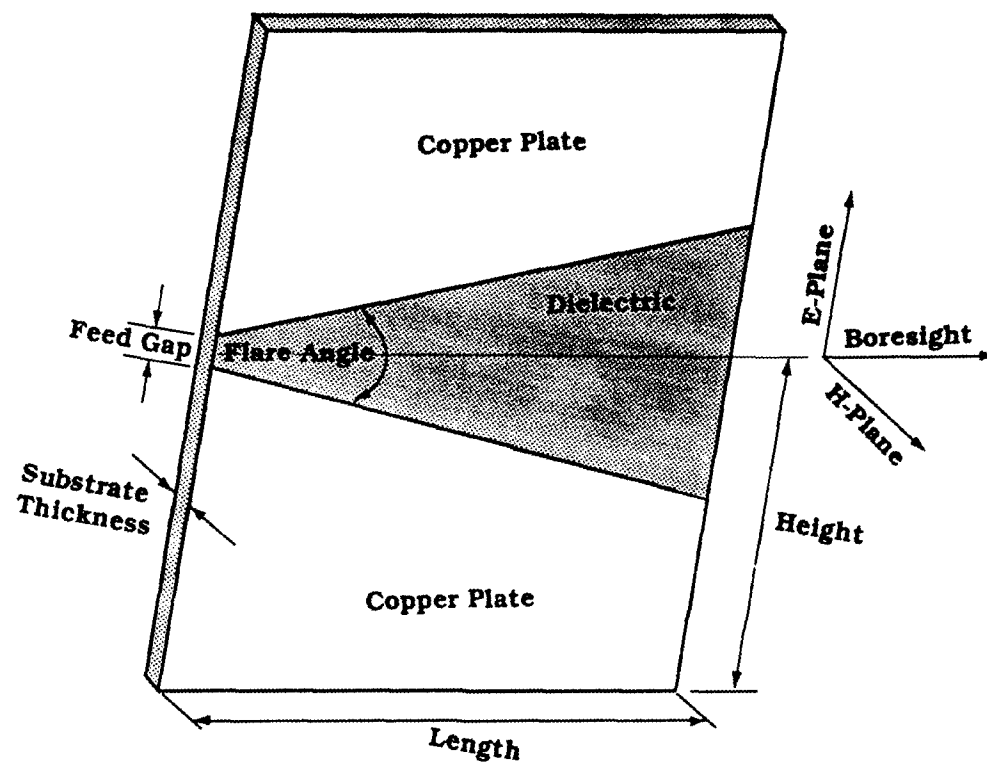
2

Figure 1.1 Oblique View of the LTSA [Ref. 2]

3

are included in chapter 2. This chapter will address the accuracy and the limitations of MOM, wire-grid modeling, and NEC. Chapter 3 addresses the LTSA wire-grid model and presents the means by which the CPU time constraint was balanced with the accuracy requirements in order to obtain the optimum wire-grid model. The wire-grid model used in the first part of Chapter 3 is based on the surface model used by Janaswamy, and the model geometry is optimized to accurately approximate the results obtained therein. In order to run his problem efficiently, Janaswamy utilized a slightly different geometry than the LTSA of Figure 1.1. Once the Janaswamy model has been accurately approximated, it is appropriate to compare the wire model against empirical data utilizing the actual LTSA geometry. The later part of Chapter 3 addresses this comparison and shows that the wire model does provide accurate radiation patterns for experimentally tested antennas.

Chapter 4 displays the ability of the wire grid model to permit a parametric study of the LTSA antenna of Figure 1.1. The antenna parameters of height, width, and flare angle are varied and the results are analyzed. Comparison with experimental results and those obtained by Kelly [Ref. 3] shows the wire model parametric study to be well-suited for use in LTSA design. Modeling results and analysis focus on the observed effects of changing beamwidths and suppressing sidelobes in the E- and H-planes. The geometry of the wire-grid models and corresponding radiation patterns are illustrated in Appendix A.

Conclusions are summarized in Chapter 5. The main emphasis is to reveal that the wire model can approximate existing computer-generated and empirical radiation patterns in an efficient manner and can be used effectively in providing a credible spectrum of design considerations for the LTSA. The efficiency of the model presented in this work may serve to motivate designers to work more extensively with the LTSA. Also, the success experienced in using the wire model method in this study may prove to be valuable in the study of other types of antennas.

II. MATHEMATICAL MODEL

A INTRODUCTION

The radiation characteristics for the LTSA models in this study were obtained using NEC. NEC is designed to provide the electromagnetic response of an arbitrary structure consisting of wires and/or surfaces in free space or over a ground plane. Since the LTSA surface structure was modeled in this study using a geometry of thin wires, NEC was chosen to perform the analysis. NEC accomplishes the analysis by the numerical solution of integral equations for induced currents. The current distribution on thin wire antennas is obtained by solving the Pocklington Integral Equation. Solving for the current distribution leads to a solution for the radiation pattern. NEC utilizes the Method of Moments (MOM), which transform the integral equation into a set of matrix equations. The matrix equations are then solved by numerical techniques. This chapter will present a general overview of the MOM, the Pocklington Integral Equation, and NEC.

B THE METHOD OF MOMENTS

1. Concept

Electromagnetic radiation problems can always be expressed as an integral equation of the general form [Ref 4: p. 306]:

$$\int I(z')K(z,z')dz' = -E^i(z) \qquad (2.1)$$

6

where $E^i(z)$ is the incident field (forcing function), $I(z')$ is the unknown current distribution, and $K(z,z')$ is the kernel. An equation of this type is known as the Electric Field Integral Equation (EFIE). Solving the EFIE for the current distribution on any antenna will lead to the solution for the radiation pattern and/or the input impedance. The EFIE can be solved by matrix techniques once it has been transformed into a set of simultaneous linear equations. The method of moments is a procedure for reducing the EFIE to a system of linear algebraic equations in terms of the unknown current $I(z')$. For thin wires the EFIE can be reduced to a scalar equation involving a line integral. This equation for a conductor of length L, known as Pocklington's Integral Equation, is of the form [Ref. 4: p. 310]:

$$\frac{1}{j\omega\varepsilon_0}\int_{-L/2}^{L/2} I(z')\left[\frac{\partial^2 \psi(z,z')}{\partial z^2} + \beta^2 \psi(z,z')\right]dz' = -E_z^i(z) \qquad (2.2)$$

where $\psi(z,z')$ is the free space Green's function defined by [Ref 3: p. 308]:

$$\psi(z,z') = \frac{e^{-j\beta R}}{4\pi R} \qquad (2.3)$$

ε_0 = permittivity of vacuum = 8.85 pF m^{-1} (2.4)

β phase constant = $2\pi/\lambda$ (2.5)

    where λ = wavelength, m   (2.6)

ω = angular frequency = $2\pi f$ rad s^{-1} (2.7)

$j = \sqrt{-1}$ (2.8)

7

and R is the distance between the observation point (x,y,z) and the source point (x',y',z'). See Figure 2.1.

$$R = \sqrt{(z + z')^2 + (x - x')^2 + (y - y')^2} \qquad (2.9)$$

Since the model developed in this study was built utilizing a grid structure made up of thin wires, a brief overview of the derivation of the Pocklington integral equation and an example of MOM to solve this equation are worthwhile.

2. Pocklington's Integral Equation Derivation

In 1897 Pocklington derived an integral equation to treat the case of wire antennas which enabled him to show that the current distribution on thin wires is approximately sinusoidal and propagates with nearly the velocity of light [Ref. 3]. To derive this equation consider the conventional assumptions for thin wire antennas and the illustrations of Figure 2.1 where the surface current density (**Js**) and the observation point (z') are at a distance a from the conductor axis (z axis).

The electric field of charges and current is given by

$$\mathbf{E} = -j\omega\mu_0\mathbf{A} - \nabla V \qquad (2.10)$$

where μ_0 = permeability of vacuum = 1260 nH m⁻¹, **A** = vector potential and V = scalar potential. We can assume that only z-directed currents are present since the wire radius is taken to be much less than the wavelength. Thus, for currents only in the z direction, equation (2.10) becomes

8
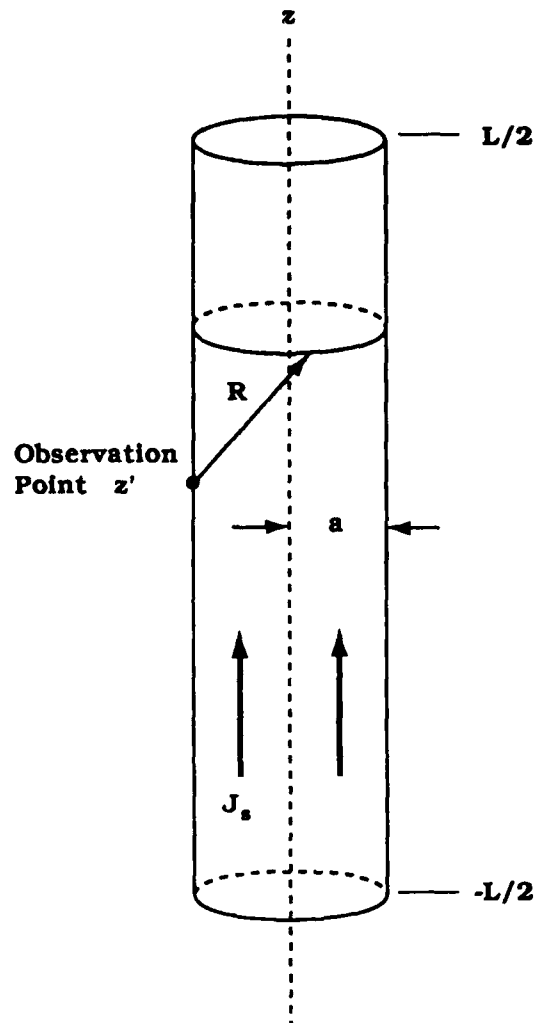
Figure 2.1 Linear Dipole Illustrated as a Wire Surface with Current Density J$_s$ and Observation Point on the Surface

9

$$E_z = -j\omega\mu_0 A_z - \frac{\partial V}{\partial z} \qquad (2.11)$$

From the Lorentz gauge condition we also have

$$\frac{\partial A_z}{\partial z} = -j\omega\varepsilon_0 V \qquad (2.12)$$

Taking the derivative of (2.11) and substituting into (2.12) we obtain

$$E_z = \frac{1}{j\omega\varepsilon_0}\left(\frac{\partial^2 A_z}{\partial z^2} + \beta^2 A_z\right) \qquad (2.13)$$

If we consider the z-directed current element $J\,dv'$

$$dE_z = \frac{1}{j\omega\varepsilon_0}\left[\frac{\partial^2 \psi(z,z')}{\partial z^2} + \beta^2 \psi(z,z')\right]J\,dv' \qquad (2.14)$$

and assume the conductivity to be infinite, and if one observes the surface current distribution from a point on the wire axis as shown in Figure 2.1, the current is confined to the wire surface and the integral over the wire volume becomes [Ref. 4: p. 308]:

$$E_z = \frac{1}{j\omega\varepsilon_0}\int_{-L/2}^{L/2} I(z')\left[\frac{\partial^2 \psi(z,z')}{\partial z^2} + \beta^2 \psi(z,z')\right]dz' \qquad (2.15)$$

We will call the quantity E_z the scattered field $E_z{}^s$, the field which is radiated in free space by the equivalent current $I(z')$. The other field present is the incident field $E_z{}^i$. On a perfect electric conductor the tangential field, E_{tan}, is equal to zero. Since

$$E_{tan} = E_z{}^s + E_z{}^i \qquad (2.16)$$

at the surface of the perfectly conducting wire and also interior to the

10

wire, the sum of the scattered field and the incident field must be zero. Therefore,

$$E_z{}^s = - E_z{}^i \qquad (2.17)$$

and equation (2.16) becomes the equation derived by Pocklington [Ref. 4].

3. Solving for Current Distribution on a Dipole

In order to demonstrate how the MOM is used to solve Pocklington's equation, a simple example of solving for the current distribution on a linear dipole will be presented. Finding the current distribution on any antenna will lead to a solution for the radiation pattern and/or input impedance. Since the idea of finding the radiation pattern of the LTSA wire models is examined in Chapters 3 and 4, this analysis is worthwhile.

Using the conventional assumptions for thin wire antennas and illustrations of Figure 2.1, the problem statement is to solve for the current, $I(z')$, on a short dipole with length, $L = 0.1\lambda$, and radius, $a = 0.005\lambda$. Assume a 1 volt center-fed excitation [Ref. 3: p. 16].

The steps used to solve Pocklington's integral equation by MOM are as follows: (a) expand $I(z')$ in a set of basis functions, (b) obtain linear equations by weighting functions and computing inner products, and (c) use matrix algebra to solve for the unknown coefficients of the basis functions [Ref. 3: p. 18].

In a simpler form, equation (2.2) can be written as

11

$$\frac{1}{j\omega\varepsilon_0} \int_{-L/2}^{L/2} I(z')K(z,z')dz' = -E_z^i(z) \qquad (2.18)$$

where the kernel,

$$K(z,z') = \left[\frac{\partial^2 \psi(z,z')}{\partial z^2} + \beta^2 \psi(z,z')\right] \qquad (2.19)$$

Approximating the current by a series of expansion (basis) functions of the form

$$I(z') = \sum_{n=1}^{N} I_n F_n(z') \qquad (2.20)$$

where I_n is a complex unknown number and $F_n(z')$ is a set of orthogonal pulse functions of the form

$$F_n(z') = \begin{cases} 1 & \text{for } z' \text{ in } z'_n \\ 0 & \text{elsewhere} \end{cases} \qquad (2.21)$$

leads to a "staircase" approximation of the actual current distribution as illustrated in Figure 2.2. $F_n(z')$ can be any set of basis functions. Figure 2.3 shows typical basis functions which can be used for $F_n(z')$. The pulse function was chosen for this example in order to keep it simple.

So far there is one linear equation in N unknowns. The number of independent linear equations must also equal N for a unique solution. The wire is divided into N segments of length $\Delta z'_n$, thus the integral equation is successively enforced at N different points on the axis of the wire. A set of weighting functions (Dirac delta functions)

$$W_m(z) = \delta(z-z_m) \qquad (2.22)$$

12
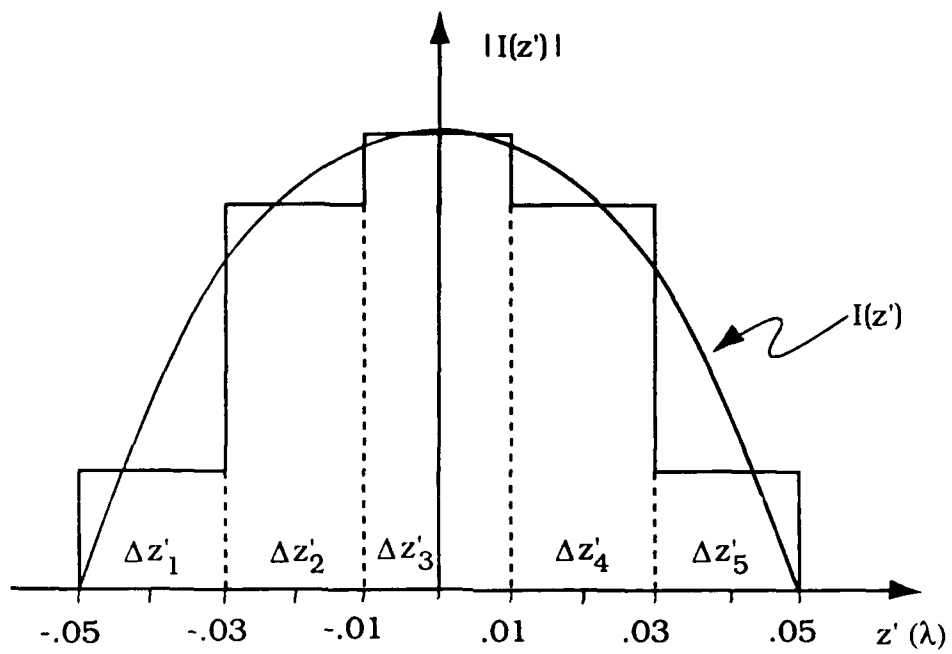
Figure 2.2 "Staircase" Approximation to an Actual Current Distribution
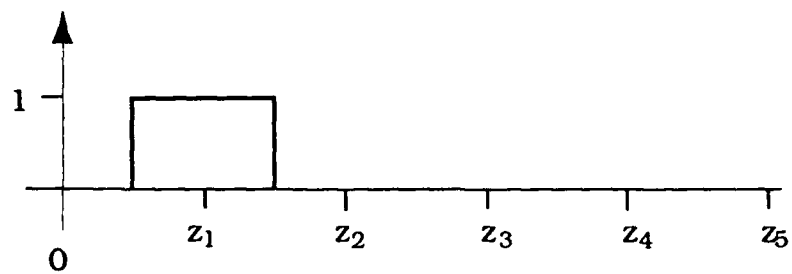
(a)   Pulse Function
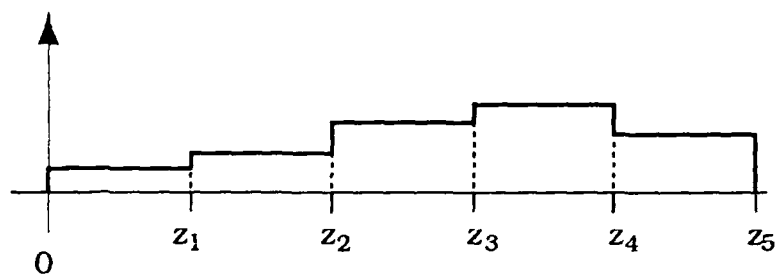
(b)   Step Approximation
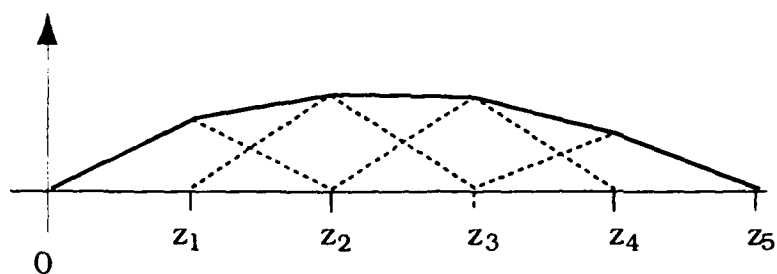
(c)   Function Represented by Triangles
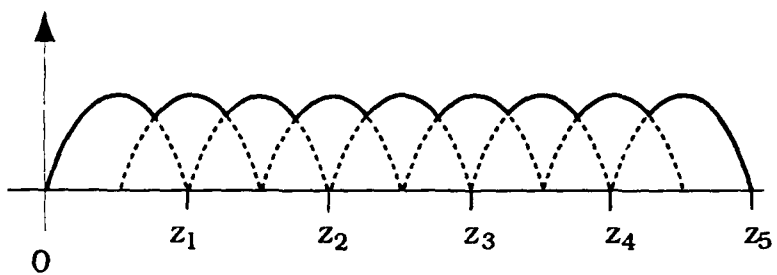
(d)   Piecewise Sinusoidal Function

Figure 2.3   Typical Basis Functions [Ref. 3]

14

with z_m taken as the midpoint of each subinterval are used to equate weighted averages of equation (2.20) for each W_m. This choice implies that the original integral equation (2.1) is now imposed at the discrete points z_m (the location of the delta functions) rather than the continuous interval. For this example N was chosen to be N = 5. The process of doing this is called point-matching. It is a special case of the more general MOM [Ref. 4; p. 312].

Substituting equation (2.20) into equation (2.18) yields

$$\frac{1}{j\omega\varepsilon_0} \sum_{n=1}^{5} I_n \int_{-L/2}^{L/2} F_n(z') K(z,z') dz' \approx - E_z^i(z) \qquad (2.23)$$

Taking the inner products in equation (2.24) produces

$$(2.24)$$

$$\frac{1}{j\omega\varepsilon_0} \sum_{n=1}^{5} I_n \int_{-L/2}^{L/2} F_n(z') K(z_m,z') dz' \approx - E_z^i(z_m)$$

The subscript, m, is considered the match point index because it is associated with the observation point at which the mth equation is valid. The second index is referred to as the source point index since it is associated with the field from the nth segment or n^{th} source [Ref 4: p.313]. Equation (2.24) is solved as a matrix equation

$$[Z_{mn}][I_n] = [V_m] \qquad (2.25)$$

where

$$z_{mn} = \frac{1}{j\omega\varepsilon_0} \int_{(n-1)L/2}^{nL/2} F_n(z') K(z_m, z') dz' \qquad (2.26)$$

$$V_m = -E_z^i(z_m)$$

The matrix $[V_m]$ must be defined before solving equation (2.25). The source model used in this example is a 1 volt center-fed excitation modeled with a magnetic frill generator and weighted delta test functions. This results in

$$[V_m] = \begin{bmatrix} 0.502 \angle -179.69° \\ 3.248 \angle -179.95° \\ 70.55 \angle -179.99° \\ 3.248 \angle -179.95° \\ 0.502 \angle -179.69° \end{bmatrix} \qquad (2.28)$$

Choosing the uniform segmentation of the wire results in an impedance matrix $[Z_{mn}]$ that is Toeplitz symmetric. (In a Toeplitz matrix, $Z_{mn} = Z_{1,|m-n|+1}$ for m≥2, n≥1.) Thus the first column (which is identical to the first row) is all that is required to fill Z_{mn}.

$$[Z_{m1}] = 10^2 \bullet \begin{bmatrix} 679.2 \angle -90.01° \\ 292.4 \angle -90.03° \\ 33.01 \angle -90.27° \\ 9.74 \angle -90.01° \\ 4.24 \angle -92.08° \end{bmatrix} \qquad (2.29)$$

Solving (2.25) for $[I_n]$ yields

$$[I_n] = 10^3 \bullet \begin{bmatrix} 0.81 \angle -89.54° \\ 1.54 \angle -89.64° \\ 2.44 \angle -89.75° \\ 1.54 \angle -89.64° \\ 0.81 \angle -89.54 \end{bmatrix} \qquad (2.30)$$

The solution for $[I_n]$ is consistent with expected results [Ref 4: p. 314].

16

The purpose of this example has been to demonstrate the MOM application to a simple antenna problem. A few key points related to the accuracy of MOM follow.

- The matrix dimension N (number of expansion modes) must be taken sufficiently large to get a convergent result but not so large as to cause numerical instability. Figure 2.4 shows how a solution for $[I_n]$ converges by increasing N for a similar problem. [Ref. 4: p. 314]

- Small numerical errors due to round-off or truncation usually have catastrophic effects if they cause apparent singularities or ill-conditioning in the matrix.

- Choice of appropriate basis functions not only improves the accuracy but reduces the matrix size needed for a convergent solution. In the case of a short dipole, the expected triangular current distribution suggests that piecewise linear or triangle basis functions should give a better representation of $I(z')$. [Ref 3: p.24]

C. NUMERICAL ELECTROMAGNETICS CODE

The Numerical Electromagnetics Code (NEC) was developed at the Lawrence Livermore Laboratory, Livermore, California, as a user-oriented computer code for analysis of the electromagnetic response of antennas and other metal structures. The analysis is accomplished by the numerical solution of integral equations for induced currents using the Method of Moments. The excitation may be an incident plane wave or a voltage source on a wire, while the output may include current and charge density, electric or magnetic field in the vicinity of the structure, and radiated fields [Ref. 5].

This study was concerned only with wire modeling of the LTSA utilizing voltage source excitation. In NEC, wires are modeled with

17
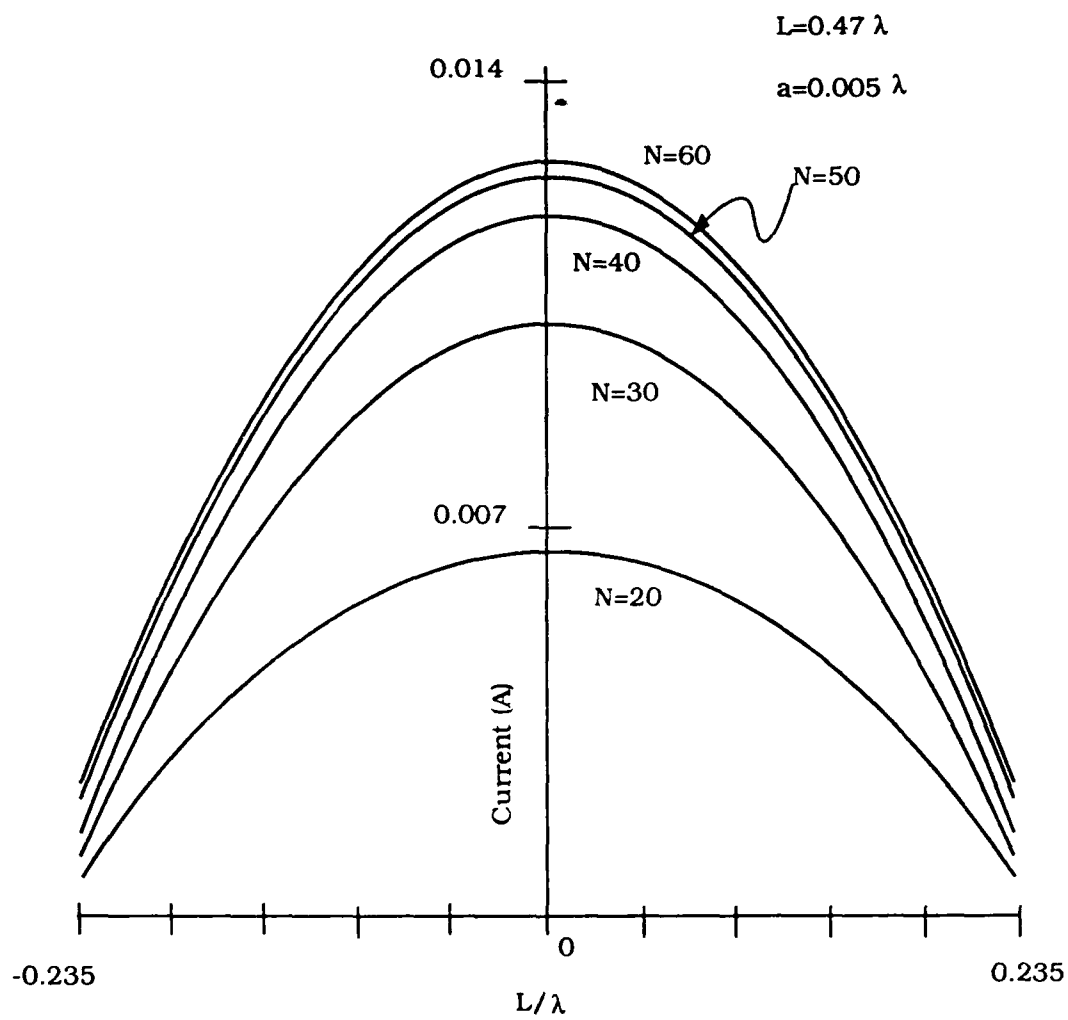
Figure 2.4 Current Distributions on a Half-wave Dipole for Various Numbers of Pulse Functions and a Unit Voltage Source [Ref. 4: p. 314].

18

strings of short straight segments, and a wire is defined by the coordinates of its two end points and its radius. The basis functions utilized by NEC are a combination of pulse, sine, and cosine functions. The weight functions are Dirac delta functions at the centers of segments, thus the boundary condition is "point matched" at the centers of segments. The main electrical consideration is segment length Δ relative to the wavelength λ. Generally, Δ should be less than about 0.1λ at the desired frequency. The size of the segments determines the resolution in solving for current on the model.

The thin-wire kernel approximations were used in this study. In the thin-wire kernel, the current on the surface of a segment is reduced to a filament of current on the segment axis. Only currents in the axial direction on a segment are considered, and there is no allowance for variation of the current around the wire circumference. The accuracy of the numerical solution for the dominant axial current is dependent on Δ/a, where a is the wire radius. The thin-wire approximation can produce non-physical results when Δ/a is too small. Studies of the computed field on a segment due to its own current have shown that with the thin-wire kernel, Δ/a must be greater than about 8 for errors of less than 1%. The angle of intersection of wire segments in NEC is not restricted, however, the number of wires joined at a single junction cannot exceed 30 because of dimension limitations of the code. At a wire junction the current satisfies Kirchoff's current law and the charge density satisfies the Wu and King condition.

In this study the wire-grid is used to model a thin conducting plate. In the past, the wire-grid modeling method has provided accurate results when modeling far-field parameters. A single current flowing on the wires represent both of the currents that would flow on opposite sides of a thin metal plate conductor. When a metal plate conductor is exposed to an incident electro-magnetic wave, a current (J_T) is induced on the top of the plate and a current (J_B) is induced on the bottom of the plate as shown in Figure 2.5. These currents are not necessarily of the same magnitude and direction. NEC models the sum current $(J_B + J_T)$ so that a single wire grid is sufficient to represent both of the currents that would flow on the opposite sides of a thin metal conductor. While information on the currents on the individual surfaces is lost, the grid will yield the correct radiated fields [Ref. 5].
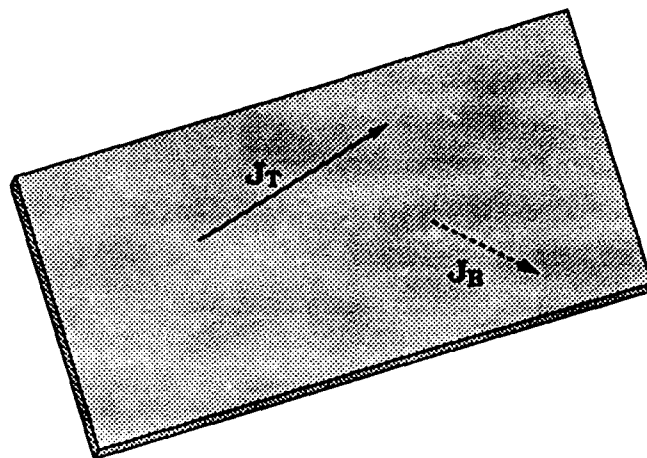
Figure 2.5   Currents Induced on a Thin Metal Plate Conductor by an Incident Field

III. LTSA WIRE MODEL

A BACKGROUND

An accurate model for the LTSA based on the MOM solution of the EFIE for the electric surface currents flowing on the conducting plates of the antenna has been presented by Janaswamy [Ref. 2]. The method is rigorous for air dielectric antennas, and approximate for dielectric supported antennas. The principal limitation of this method is that large CPU times are needed to obtain the solution [Ref. 2]. This chapter presents an alternative wire-grid model of the LTSA that utilizes the same geometry used by Janaswamy. To simplify the modeling of the surface currents of the LTSA antenna shown in Figure 3.1a, Janaswamy used a slightly different geometry in order to keep the unknowns to a manageable number. This modified geometry, illustrated in Figure 3.1b, does not change the physics that governs the radiation mechanism of the antenna [Ref. 2]. The solid structure of the antenna is replaced by a wire grid configuration in order to reduce the time required to fill the impedance matrix of the MOM solution. Present analysis indicates that the wire grid model provides an accurate approximation to the results obtained by Janaswamy while significantly reducing the CPU time required to obtain the solution. This similarity of results obtained by using two different computer models natural leads to a comparison of the wire-grid model radiation patterns with radiation patterns obtained experimentally.

22
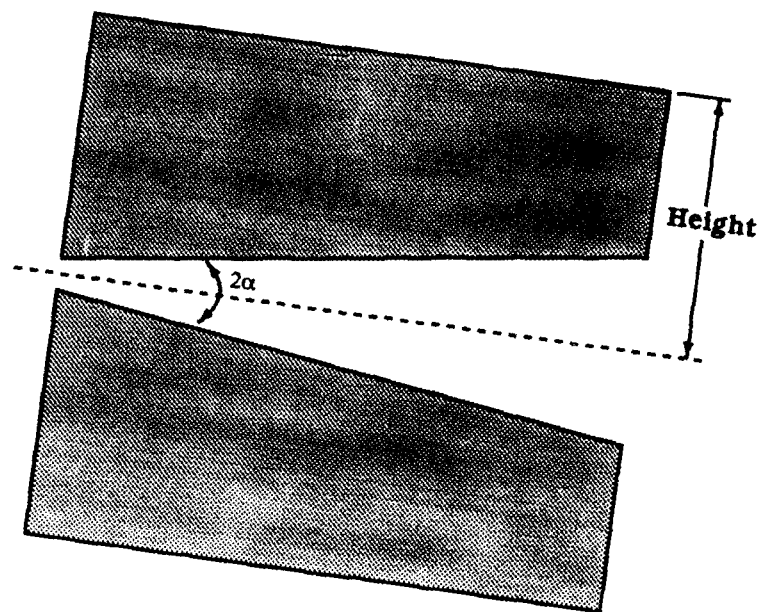
Figure 3.1a LTSA Surface Geometry
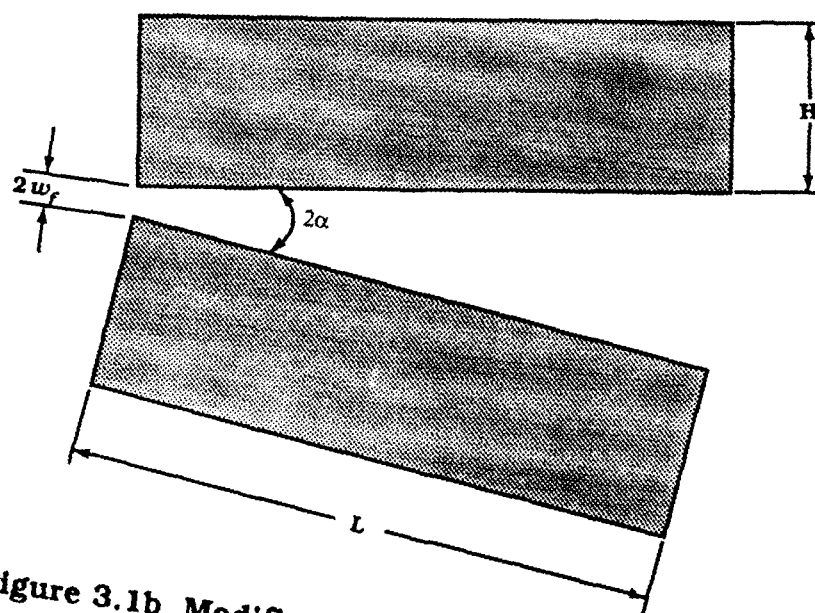
Figure 3.1b Modified LTSA Geometry for Modeling

23

B. COMPARISON OF WIRE MODEL AND SURFACE MODEL

The criteria set for this study was to accurately approximate the results for the LTSA (without a dielectric substrate) obtained by Janaswamy while keeping the computer run time required to obtain the solution under 15 minutes. For an antenna with $L/\lambda = 5.2$ and $H/\lambda = 0.9$, Janaswamy's model needed a CPU time of approximately 9 hours running on a VAX 11/785. The majority of this time was spent filling the impedance matrix $[Z_{mn}]$. In Janaswamy's model there were 143 unknowns on each plate, thus the computer had to solve 40,898 two-dimensional surface integrals in order to fill the two 143 X 143 impedance matrix. Kelly, working with the same surface model (267 unknowns) and utilizing VS Fortran code on an IBM 3033/4381 system was able to reduce the run time to 70 minutes [Ref. 3]. Using the wire model reduces the integral equation to one-dimension, therefore, the impedance matrix can be filled much faster. The NEC software used in this study was run on the IBM 3033/4381 system. It was decided that producing accurate results using a wire grid model of the LTSA for this particular problem in less than 15 minutes would lead to efficient study of other LTSA antenna designs.

The first step was to model the LTSA using a simple wire structure consisting of 9 wires. The wire model, illustrated in Figure 3.2, was excited by a unit volt voltage source connected to wire number 1, with equal length segments adjacent to the source. The frequency of operation was 300 MHz. At this frequency the wavelength (λ) is equal to 1 m, $L = 5.2\lambda$ and $H = 0.9\lambda$. These

24
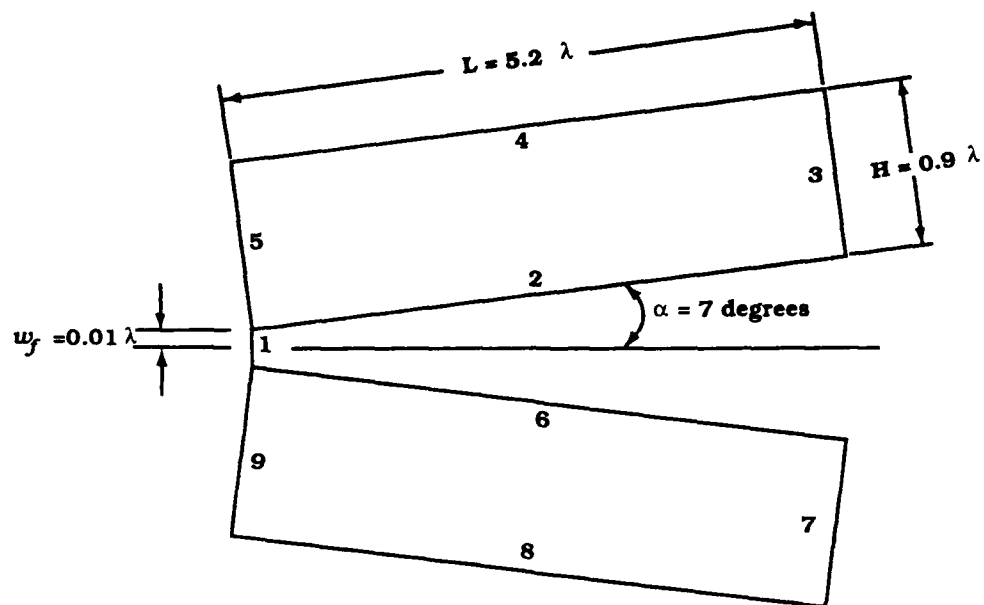
Figure 3.2 Basic Wiregrid Structure

dimensions are consistent with those used by Janaswamy. The thin wire kernel was utilized so that the current on the surface of the segment was reduced to a filament of current on the segment axis. The wires were of constant radius equal to 0.001 m, and were segmented at all junctions.

Although it was obvious that this simple structure would not approximate the results obtained by Janaswamy, an analysis of this model provided valuable insight. Several factors, which needed to be explored before a more elaborate model could be built, were determined using the simple model. First, it was necessary to determine whether or not a convergent solution could be found for the simple structure. By gradually increasing the number of segments per wavelength it was determined that a convergent solution could be obtained and that the number of segments/wavelength that would accurately approximate this solution was 7. Using 7 segments per wavelength, Δ is equal to 0.1428λ. This leads to a ratio of Δ/a of 142.8. Recall from chapter 2 that for errors less than 1%, Δ/a must be greater than 8. Secondly, it was necessary to determine whether or not using a ground plane instead of the lower symmetric half of the antenna in the model would decrease the run time without changing the results. This analysis proved that, since the geometry of the antenna is symmetric, the computer run time could be further decreased, without sacrificing the accuracy of the model, by using a ground plane in place of the lower symmetric half of the antenna.

Utilizing the information obtained in the analysis of the basic structure and Kirchoff's current law, no less than a dozen different wire grid geometries were analyzed. At first, only a few wires were added to the basic structure. The idea was to analyze various simple geometries to determine which would produce a radiation pattern similar to the pattern obtained by Janaswamy. The radiation patterns of several different simple geometries were studied to determine the best wire pattern. Examples of these geometries are illustrated in Figure 3.3. It was discovered that if wires within the basic structure were placed such that each of the wires originated at the lower left corner where the source was located (as illustrated in Figure 3.3b), the resultant radiation pattern produced a shape similar to the pattern obtained by Janaswamy. This result is consistent with theory in that placing the origin of all wires at the source point will facilitate a smooth current transition from the fed to the wires of the model.

The next step was to work within this basic wire pattern, adding more wires until results that accurately approximated Janaswamy's results were obtained. Increasing the number of wires, one at a time, the radiation pattern similarity grew closer to Janaswamy's. The wire grid configuration illustrated in Figure 3.4 proved to optimally meet the time criteria. The height along the end farthest from the source is divided into 5 short wires (length = 0.18 m), and a radial wire was attached to the junction of each of the short wires. Similarly the length along the top of the structure is divided into 8 short wires (length = 0.65 m) with a radial wire attached at each junction. The
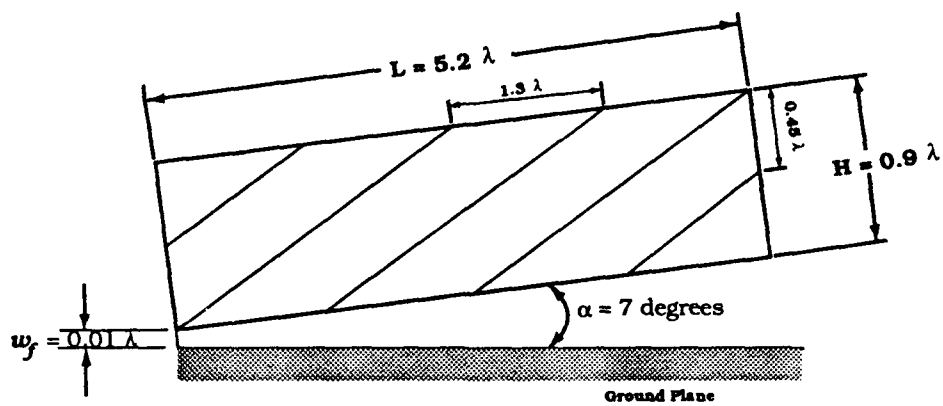
(a)
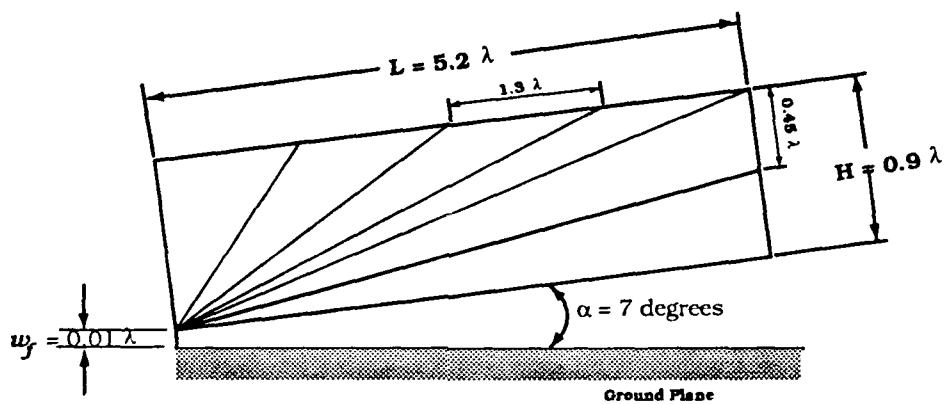
(b)
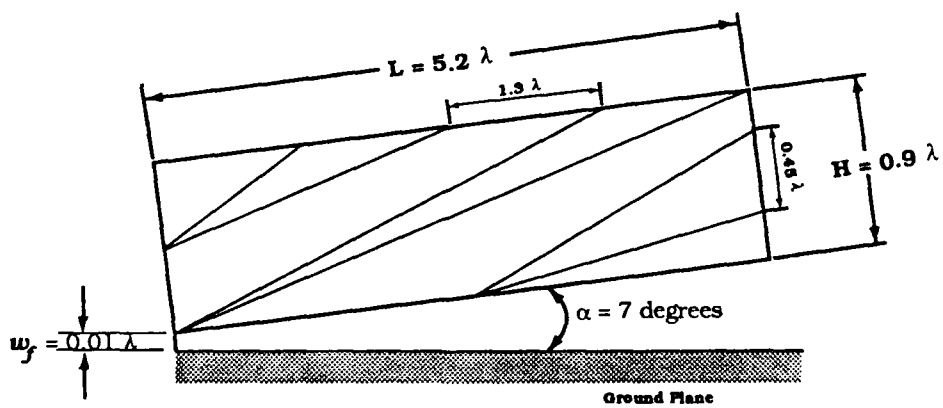
(c)

Figure 3.3 Experimental Wire-grid Patterns

28
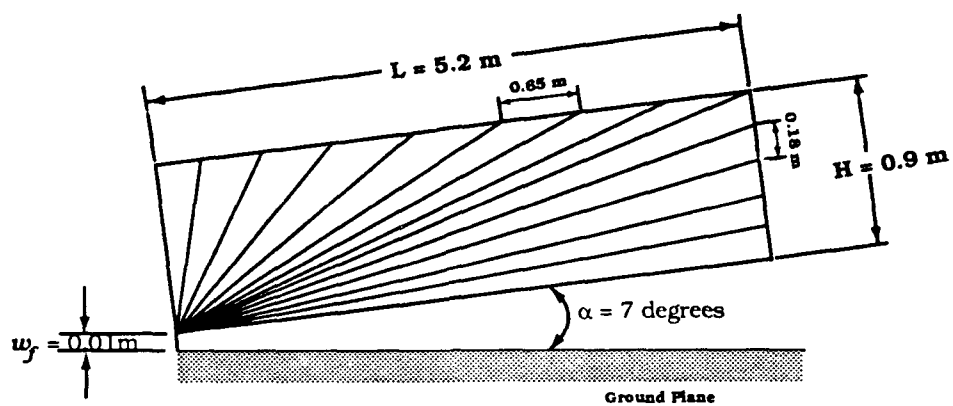
Figure 3.4 Optimum Wiregrid Structure

29

total number of wires used in this model is 28. The number of unknowns in this structure is 397. The run time for this model was approximately 15 minutes and the resultant radiation pattern approximated the pattern obtained by Janaswamy. Figure 3.5 shows the comparison of the wire grid model radiation pattern and the radiation pattern using Janaswamy's model. Several attempts to improve this geometry by adding smaller wires branching out from the main radial wires showed no significant improvement in the radiation pattern.

Although a more accurate approximation could be obtained by adding more radial wires to the model, the efficiency would decrease. Before sacrificing the 15 minute run time criteria it was appropriate to compare results obtained from this wire model with experimental ones.

C. COMPARISON OF WIRE MODEL AND EXPERIMENTAL LTSA

Once it was determined that a wire grid model could accurately approximate the results obtained by Janaswamy within the time constraint of 15 minutes, the next step was to model an actual LTSA and compare the model radiation pattern to experimental results. The wire-grid illustrated in Figure 3.6 models an LTSA for which experimental results were computed at frequencies of 8 GHz and 10 GHz [Ref. 7]. The wavelengths are 3.75 cm and 3.00 cm respectively. The experimental antenna was mounted on one-half inch styrofoam. The relative permittivity of styrofoam is $\varepsilon_r = 1.03$, which is approximately equal to the relative permittivity of air ($\varepsilon_r = 1.0006$). A

Optimal Wire Model vs. Janaswamy Model
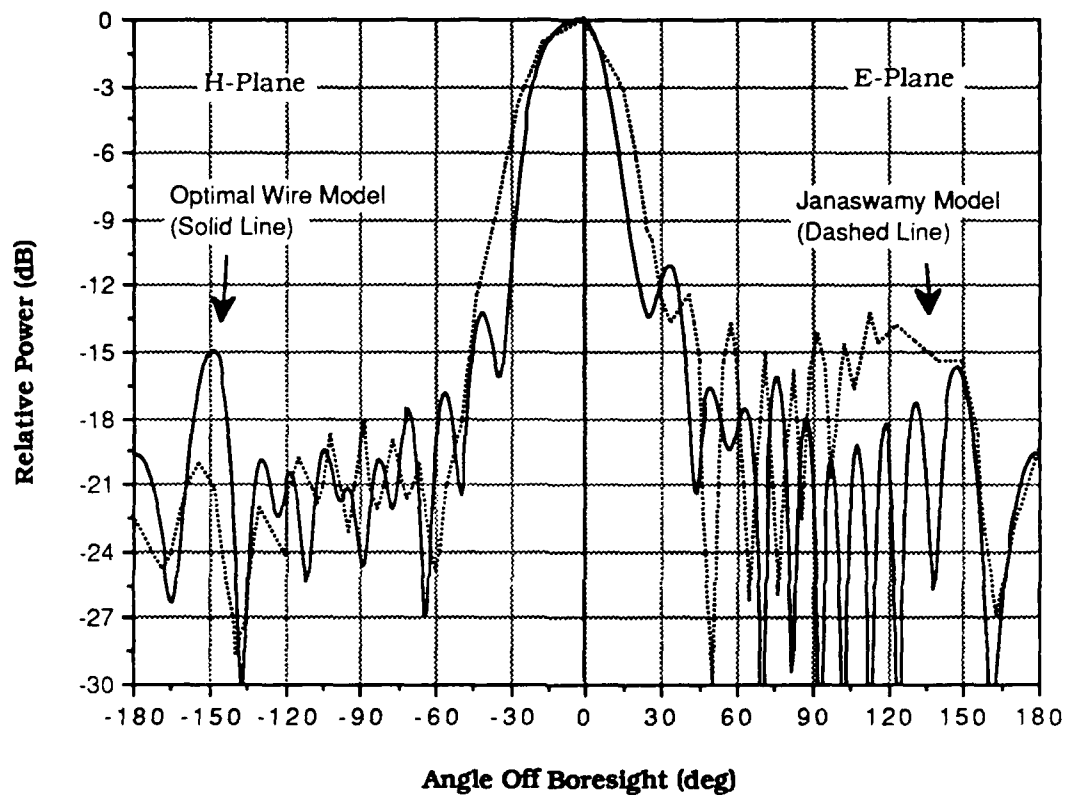
Figure 3.5   Comparison of radiation Patterns of the Janaswamy Model
and the Wire Model
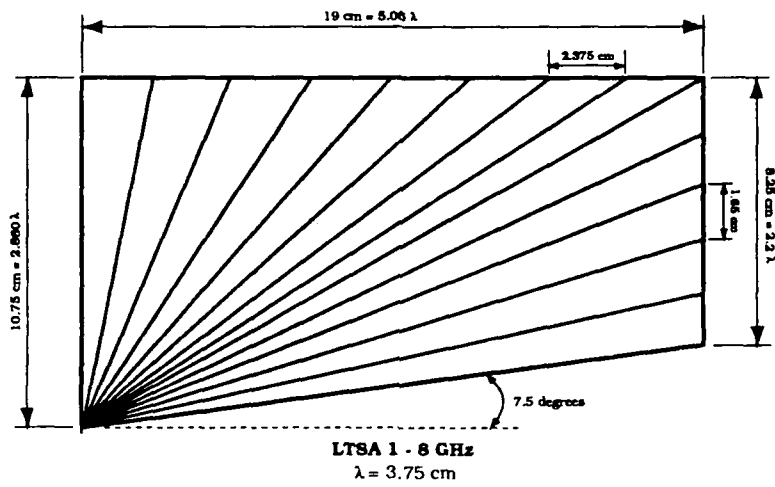
Figure 3.6a Wire Model of Experimental LTSA at 8 GHz
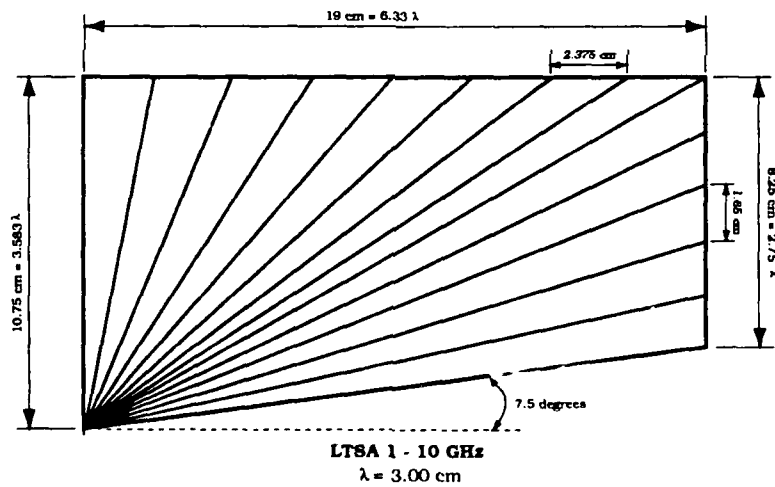
Figure 3.6b Wire Model of Experimental LTSA at 10 GHz

microwave detector diode was placed across the feed gap to receive a 1 KHz modulated RF signal.

The wire radius used in this model is equal to 0.0003. This leads to a Δ = .00428 and a Δ/a equal to 14.28 for 8 GHz and Δ = .00535 and a Δ/a equal to 17.85 for 10 GHz. Since the Δ/a ratios are greater than 8, the errors in the computed field will be less than 1% [Ref. 6]. The number of wires used in this model is 28. Using 7 segments per wavelength leads to 526 unknowns for the 8 GHz case and 629 unknowns for the 10 GHz case.

Figure 3.7 compares the radiation pattern of the wire model with the results obtained experimentally. These results show that the wire model produces a very good approximation of the actual LTSA. There is a noticeable difference in the sidelobes. however. the sidelobes of the radiation pattern of the experimental antenna are somewhat obscure because the dynamic range of the microwave detector diode was less than 15 dB. The wire model radiation patterns shown in Figure 3.7 are consistent with known characteristics and thus the wire model has proved to be an accurate approximation of the experimental results.

Wire Model vs. Experimental LTSA 8GHz
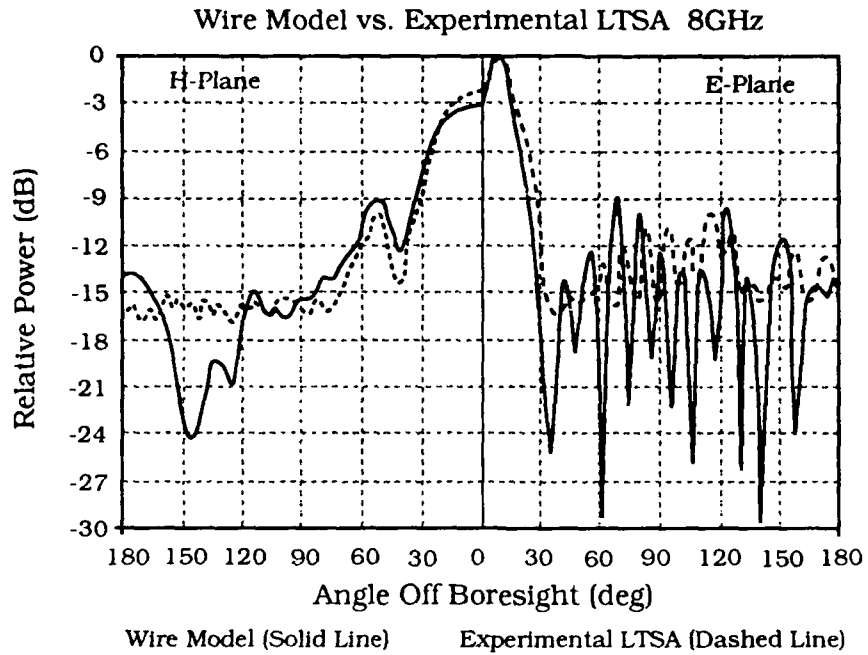
Figure 3.7a Comparison of Radiation Patterns
of the Wire Model and Experimental LTSA at 8GHz

Wire Model vs. Experimental LTSA 10GHz
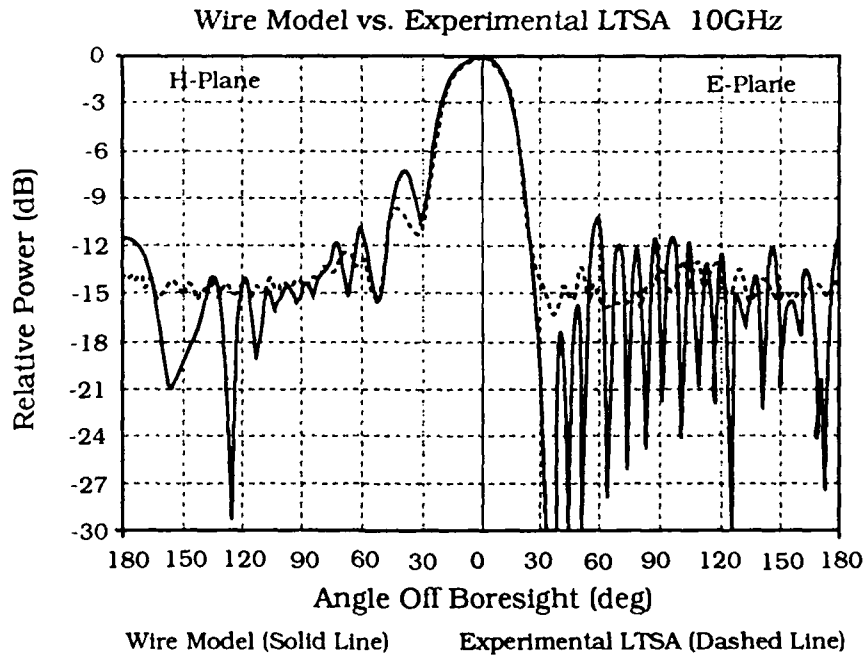
Figure 3.7b Comparison of Radiation Patterns
of the Wire Model and Experimental LTSA at 10GHz

34

IV. PARAMETRIC STUDY

A INTRODUCTION

The ability of the wire model to accurately predict radiation pattern behavior in a reasonable amount of time leads to efficient and effective study of LTSA design. The theoretical model provides the opportunity to develop specific parametric analysis of the LTSA. Parametric analysis had only been experimentally performed until Kelly studied the effects of changing the height, length, flare angle, and dielectric substrate on the radiation pattern of the LTSA using his surface model [Ref. 3]. This study was valid, however, due to the large amount of CPU time required, it was somewhat limited. The rectangular geometry utilized by Kelly also presented some limitations. Kelly utilized the same rectangular surface model as used by Janaswamy (this geometry is illustrated in Figure 3.1b). This geometry worked well for Janaswamy's purposes, however, Kelly could not vary the parameters very far from the reference structure without distorting results. It can be seen from Figure 3.1 that the actual LTSA and the modified LTSA structure used by Janaswamy are relatively similar in shape and size and Janaswamy has shown that the physics that governs the radiation mechanism of the antenna is not changed by utilizing the modified geometry [Ref. 2]. However, Figure 4.1, and the results of this study indicate that when the parameters are changed

35
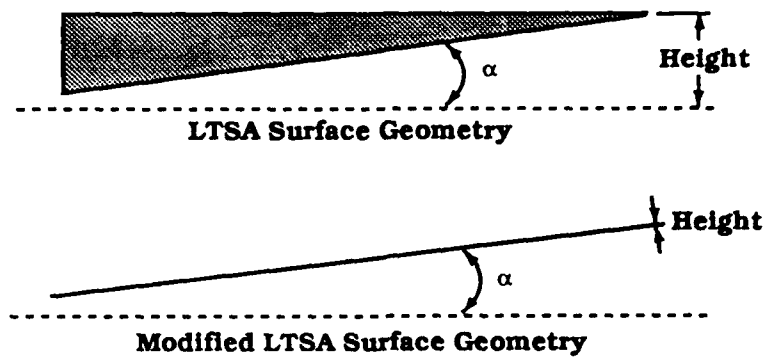
Figure 4.1a Effects of Minimizing Height on the Geometry of the LTSA Surface Model and the Modified LTSA Geometry
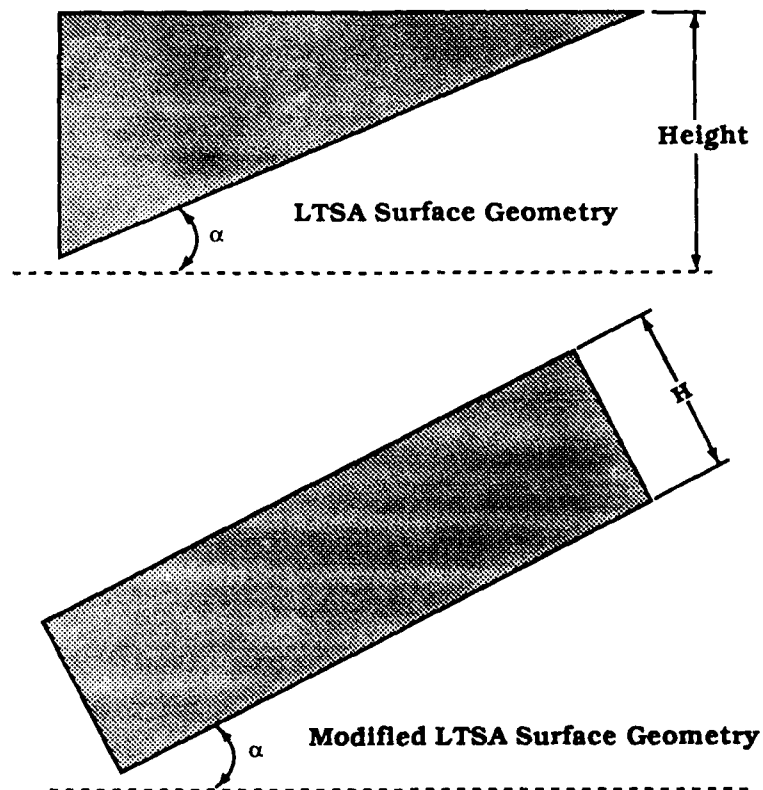
Figure 4.1b Effects of Maximizing Flare Angle on the Geometry of the LTSA Surface Model and the Modified LTSA Geometry

towards the extreme, the rectangular geometry no longer gives an accurate approximation for the LTSA structure.

The solution for the radiation pattern using the wire model is obtained in less than one-quarter of the time required by Kelly's model and thus facilitates the study of larger and more varied LTSA structures. This is particularly true of the air dielectric antennas. For example, the largest structure Kelly was able to study had a height of $1.5\lambda_0$ and a length of $5\lambda_0$, whereas the present study was able to efficiently consider a structure with H = $2.2\lambda_0$ and L = $6.33\lambda_0$. Also, because the wire model has the same geometry as the LTSA, it will provide more accurate results when the parameters are varied far from the reference parameters. It could be argued that straying too far from the reference parameters would be wandering outside of the practical operating range of the antenna, and in some instances this proved to be true. In many of these cases the main beam was not well formed. However, in other cases, stretching the limits of the parameters provided useful insight.

It is necessary to define a valid set of design parameters before correlating the behavior to design changes. As a reference for the parametric study the LTSA design parameters are shown in Table 4.1. The predicted radiation pattern for the reference data is shown in Figure 4.2. In this study the parameters of length, height, and flare angle will be varied and the resulting radiation patterns analyzed. The analysis proceeds by varying one design parameter at a time and observing the effects on the radiation pattern. Appendix A contains

37

LTSA Design Parameters		
Frequency	8 GHz (λ_0 = 3.75 cm)	10 GHz (λ_0 = 3.00 cm)
Height	2.2 λ_0	2.75 λ_0
Length	5.06 λ_0	6.33 λ_0
Flare Angle	15 degrees	15 degrees
Feed Gap	.0093 λ_0	.0116 λ_0
Dielectric	Air	Air

Table 4.1   Reference LTSA design parameters for parametric study
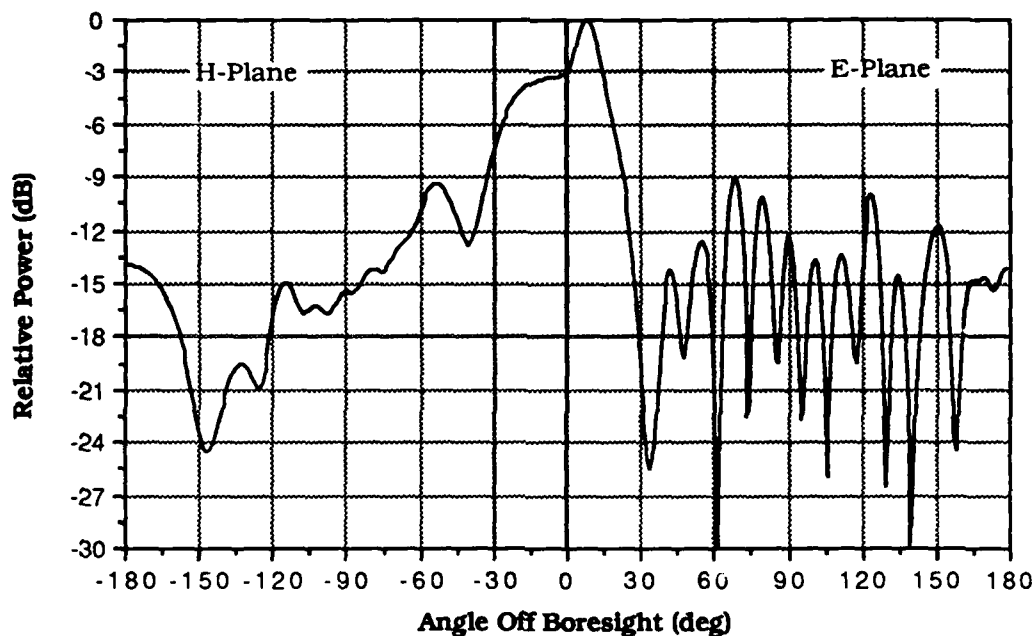
Figure 4.2a Predicted Radiation Pattern for the Wiregrid Model of the Emphirical Design - 8GHz
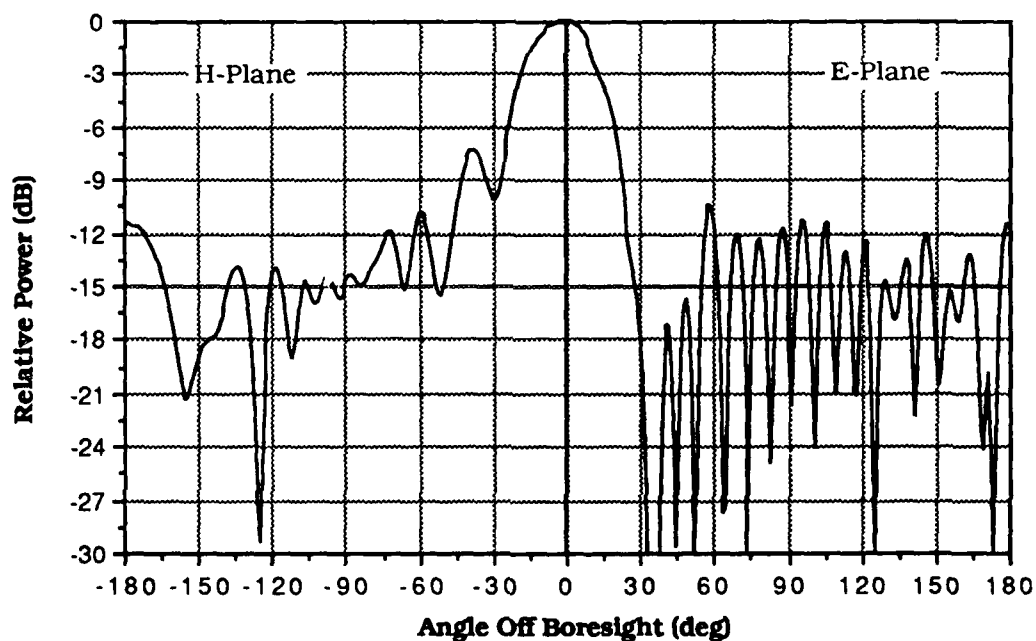
Figure 4.2b Predicted Radiation Pattern for the Wiregrid Model of the Emphirical Design - 10GHz

39

the detailed radiation pattern and wire geometry comparisons. In this chapter radiation pattern comparisons are made by analyzing the half-power or 3 dB beamwidths (HP_E, HP_H) of the main beam and relative gain of the highest sidelobe.

Together these attributes indicate the directivity of the antenna and provide a basis with which to compare antenna designs. The equation used to approximate the directivity of the LTSA is

$$D = 52,525/(HP_E\ HP_H) \tag{4.1}$$

where HP_E and HP_H are in degrees and a smooth elliptical main beam cross-section is assumed [Ref. 3: p. 41].

B. HEIGHT OF THE LTSA

Experiments with an air dielectric LTSA (L = $7.2\lambda_0$) showed that a progressively narrower E-plane beamwidth is obtained when the height was shortened to $1.5\lambda_0$, but that at $0.75\lambda_0$ the HP_E broadened again [Ref. 3]. This is consistent with the predicted behavior from the wire model shown in Figure 4.3a and Figure 4.4a for L = $5.06\lambda_0$ and L = $6.33\lambda_0$, respectively. In both cases there is a distinct narrowing of HP_E when the height is approximately equal to $1.0\lambda_0$ (H = $.88\lambda_0$ for L = $5.06\lambda_0$ and at H = $1.10\lambda_0$ at L = $6.33\lambda_0$). This represents a directivity increase of about 2 dB compared to H = $1.5\lambda_0$. In the E-plane, the relative gain of the highest sidelobe is at a minimum when H = $.8\lambda_0$ to H= $1.3\lambda_0$ for L = $5.06\lambda_0$ and when H = $1.6\lambda_0$ to H = $2.3\lambda_0$ for L = $6.33\lambda_0$. These results are also consistent with the results obtained by Kelly.

40
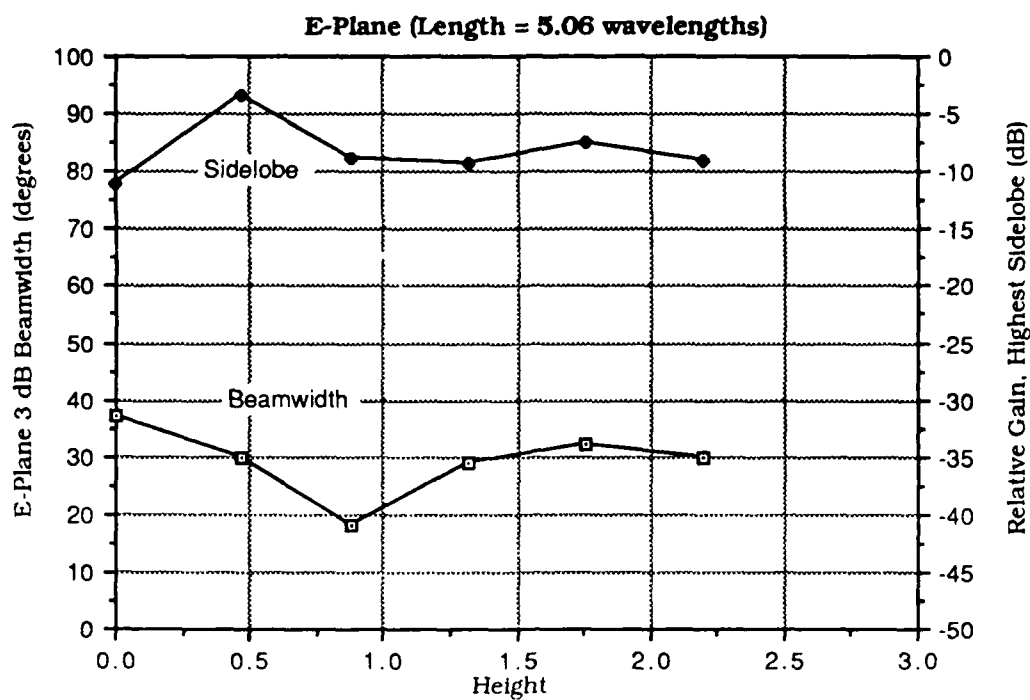
Figure 4.3a   E-Plane Effects of Changing Height - 8GHz
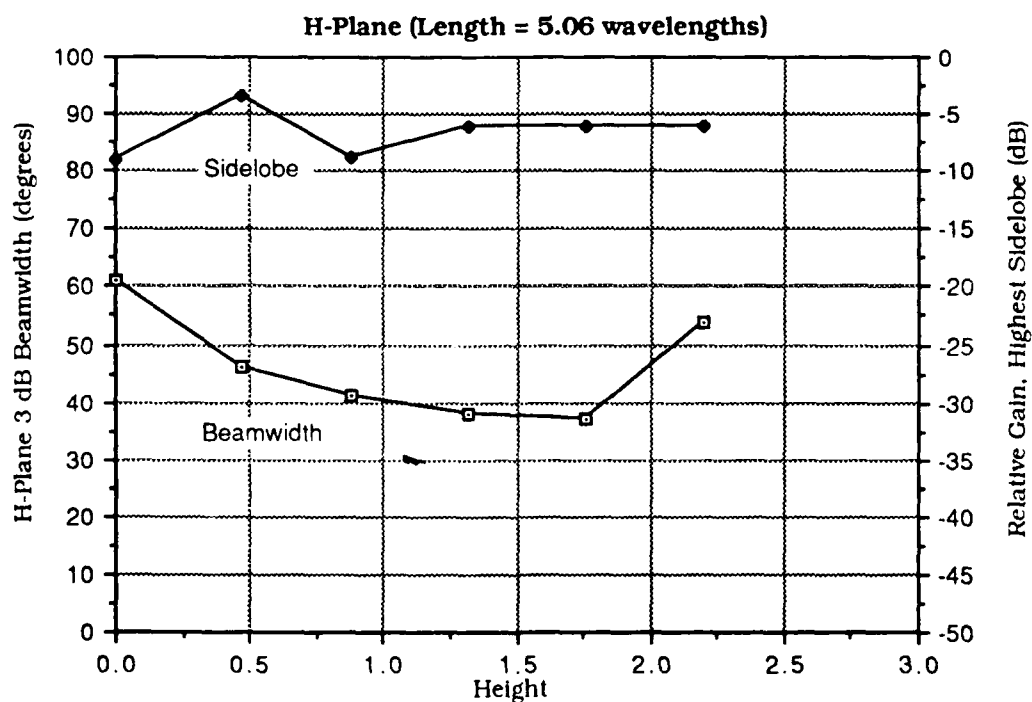
Figure 4.3b   H-Plane Effects of Changing Height - 8GHz

41

E-Plane (Length = 6.33 wavelengths)
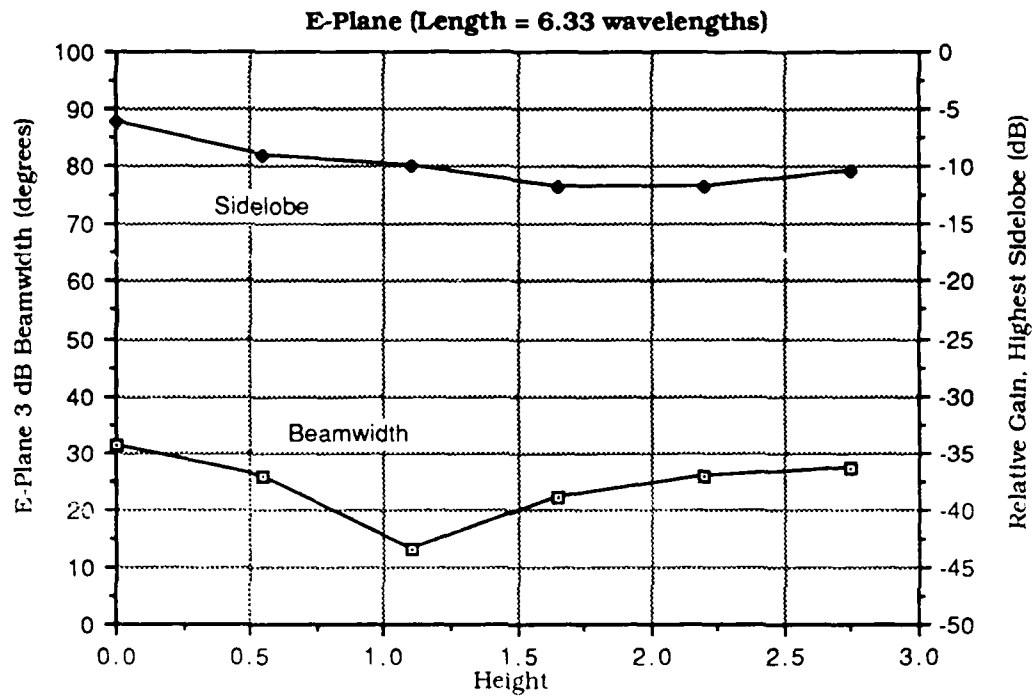
Figure 4.4a   E-Plane Effects of Changing Height - 10GHz

H-Plane (Length = 6.33 wavelengths)
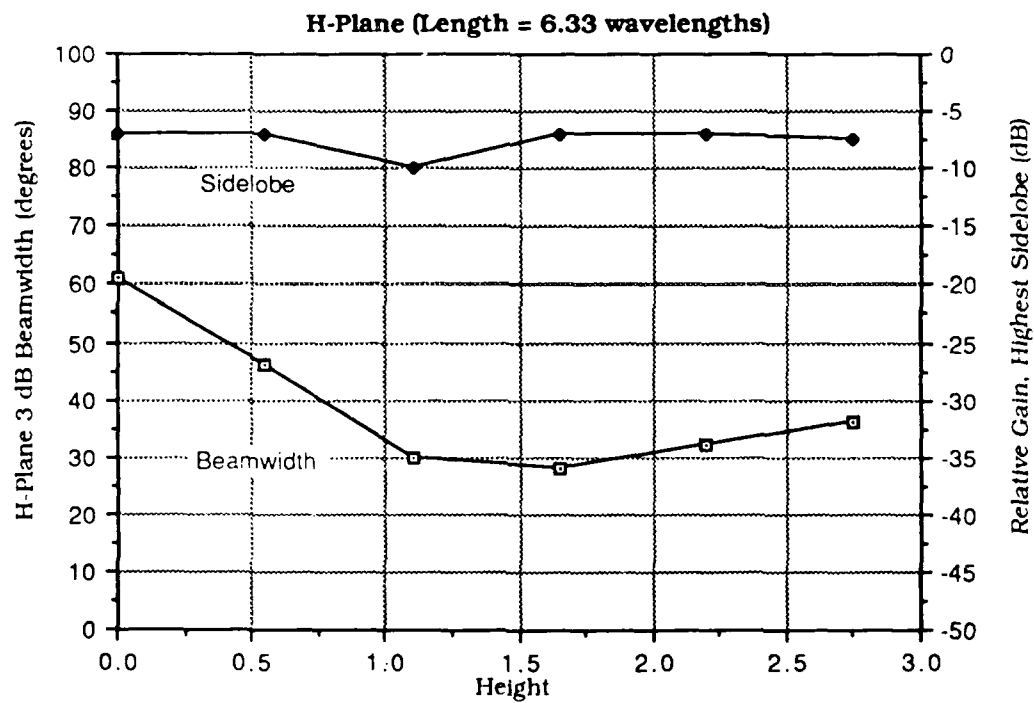
Figure 4.4b   H-Plane Effects of Changing Height - 10GHz

42

In the H-plane the cited experiments and Kelly's model showed a broadening of HP_H for decreasing height [Ref. 3]. This is consistent with the results obtained from the wire model as shown in Figure 4.3b and Figure 4.4b. However, the cited experiments and the results obtained by Kelly did not consider heights greater than $1.5\lambda_0$. This study revealed that HP_H also broadened when the height was above H = $1.7\lambda_0$.

One significant difference noted between the results obtained by Kelly and the results of the wire model was when the height of the LTSA was below $0.75\lambda_0$. Kelly claimed that the beamwidth tapered off in this area whereas the wire model results showed that the beamwidth increased. The difference could be due to the fact that Kelly used the same rectangular geometry which was used by Janaswamy and the wire model geometry is shaped more like the actual LTSA. When the height is reduced towards zero, Kelly's model begins to resemble a straight wire while the wire model maintains the shape of a wedge as shown in Figure A.21. Janaswamy had stated that using the alternate geometry does not change the physics that govern the radiation mechanism of the antenna for antenna dimensions in the region of practical use [Ref. 2]. However, Janaswamy's length to height ratio was constant at $5.2\lambda_0/0.9\lambda_0 = 5.77$.

Figures 4.3a and 4.3b reveal that there are very high sidelobes when the height of the antenna is reduced below $0.5\lambda_0$. For heights in this range, the backlobe becomes more prominent and limits the use of the antenna. It is the highest sidelobe that is plotted in Figures 4.3a

43

and 4.3b. For certain heights, the backlobe is greater than the sidelobes and is plotted in Figures 4.3a and 4.3b instead. The sidelobe level decreases again as the antenna height approaches zero. This suggests that, within a certain range of height, much of the propagated wave is being reflected and thus there is an impedance mismatch.

In this study, dimension multiples of approximately $\lambda_0/2$ are used for the height and length, thus good judgement must be used in the interpolation of data points. It also must be kept in mind that these results may vary somewhat with changing contributions of other fixed design parameters. Choosing the criteria for optimum design of an LTSA that produces a radiation pattern showing a narrow main beam and low sidelobe levels and keeping the above mentioned factors in mind has revealed that the height of the LTSA should be kept approximately between 1.1 and 1.7 wavelengths. This result is significant when making decisions concerning cost, weight, and size limitations.

C. FLARE ANGLE OF THE LTSA

Experiments performed in the past have shown that when the flare angle (2α) is varied, the effects on the LTSA radiation pattern result from two competing phenomena. First, it has been shown that increasing the flare angle in similar traveling wave antennas has demonstrated that HP_E narrows proportional to $1/2\alpha$ and that HP_H is generally insensitive to flare angle changes. These results are justified in part by analogy to aperture antennas in which narrower beamwidths are obtained by increasing the aperture size. The second effect

44

(which occurs in dielectric supported antennas) results from the relationship between flare angle and phase velocity. Experiments have shown that increasing 2α results in a broader beamwidth due to increased phase velocity. The phase velocity increases because the fields between the plates are weakened as the plates move farther apart. The phase velocity is inversely proportional to the energy stored in the fields. When the flare angle is increased, the slow-wave effect supporting a narrow beam is reduced and the beam widens [Ref. 3: p. 49].

Kelly's analysis revealed that when the flare angle was below 21 degrees the beamwidths were insensitive to flare angle changes and thus concluded that, in general, the relative contributions of the cited competing factors seemed to offset one another in modeling below 21 degrees [Ref.3: p.49]. This is somewhat consistent with the behavior shown in Figures 4.5 and 4.6, however, a slight difference is noticed. Figures 4.5b, 4.6a, and 4.6b show HP_E and HP_H decreasing slightly as the flare angle approaches 21 degrees. This decrease is most likely caused by the fact that the height is decreasing towards $1.7\lambda_0$ as the flare angle approaches 21 degrees (as illustrated in Figures A.25, A.27, A.29, A.31, A.33, and A.35). It can be seen from Figures 4.2a, 4.3a, and 4.3b that, as the height approaches $1.7\lambda_0$, HP_E and HP_H decrease. Looking at Figure 4.5a vs. 4.3a we notice similar results. In Figure 4.4a HP_E is approximately constant below 21 degrees, and Figure 4.3a shows that HP_E also remains approximately constant above $1.7\lambda_0$.
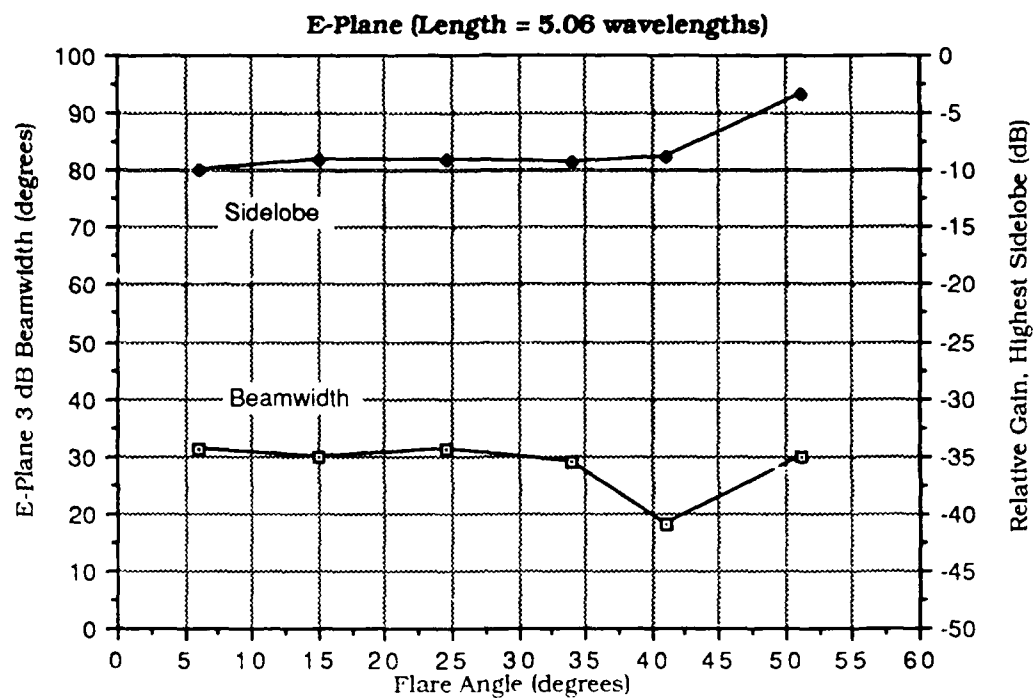
Figure 4.5a   E-Plane Effects of Changing Flare Angle - 8GHz
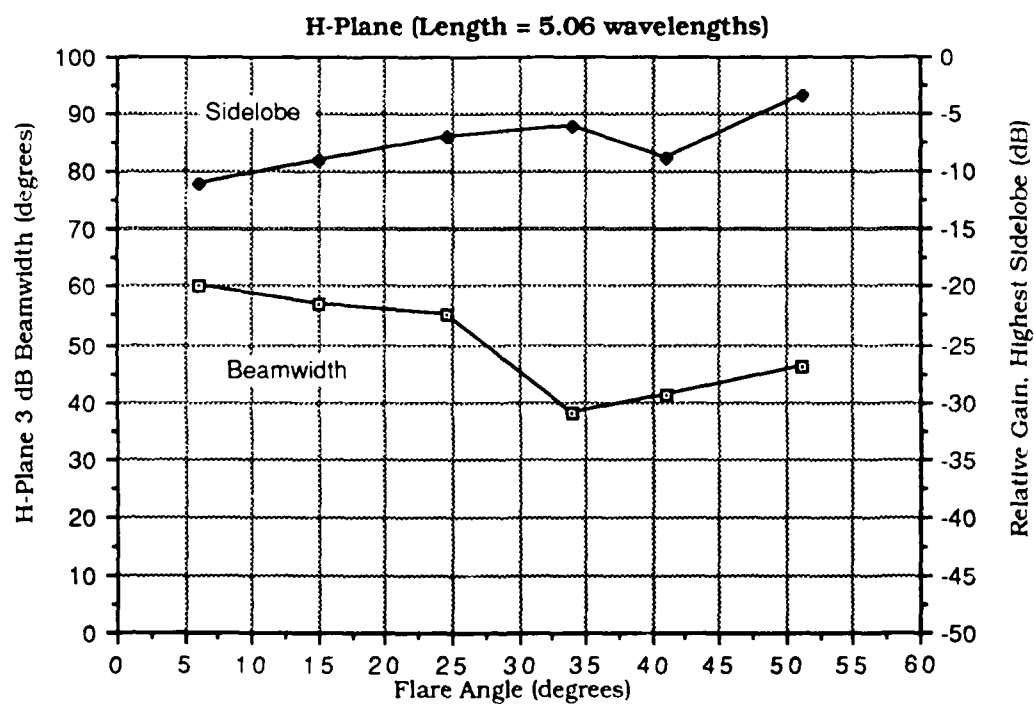
Figure 4.5b   H-Plane Effects of Flare Angle - 8GHz

46

E-Plane (Length = 6.33 wavelengths)
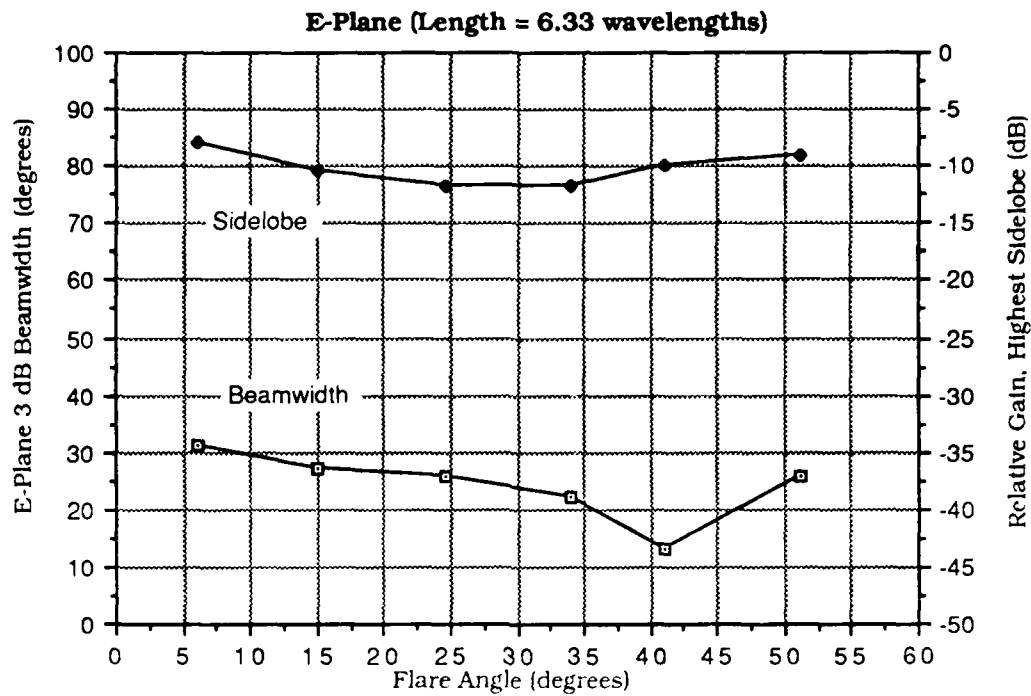
Figure 4.6a   E-Plane Effects of Changing Flare Angle - 10GHz

H-Plane (Length = 6.33 wavelengths)
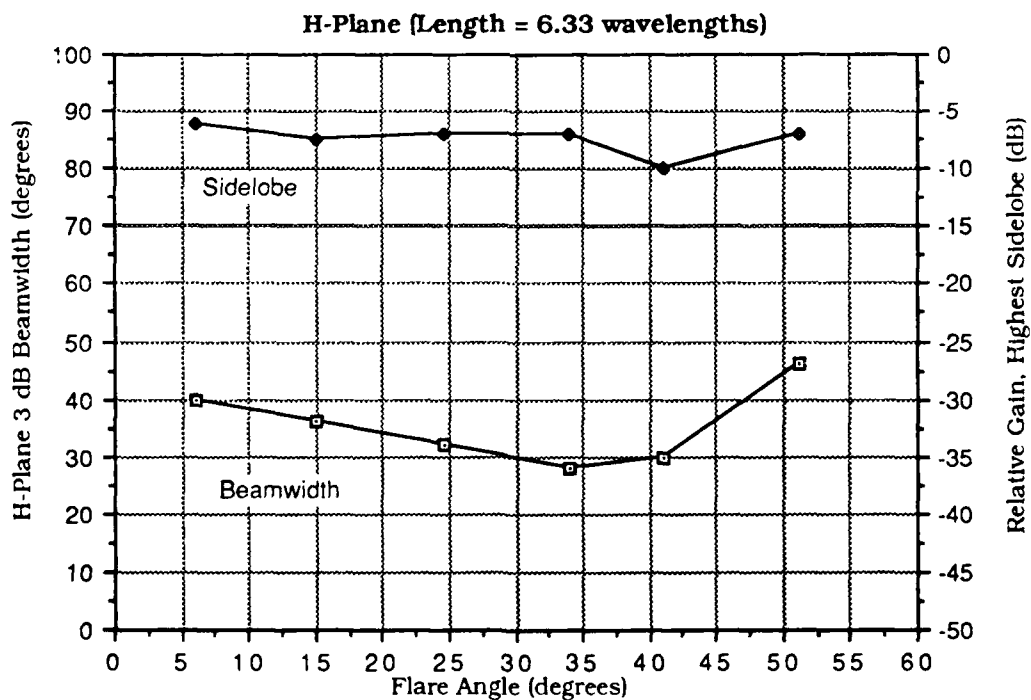
Figure 4.6b   H-Plane Effects of Changing Flare Angle - 10GHz

47

Because of the geometry of the LTSA it is not possible to keep all of the parameters constant when changing the flare angle. Thus the height and the flare angle both vary and both have an effect on the radiation pattern. Since Kelly used a rectangular geometry, he could vary the flare angle and not effect any of the other parameters. The wire model, because it maintains the shape of the LTSA, will give a more realistic approximation of the antenna, especially when the parameter changes are extreme. It can be seen from this study that the height/flare angle variable must be considered when performing a parameter analysis.

Figures A.33 through A.48 reveal that the main beam is not well formed for flare angles above 33 degrees. The data collected in this study indicates that the best-formed main beam occurs when the flare angle is under 15 degrees and the height of the LTSA is approximately between 1.1 and 1.7 wavelengths.

D. LENGTH OF THE LTSA

It has been demonstrated by earlier theory and experiment, that for LTSA lengths (L) of three to ten wavelengths, narrower beamwidths are obtained by increasing L [Ref. 3: p. 41]. The radiation patterns of an LTSA with α = 11.2 degrees without a dielectric have also been measured as a function of actual length. The results show that the LTSA without a dielectric is a traveling-wave antenna in the sense that the beamwidths approximately follow the

48

$$\frac{1}{\sqrt{L/\lambda_0}}$$ (4.2)

dependence [Ref. 1]. This theory also indicates that as the length is increased, the beamwidth will decrease.

Figure 4.7 indicates that the results obtained in this study are consistent with theory and consistent with the results obtained by Kelly [Ref. 3: p.44]. Because of the CPU run time limitation Kelly was not able to consider lengths greater than $5\lambda_0$. It can be seen from Figure 4.7 that the beamwidth at $6.33\lambda_0$ is somewhat narrower that the beamwidth at $5\lambda_0$ and thus may be the better choice to use in design of a narrow beam LTSA.

E-Plane (Height = 2.5 wavelengths)
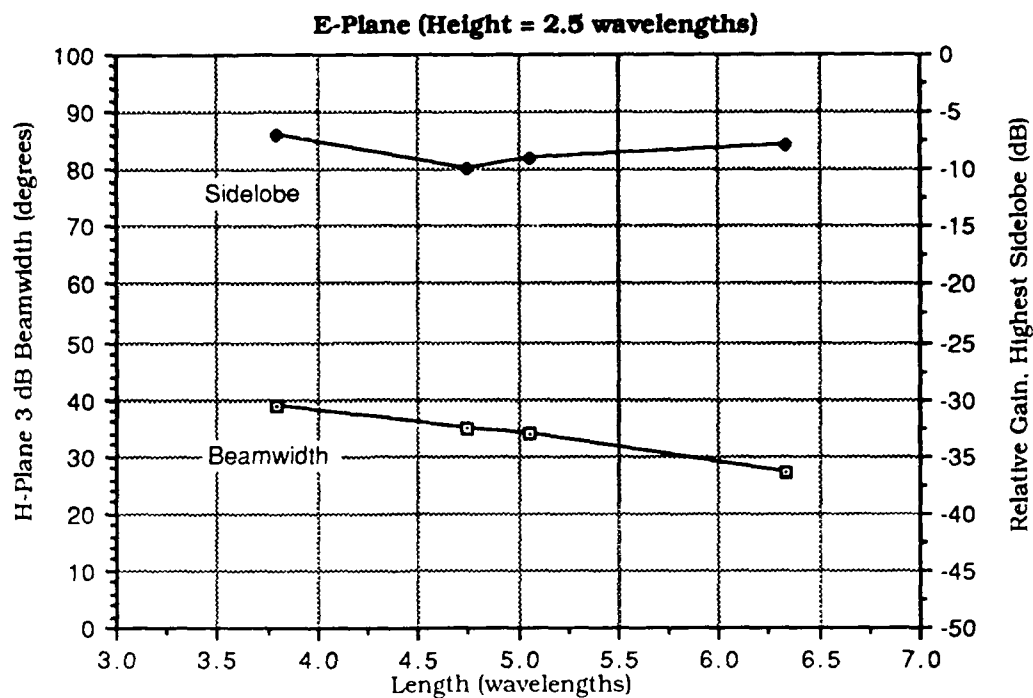
Figure 4.7a   E-Plane Effects of Changing Length - 8GHz

H-Plane (Height = 2.5 wavelengths)
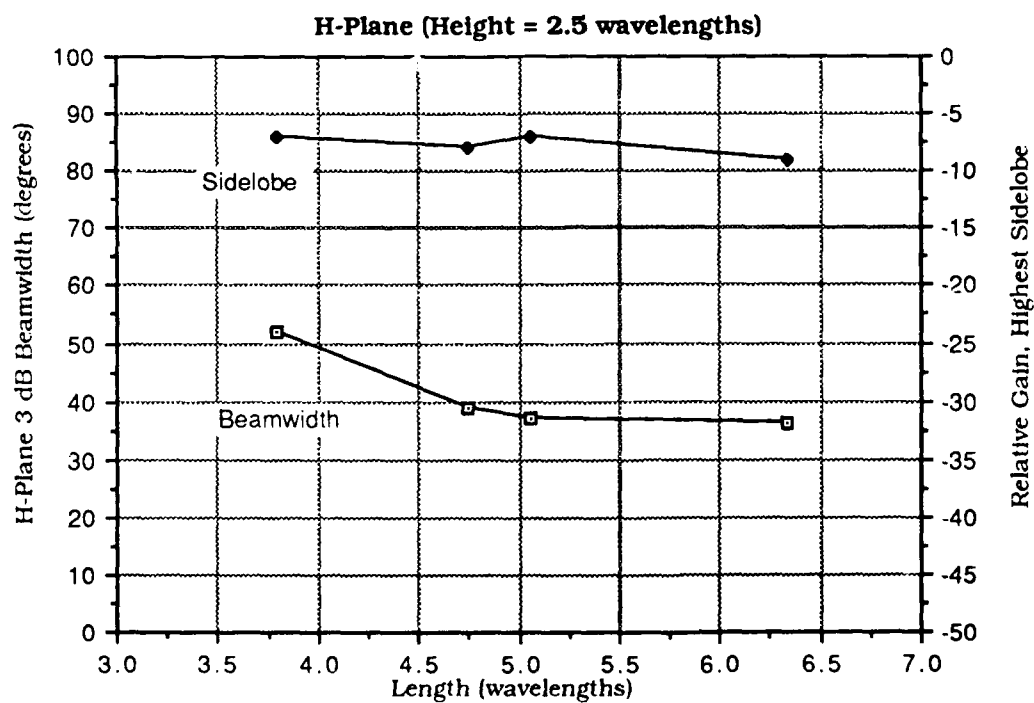
Figure 4.7b   H-Plane Effects of Changing Length - 8GHz

50

V. CONCLUSIONS

The purpose of this study was to develop a wire-grid model of the LTSA which would accurately predict its behavior while significantly reducing the CPU time required by current models. The Method of Moments as applied by NEC provided the supporting theory. By producing the numerical solution of integral equations for induced currents, the radiation patterns for wire-grid structures were obtained. The wire-grid structure was optimized through comparison with results obtained by Janaswamy's computer model and then by comparison with experimental data. Demonstrative application was provided by a parametric study of 28 LTSA designs. The results of the study proved to be consistant with known empirical data. Thus, it has been shown that the wire-grid method of modeling the LTSA is an effective and efficient tool for design.

The conclusions that can be drawn from the parametric study are as follows:

- The length of the LTSA should be determined by the desired directivity of the antenna.

- For a given length, there will be a range of optimum height/flare angle combinations.

This study will enhance future development of the LTSA. Since the air dielectric was the only case considered in this study, the next step is to use the wire-grid method to model the LTSA with a dielectric substrate. An approximate method of treating the dielectric

51

is by the use of impedance boundary conditions. Further study could also include different types of endfire slot antennas such as the exponentially tapered Vivaldi antenna or the Constant Width Slot Antenna (CWSA). The exponential taper could be approximated by a series of short wire segments offset at slightly different angles. The efficiency of the model presented in this work may serve to motivate designers to work more extensively with the LTSA. Also, the success experienced in using the wire model method in this study may prove to be valuable in the study of other types of antennas.

APPENDIX A

LTSA GEOMETRIES AND RADIATION PATTERNS

The LTSA geometries and associated radiation patterns used in the parametric analysis are outlined in this appendix. The odd numbered figures show the geometry and the even numbered figures show the radiation pattern. The analysis begins with the reference parameters as indicated in Table 4.1 and illustrated in Figures A.1 and A.2. Figures A.3 through A.24 illustrate the details of the height parameter analysis. Figures A.25 through A.48 illustrate the details of the flare angle parameter analysis. Figures A.49 through A.56 illustrate the details of the length parameter analysis.

LTSA 1 - 8 GHz
λ = 3.75 cm
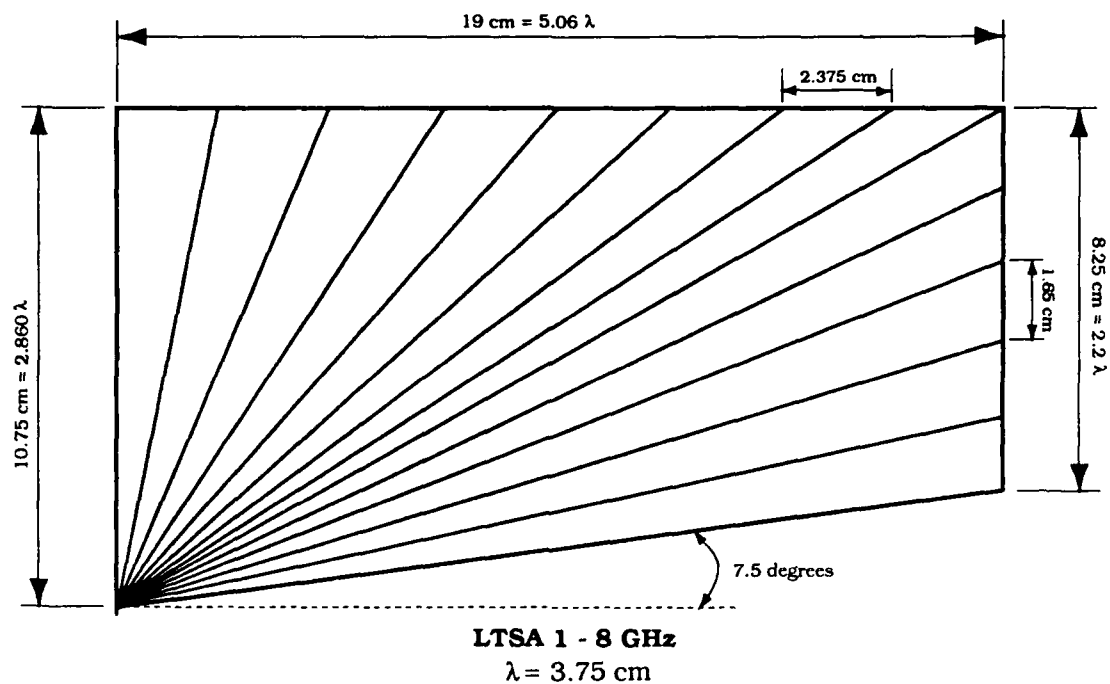
Figure A.1   LTSA Geometry Modeled After Emphirical Design - 8GHz

LTSA 1 - 8 GHz
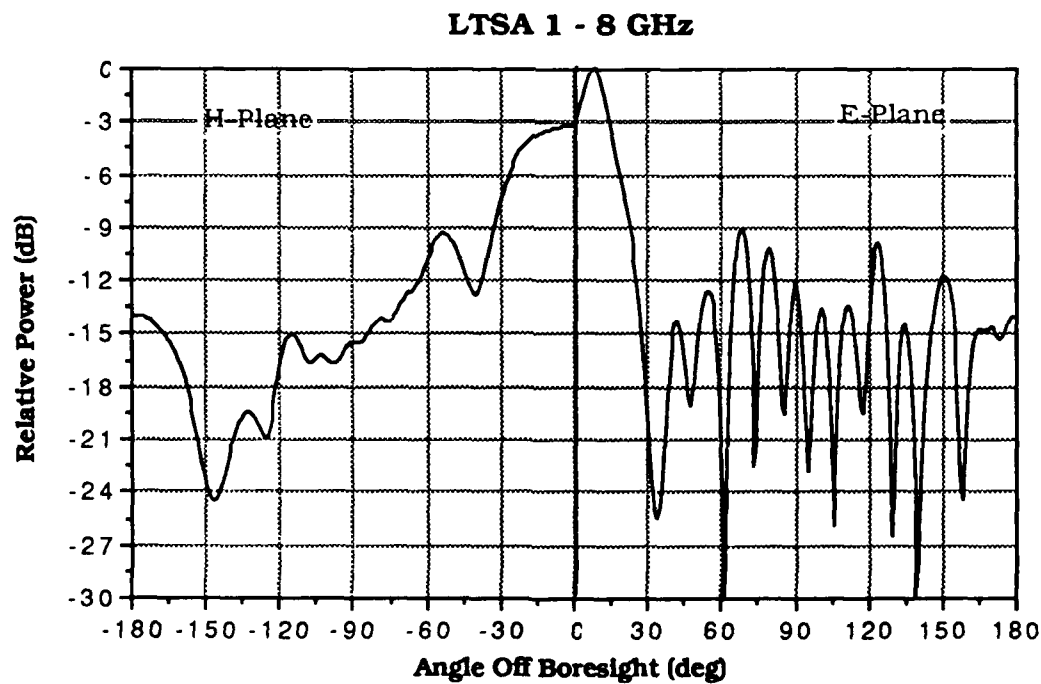
Figure A.2   Predicted Radiation Patterns for Emphirical Design - 8GHz

54

19 cm = 6.33 λ

2.375 cm

10.75 cm = 3.583λ

8.25 cm = 2.75 λ

1.65 cm

7.5 degrees

LTSA 1 - 10 GHz
λ = 3.00 cm
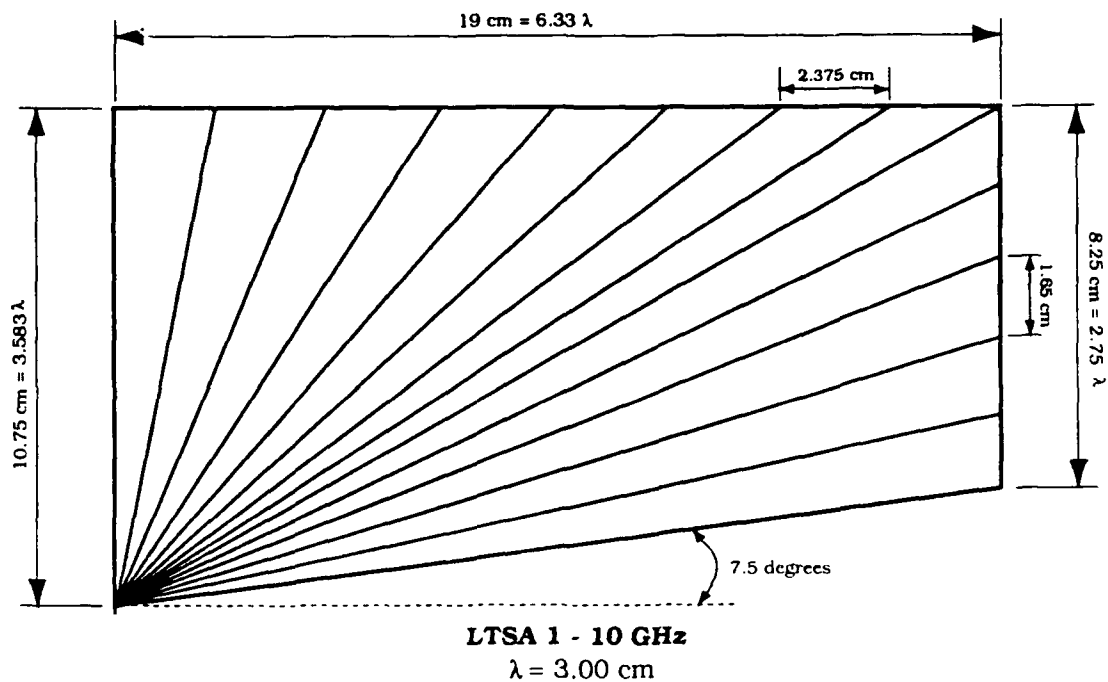
Figure A.3   LTSA Geometry Modeled After Emphirical Design - 10GHz

LTSA 1 - 10 GHz

H-Plane

E-Plane

Relative Power (dB)

Angle Off Boresight (deg)
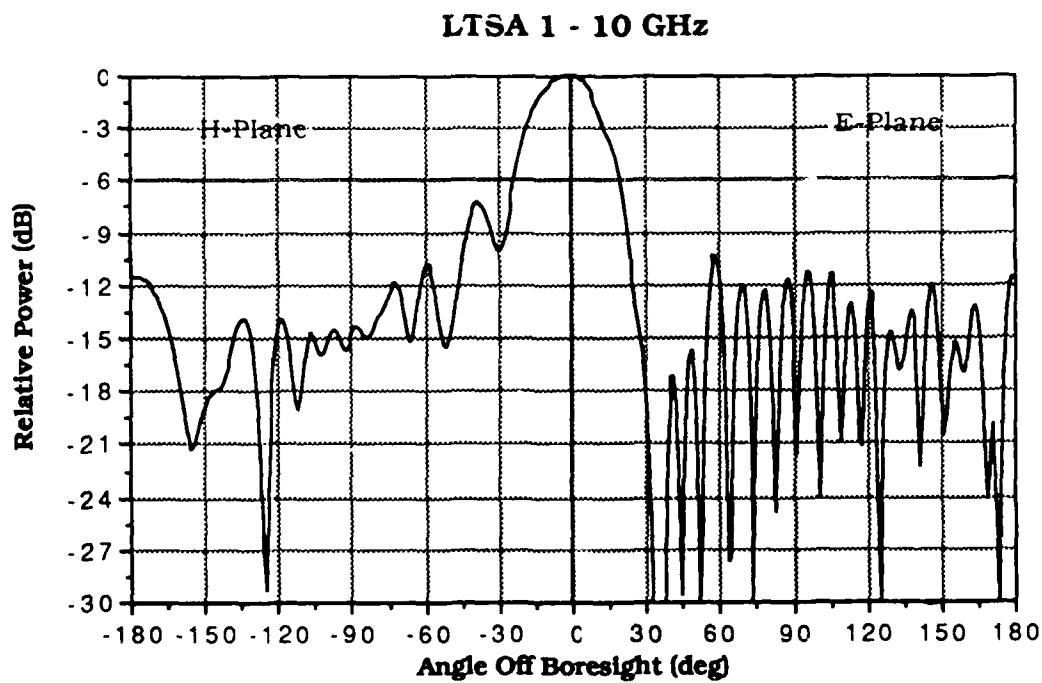
Figure A.4   Predicted Radiation Patterns for Emphirical Design - 10GHz

55
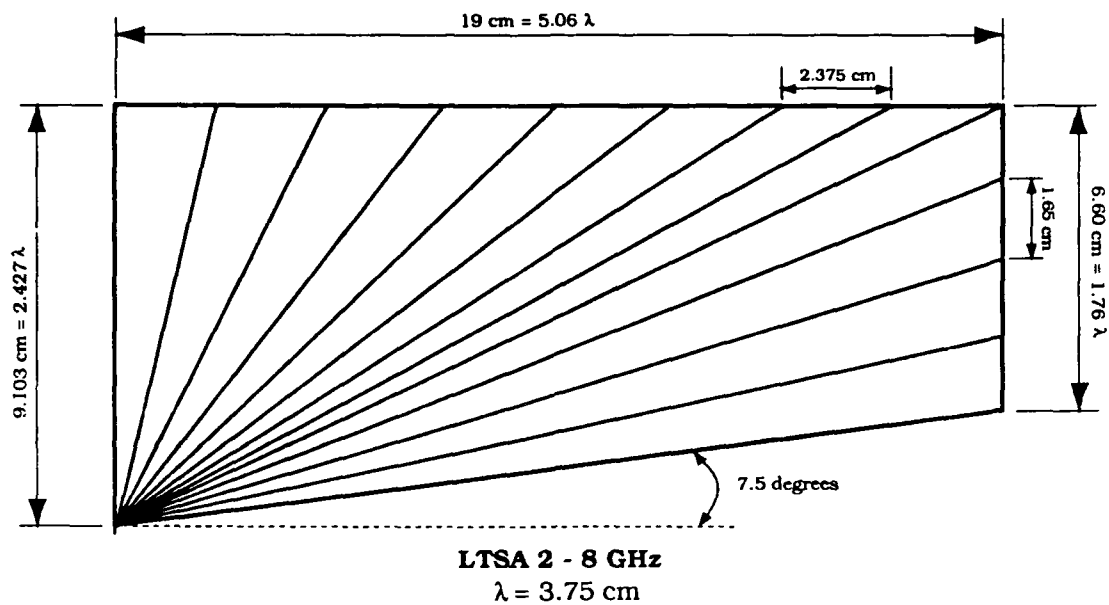
Figure A.5 LTSA Geometry Decreasing Height to 1.76λo - 8GHz

LTSA 2 - 8 GHz
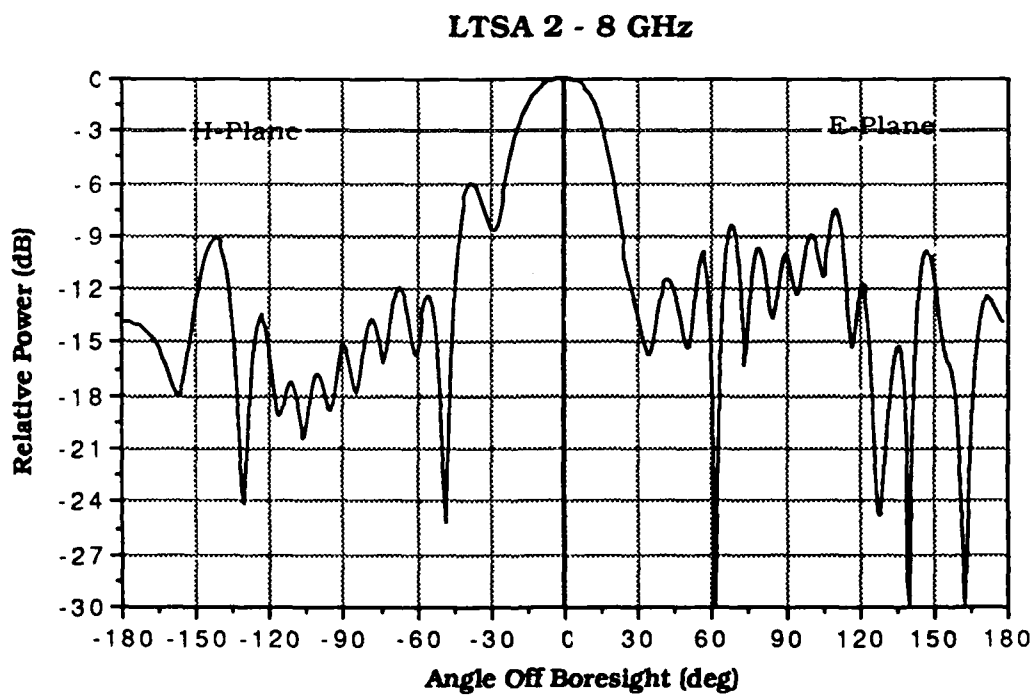
Figure A.6   Effects of Decreasing Height to 1.76λo - 8GHz

56

19 cm = 6.33 λ

2.375 cm

6.60 cm = 2.20 λ

1.65 cm

9.103 cm = 3.034 λ

7.5 degrees

LTSA 2 - 10 GHz

λ = 3.00 cm
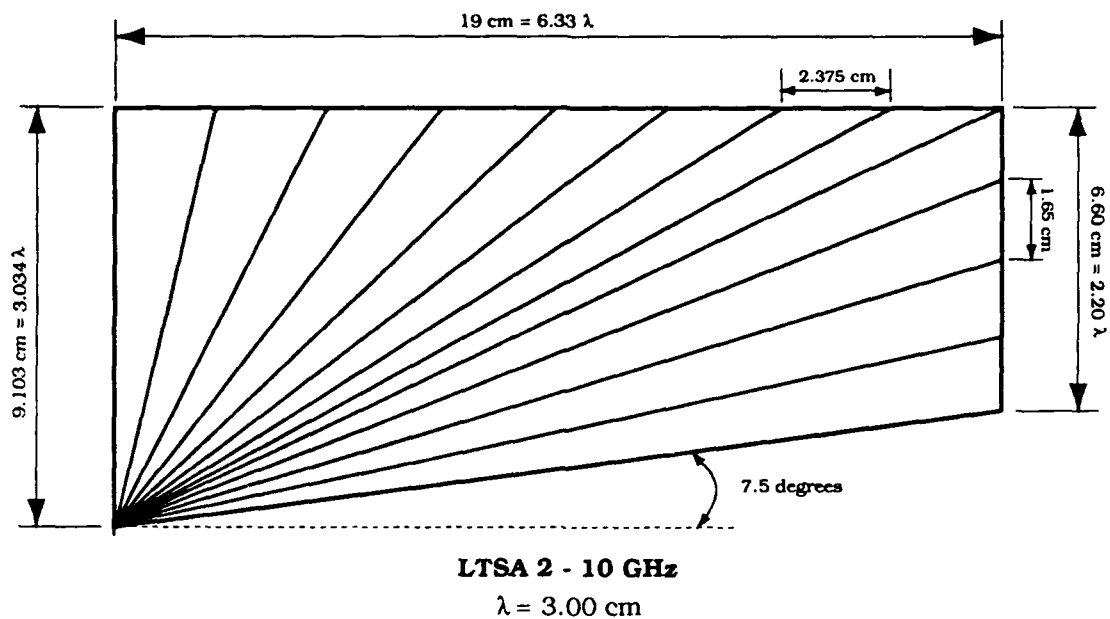
Figure A.7   LTSA Geometry Decreasing Height to 2.20λo - 10GHz

LTSA 2 - 10 GHz

H-Plane

E-Plane

Relative Power (dB)

Angle Off Boresight (deg)
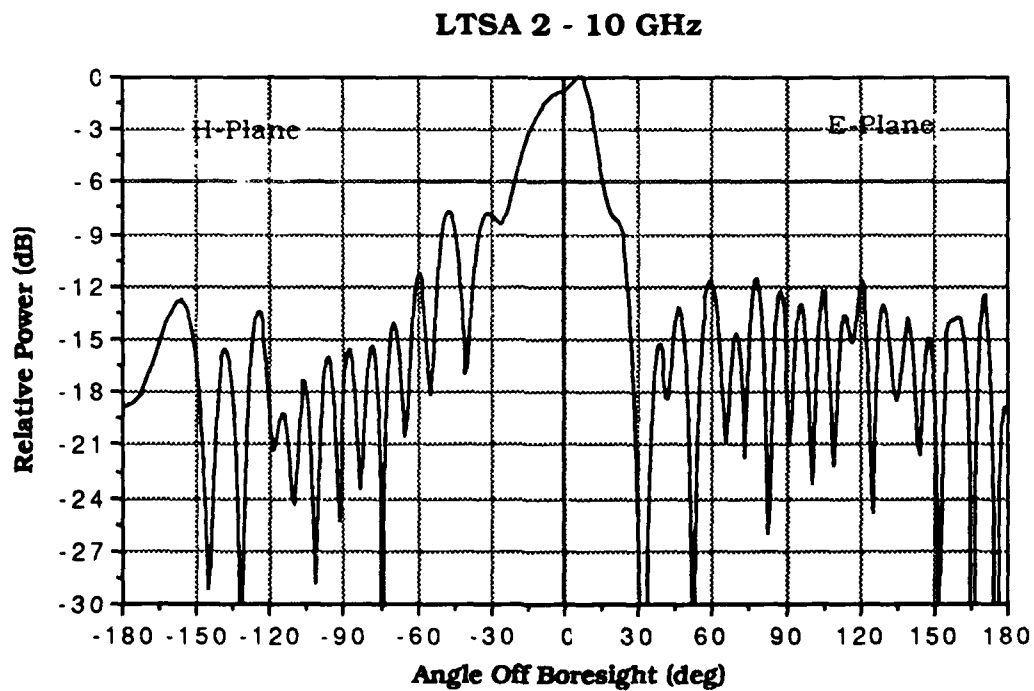
Figure A.8   Effects of Decreasing Height to 2.20λo - 10GHz

57

19 cm = 5.06 λ

2.375 cm

1.85 cm

4.95 cm = 1.32 λ

7.465 cm = 1.988 λ

7.5 degrees
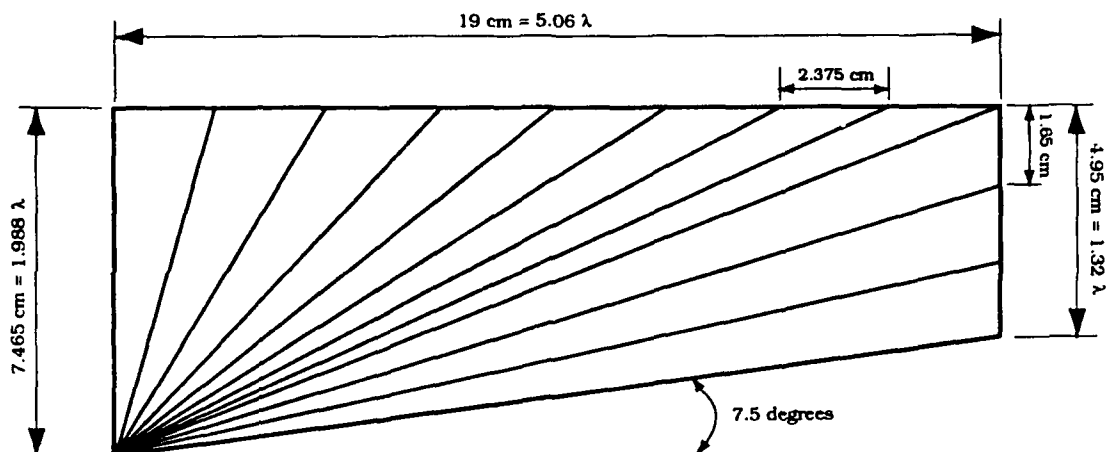
LTSA 3 - 8 GHz
λ = 3.75 cm

Figure A.9   LTSA Geometry Decreasing Height to 1.32λo - 8GHz

LTSA 3 - 8 GHz

H-Plane

E-Plane

Relative Power (dB)

Angle Off Boresight (deg)
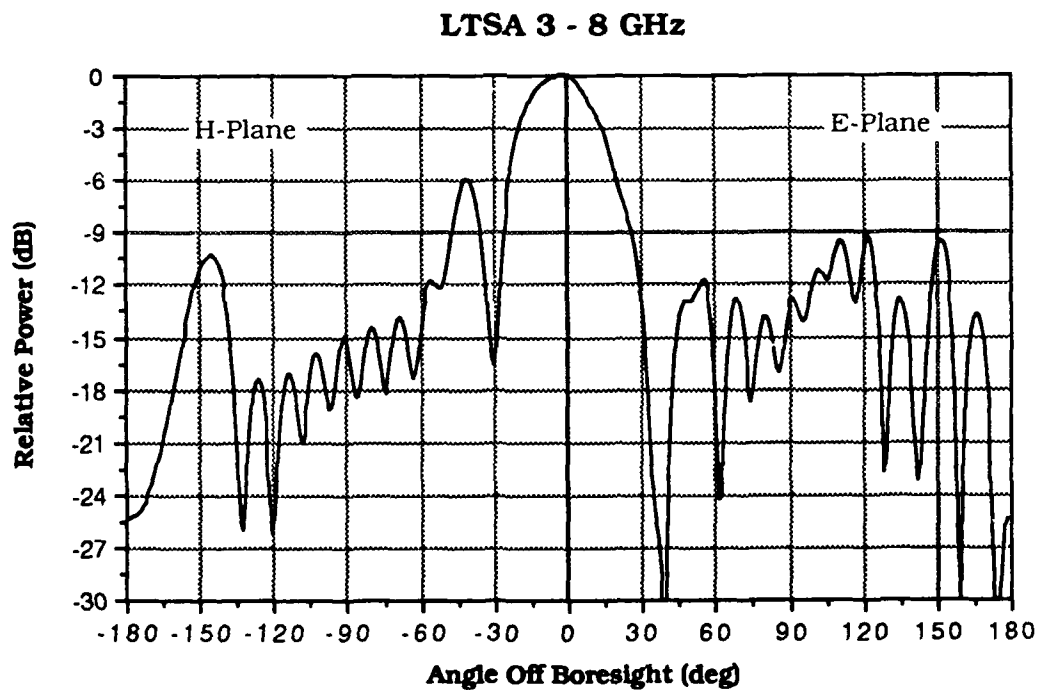
Figure A.10   Effects of Decreasing Height to 1.32λo - 8GHz

58

LTSA 3 - 10 GHz
λ = 3.00 cm
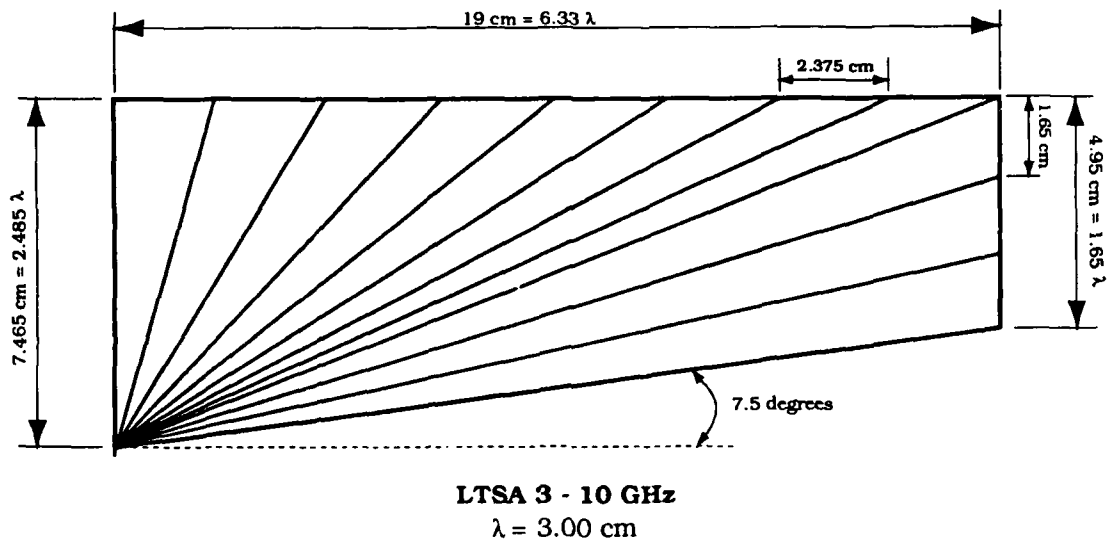
Figure A.11   LTSA Geometry Decreasing Height to 1.65λo - 10GHz
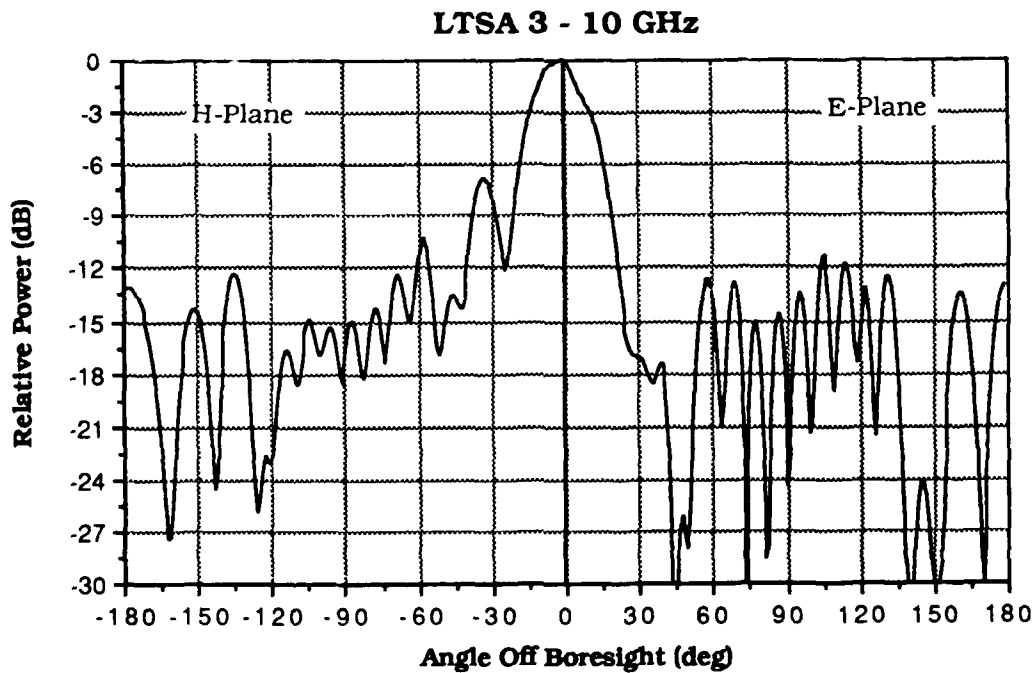
Figure A.12   Effects of Decreasing Height to 1.65λo - 10GHz

59

LTSA 4 - 10 GHz
λ = 3.00 cm
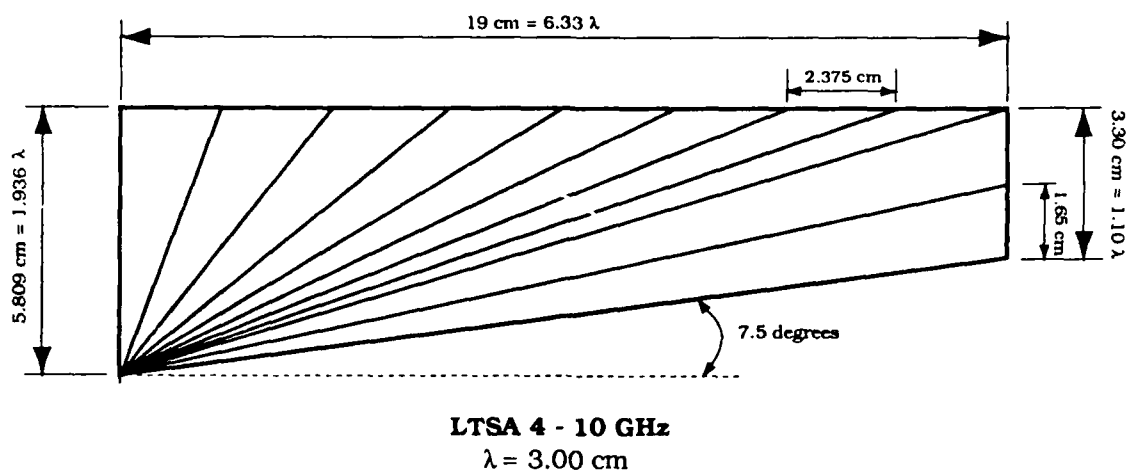
Figure A.13   LTSA Geometry Decreasing Height to 0.88λo - 8GHz

LTSA 4 - 8 GHz
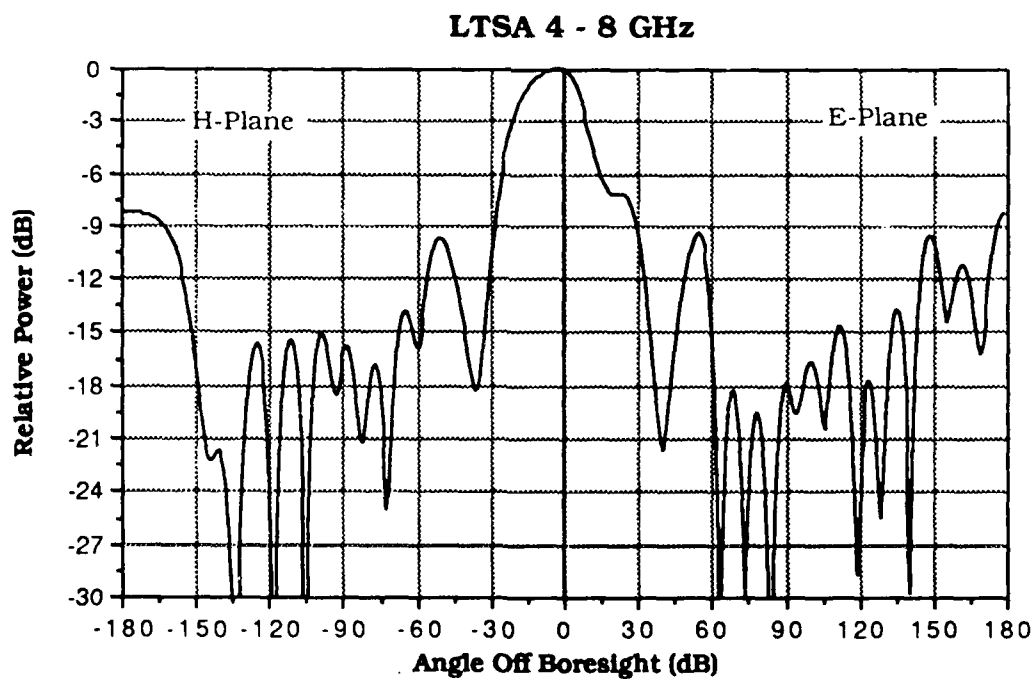
Figure A.14   Effects of Decreasing Height to 0.88λo - 8GHz

60

19 cm = 6.33 λ

2.375 cm

5.809 cm = 1.936 λ

3.30 cm = 1.10 λ

1.65 cm

7.5 degrees

LTSA 4 - 10 GHz
λ = 3.00 cm
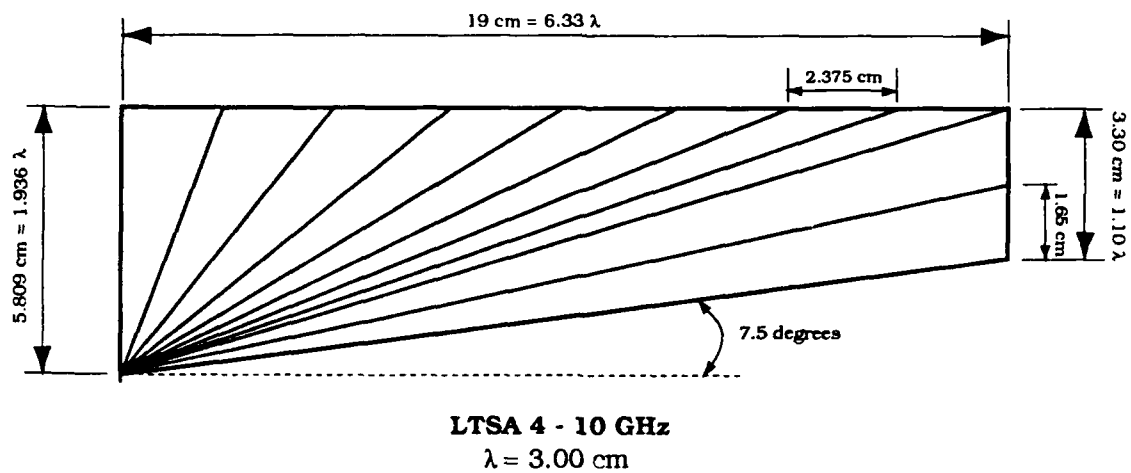
Figure A.15   LTSA Geometry Decreasing Height to 1.10λo - 10GHz

LTSA 4 - 10 GHz

H-Plane

E-Plane

Relative Power (dB)

Angle Off Boresight (deg)
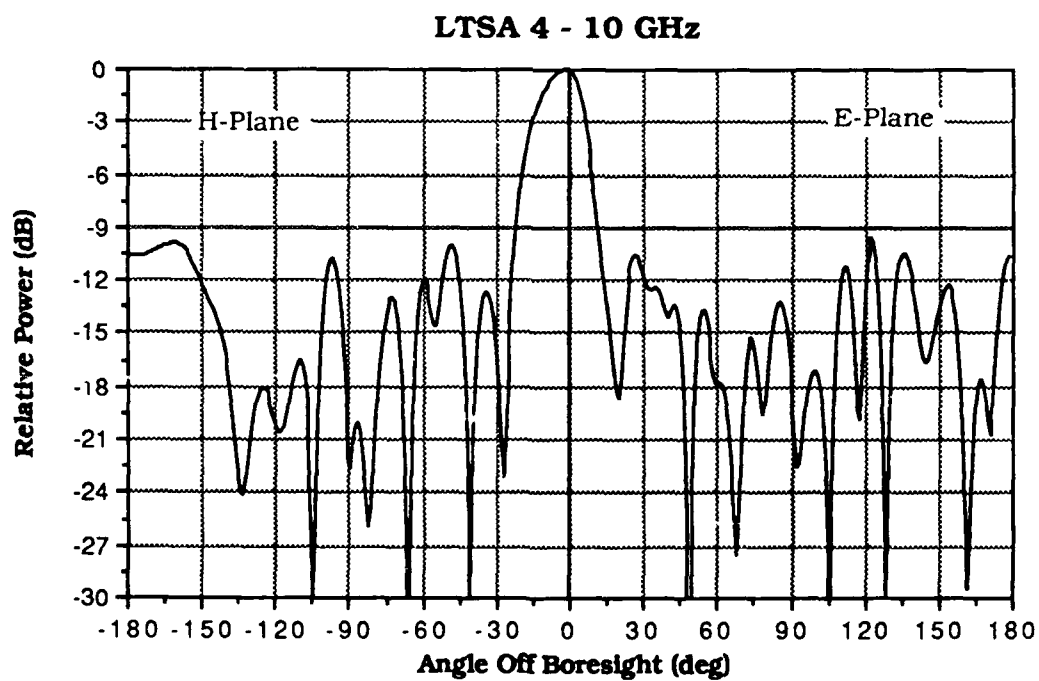
Figure A.16   Effects of Decreasing Height to 1.10λo - 10GHz

61

19 cm = 5.06 λ

2.375 cm

4.162 cm = 1.109 λ

1.65 cm = 0.47 λ

1.65 cm

7.5 degrees

LTSA 5 - 8 GHz

λ = 3.75 cm
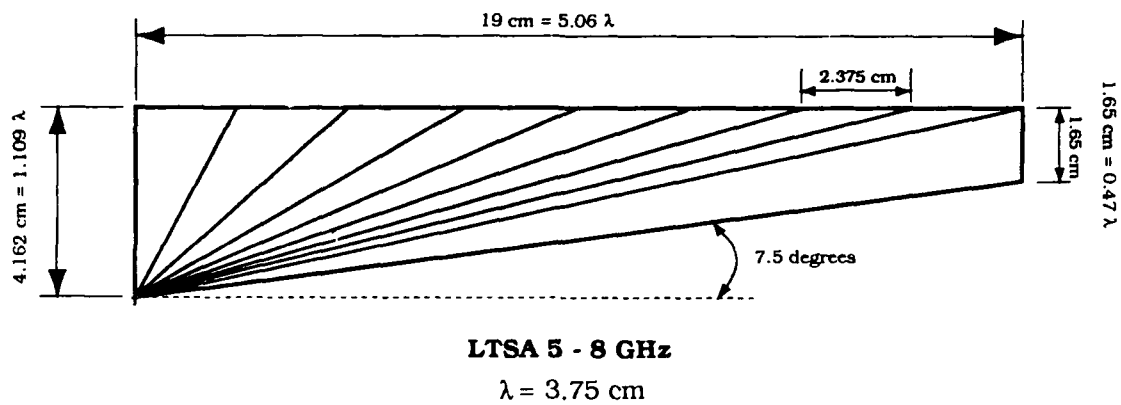
Figure A.17   LTSA Geometry Decreasing Height to 0.44λo - 8GHz

LTSA 5 - 8 GHz

H-Plane

E-Plane

Relative Power (dB)

Angle Off Boresight (deg)
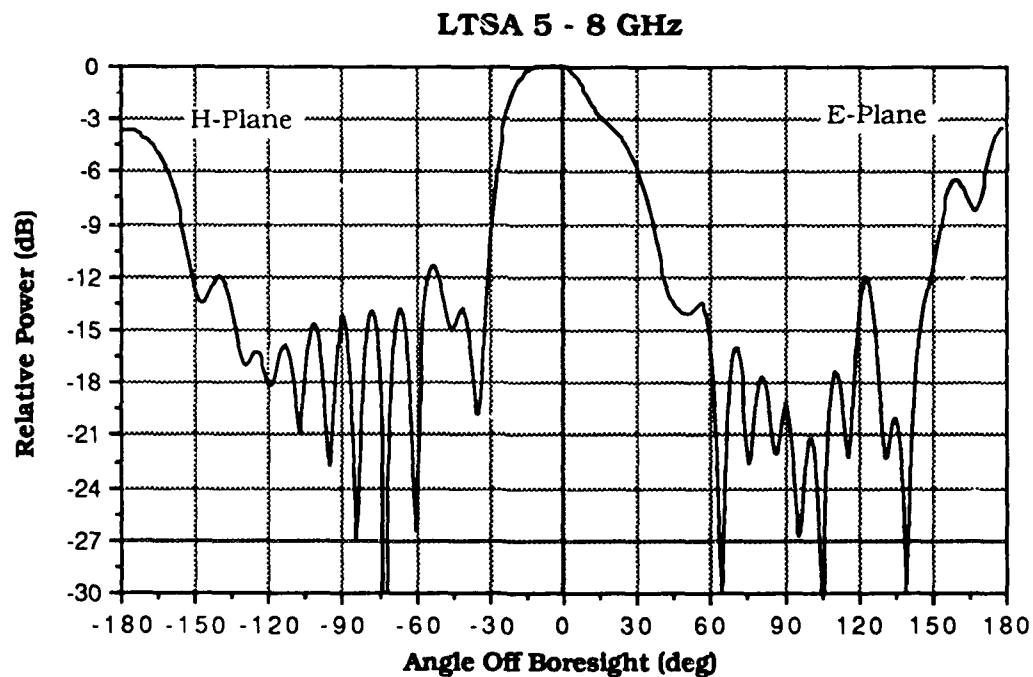
Figure A.18   Effects of Decreasing Height to 0.44λo - 8GHz

62

LTSA 5 - 10 GHz
$\lambda = 3.00$ cm
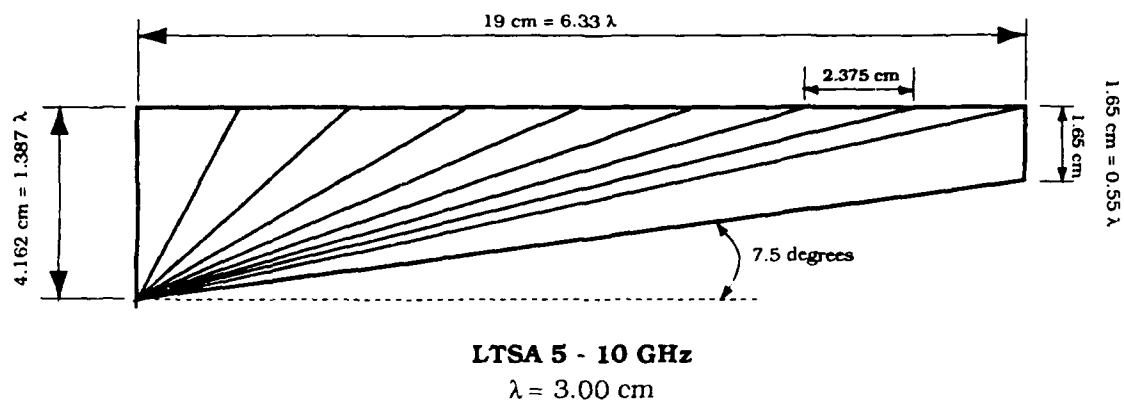
Figure A.19   LTSA Geometry Decreasing Height to $0.55\lambda o$ - 10GHz
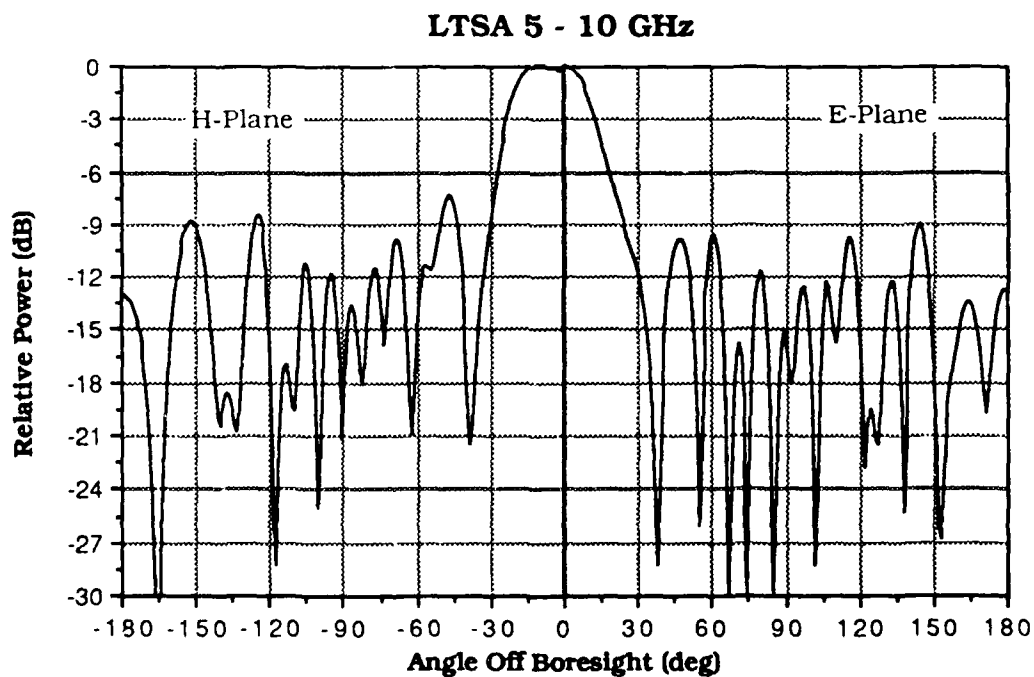
Figure A.20   Effects of Decreasing Height to $0.55\lambda o$ - 10GHz

19 cm = 5.06 λ

2.375 cm

2.515 cm = .67 λ

7.5 degrees

LTSA 6 - 8 GHz

λ ≈ 3.75 cm
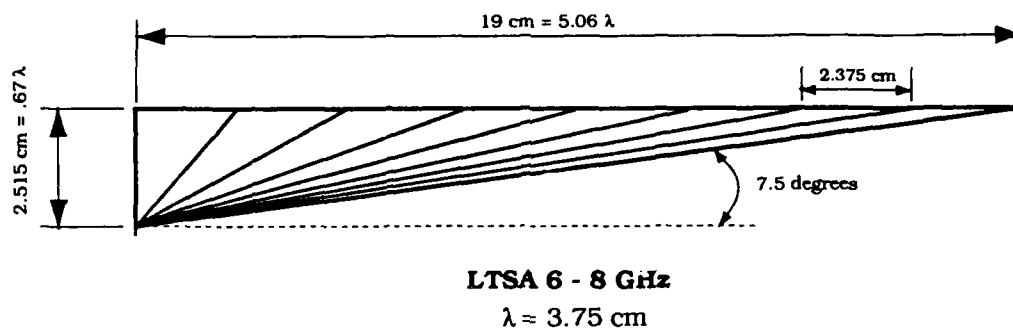
Figure A.21   LTSA Geometry Decreasing Height to 0.0λo - 8GHz

LTSA 6 - 8 GHz

H-Plane

E-Plane

Relative Power (dB)

Angle Off Boresight (deg)
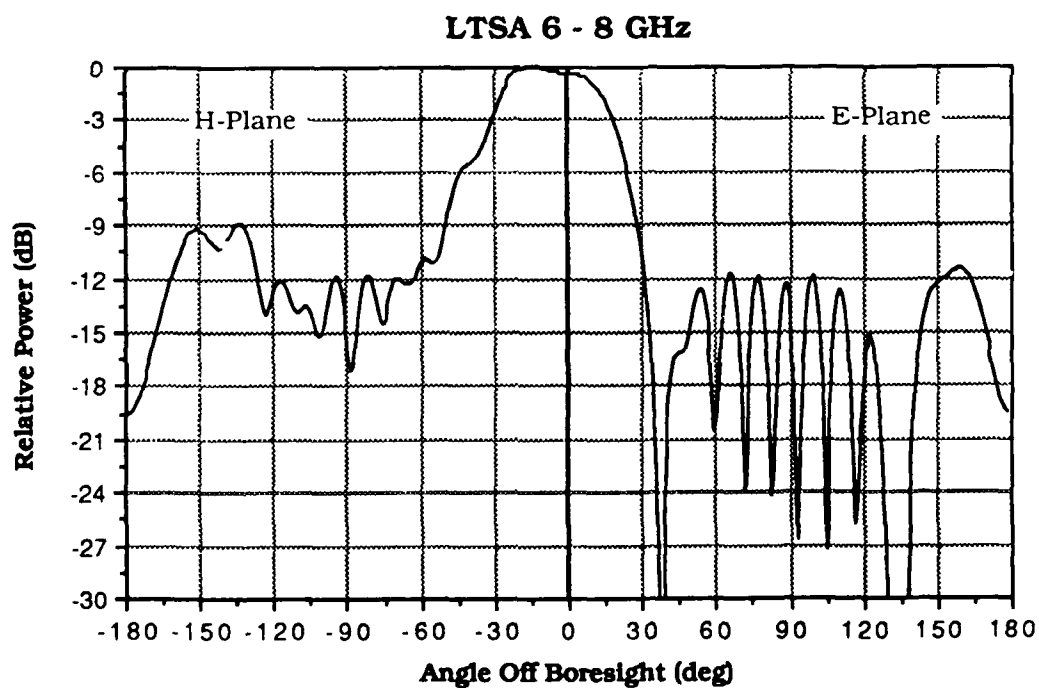
Figure A.22   Effects of Decreasing Height to 0.0λo - 8GHz

64
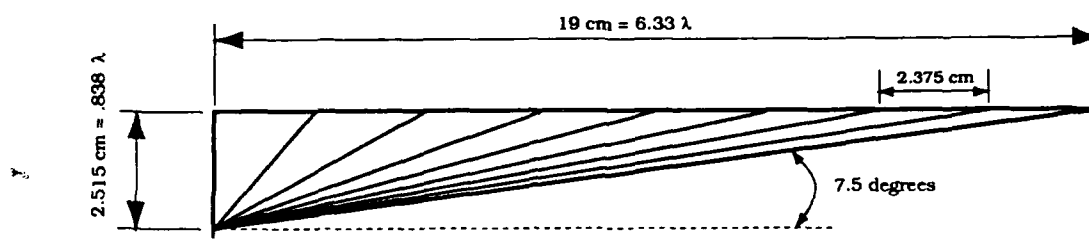
LTSA 6 - 10 GHz

$\lambda = 3.00$ cm

Figure A.23 LTSA Geometry Decreasing Height to 0.0λo - 10GHz
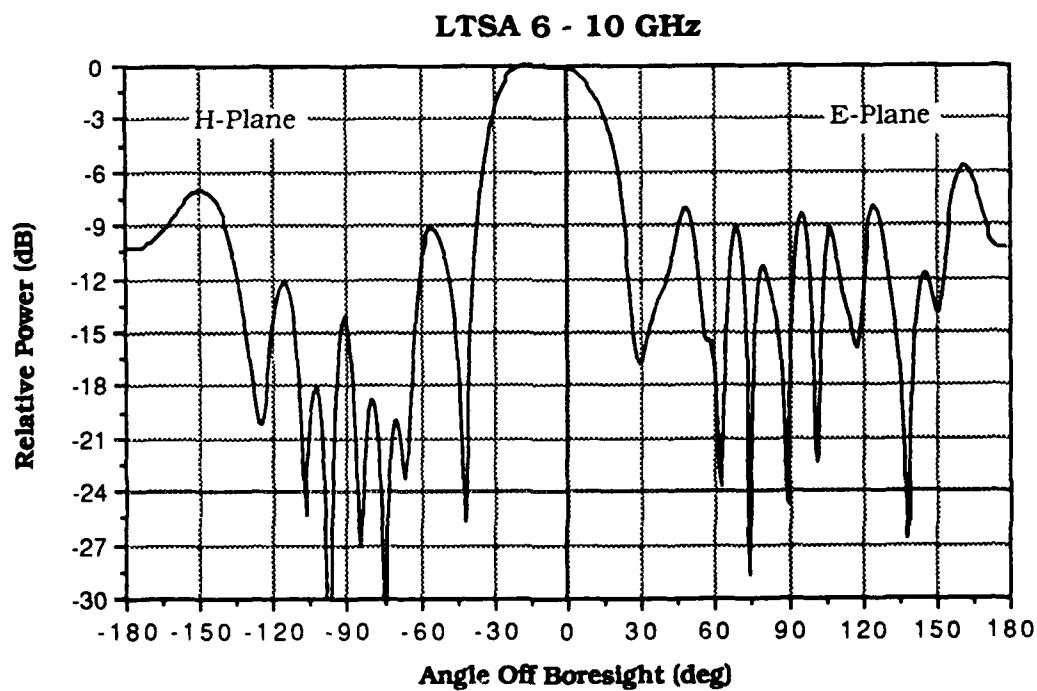
Figure A.24 Effects of Decreasing Height to 0.0λo - 10GHz

65

19 cm = 5.06 λ

2.375 cm

10.75 cm = 2.860 λ

9.9 cm = 2.64 λ

1.65 cm

3 degrees

LTSA 7 - 8 GHz
λ = 3.75 cm
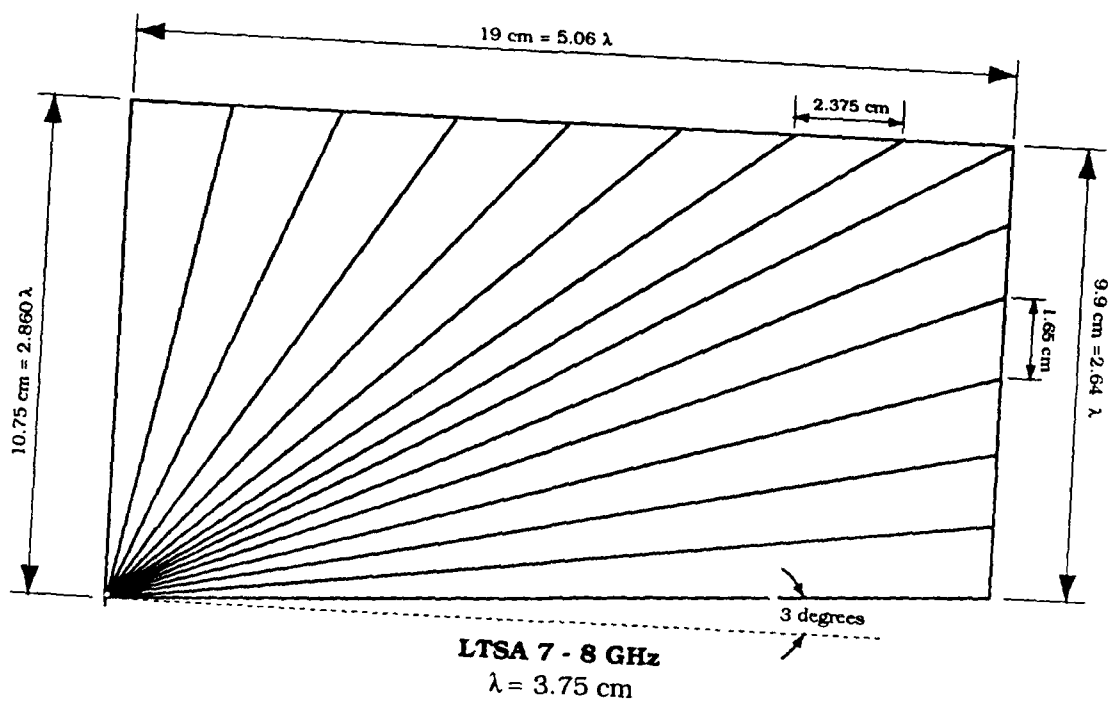
Figure A.25   LTSA Geometry with Flare Angle = 6 degrees - 8GHz

LTSA 7 - 8 GHz

H-Plane

E-Plane

Relative Gain (dB)

Angle Off Boresight (degrees)
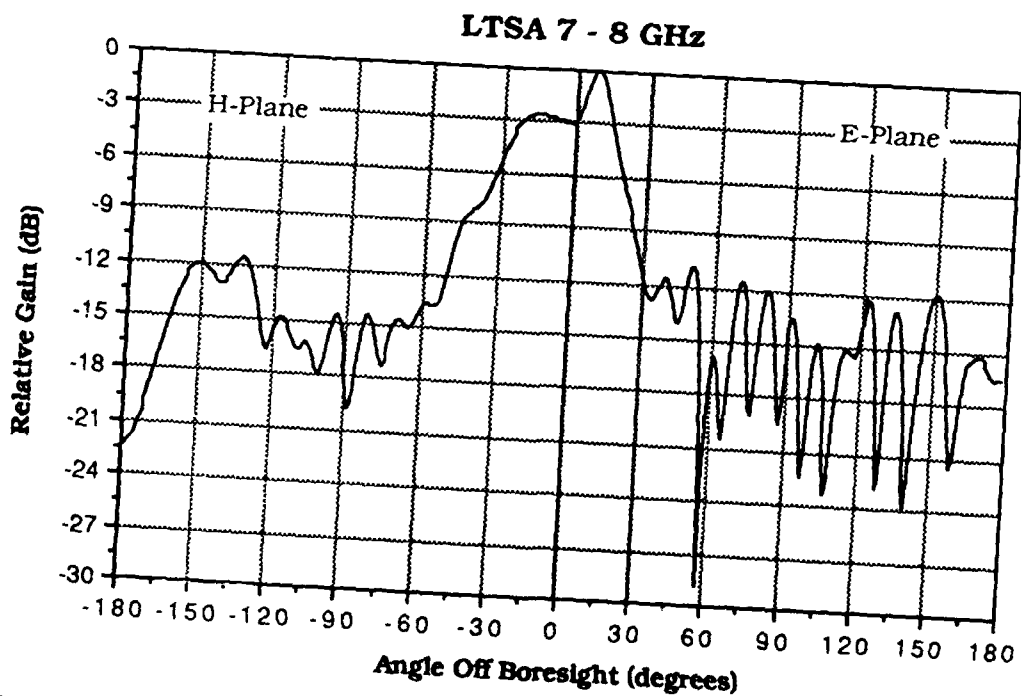
Figure A.26   Effects of Changing Flare Angle to 6 degrees - 8GHz

66

19 cm = 6.33 λ

2.375 cm

10.75 cm = 3.583 λ

9.90 cm = 3.3 λ

1.65 cm

3 degrees

LTSA 7 - 10 GHz

λ = 3.00 cm
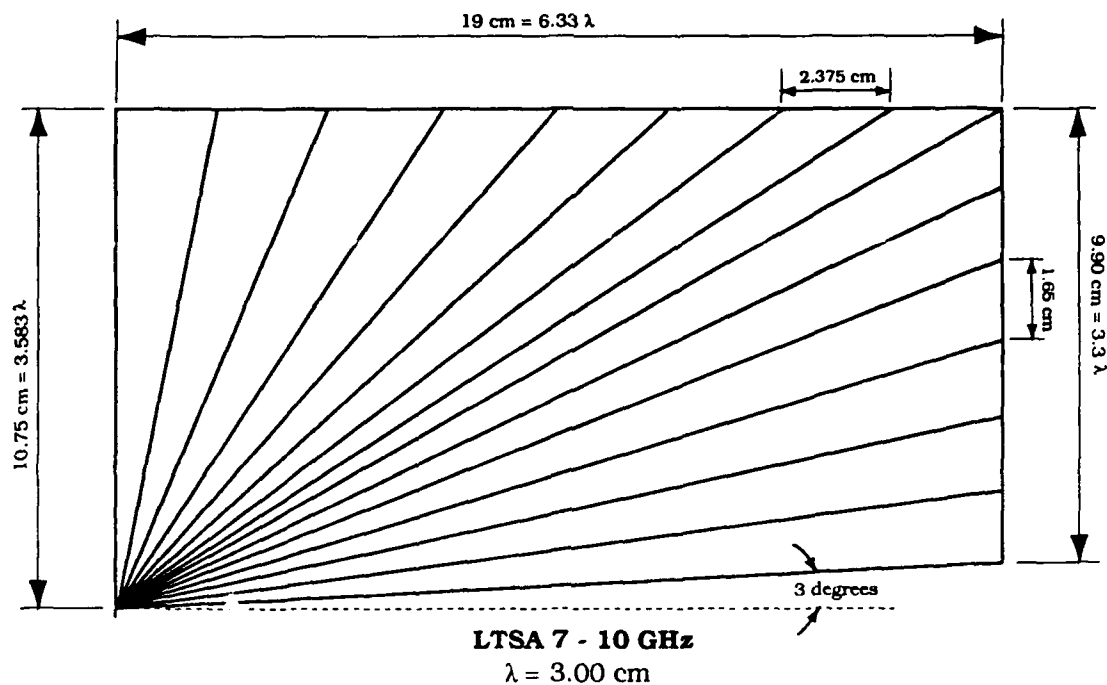
Figure A.27   LTSA Geometry with Flare Angle = 6 degrees - 10GHz

LTSA 7 - 10 GHz

H-Plane

E-Plane

Relative Power (dB)

Angle Off Boresight (deg)
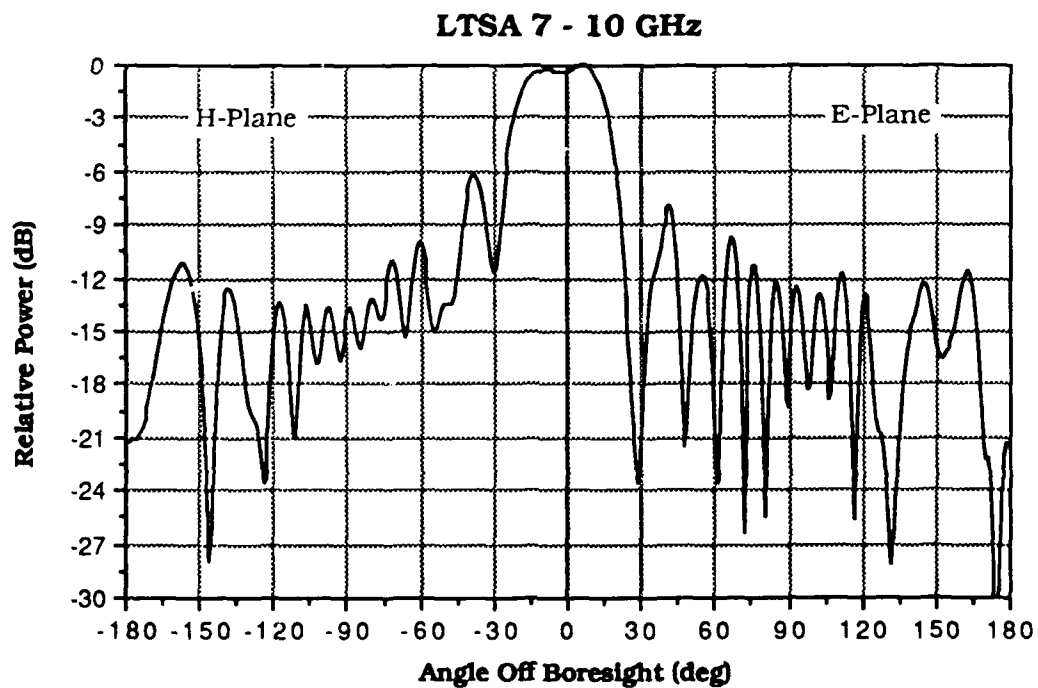
Figure A.28   Effects of Changing Flare Angle to 6 degrees - 10GHz

67

19 cm = 5.06 λ

2.375 cm

10.75 cm = 3.071 λ

6.60 cm = 1.76 λ

1.65 cm

12.36 degrees

LTSA 8 - 8 GHz
λ ≈ 3.75 cm
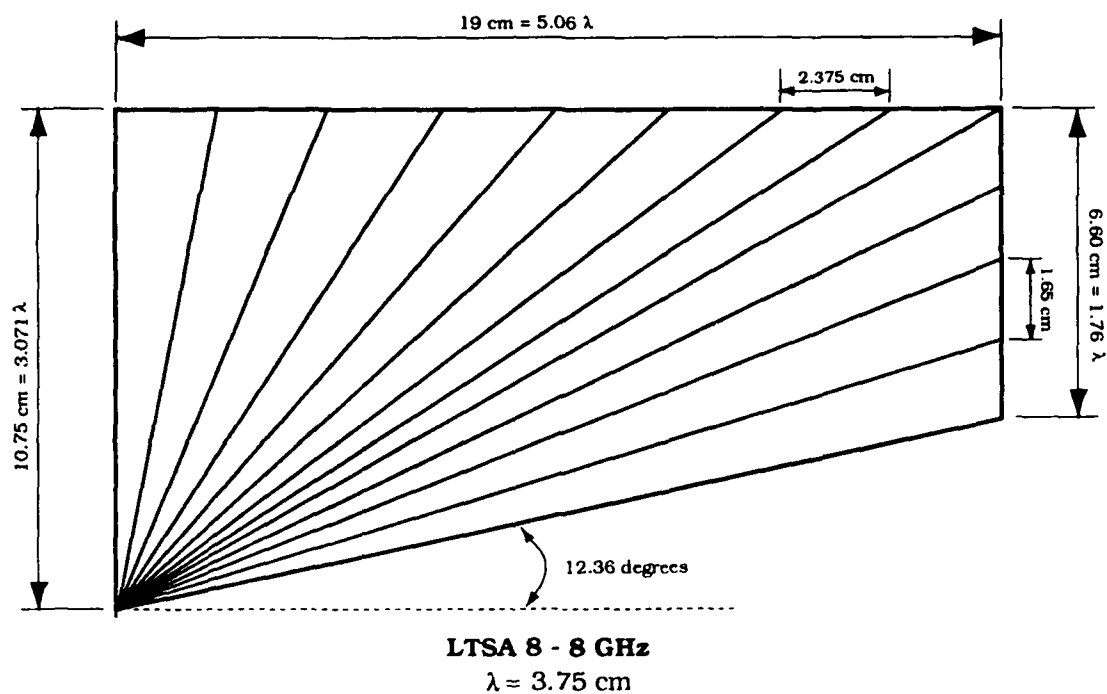
Figure A.29   LTSA Geometry with Flare Angle =24.72 degrees - 8GHz

LTSA 8 - 8 GHz
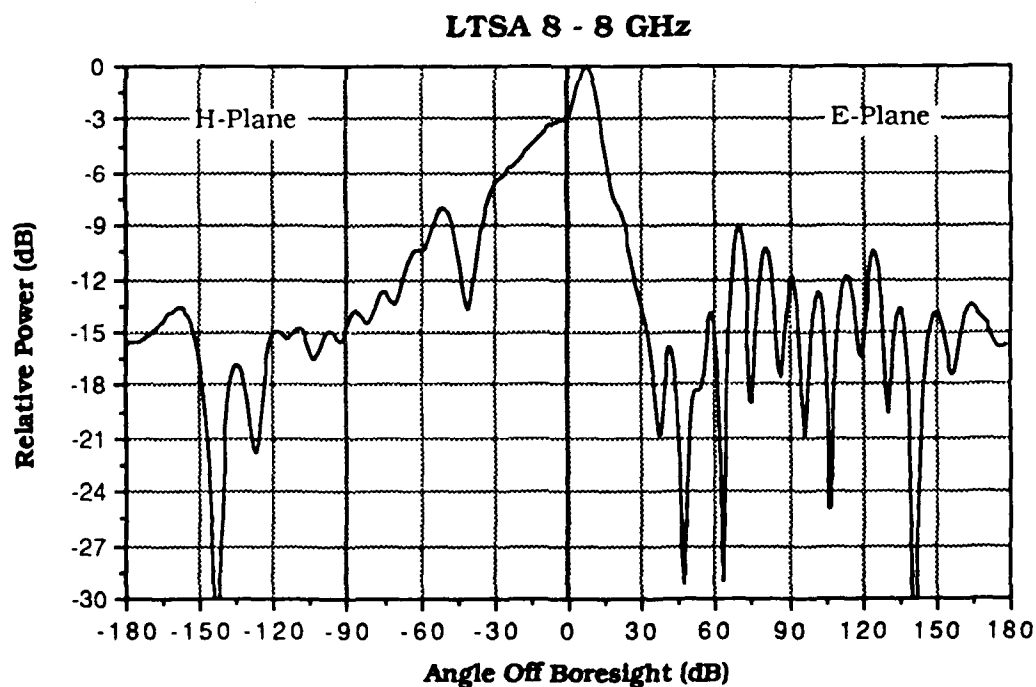
Figure A.30   Effects of Changing Flare Angle to 24.72 degrees - 8GHz
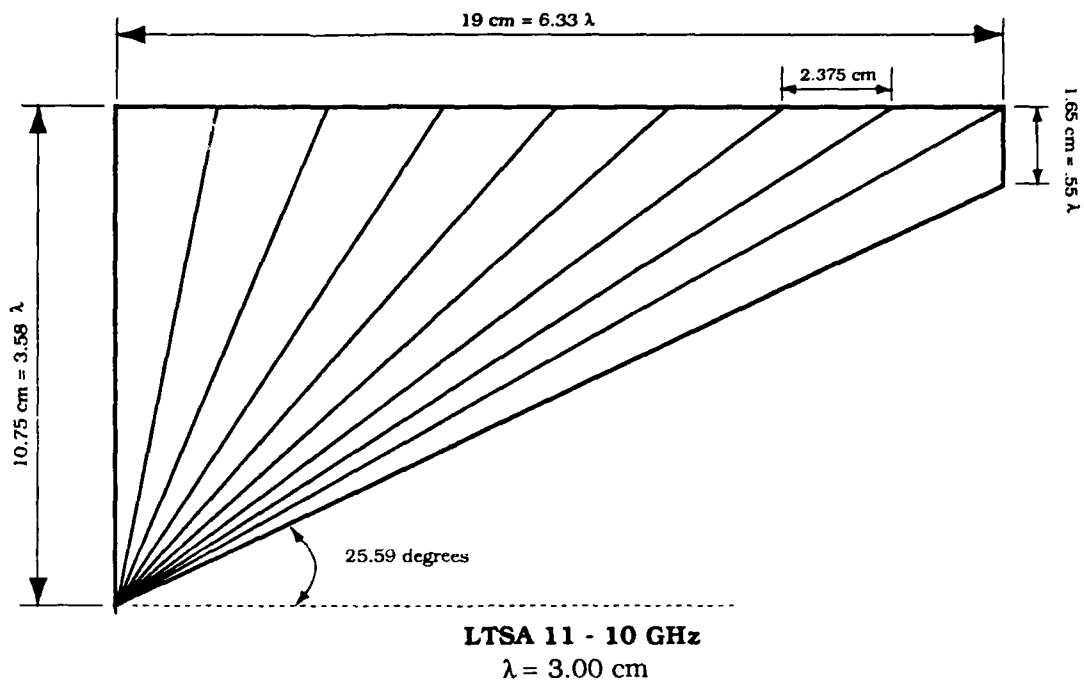
68

LTSA 8 - 10 GHz
$\lambda = 3.00$ cm
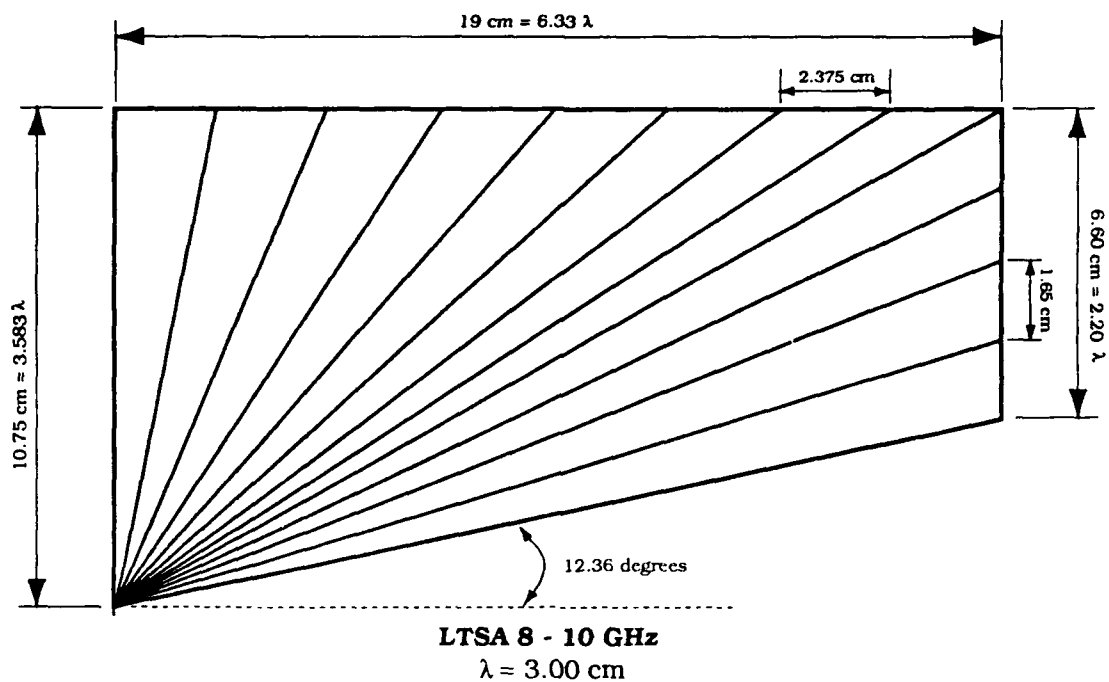
Figure A.31   LTSA Geometry with Flare Angle = 24.72 degrees - 10GHz
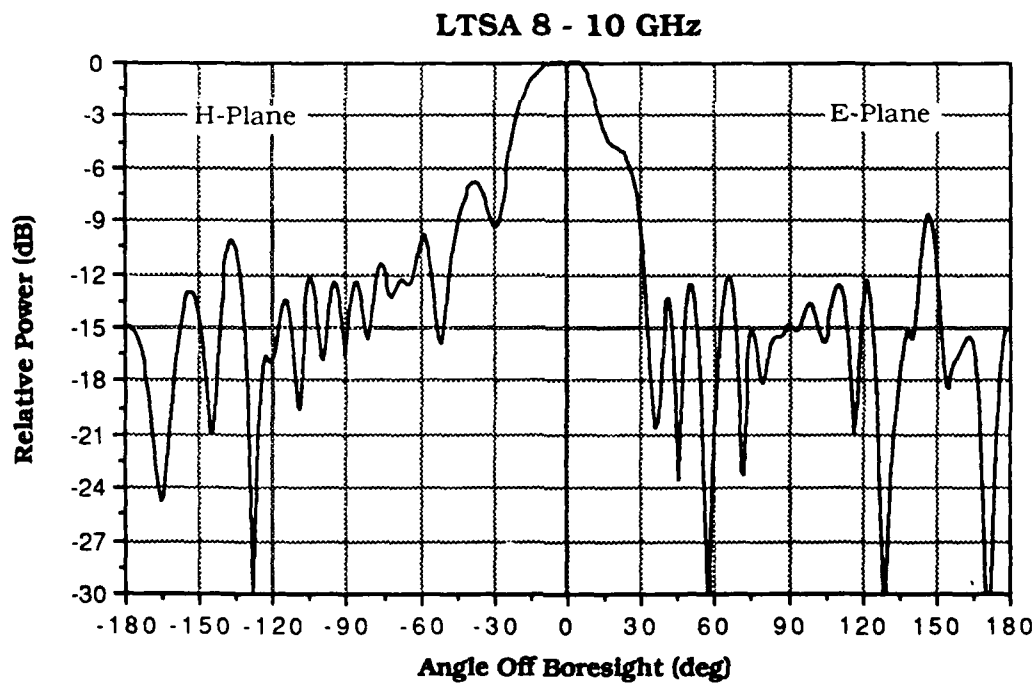
Figure A.32   Effects of Changing Flare Angle to 24.72 degrees - 10GHz

69

LTSA 9 - 8 GHz
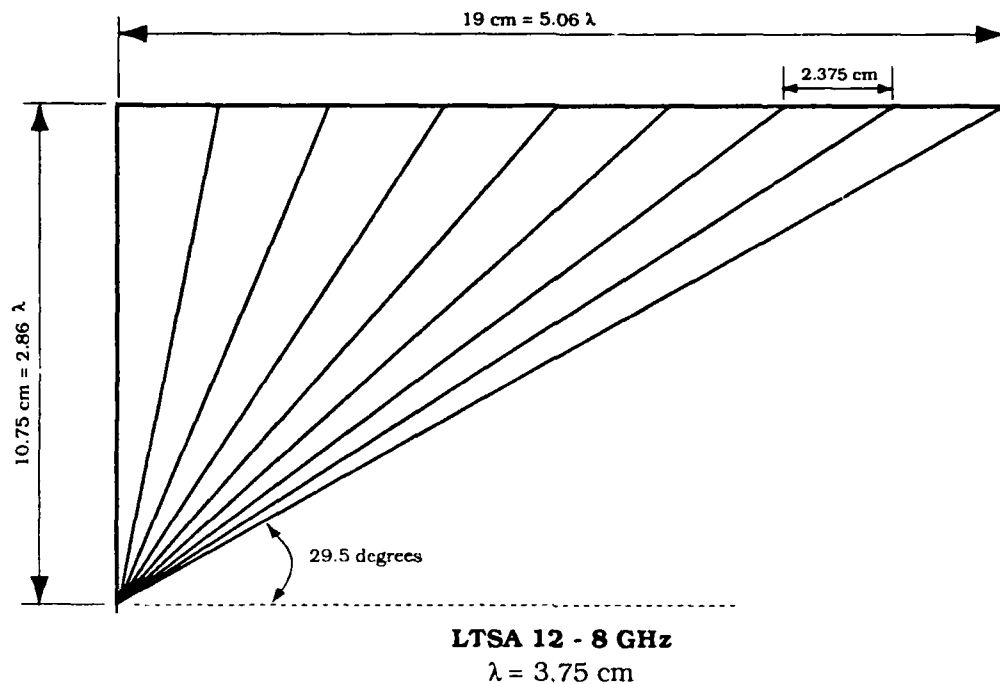λ = 3.75 cm
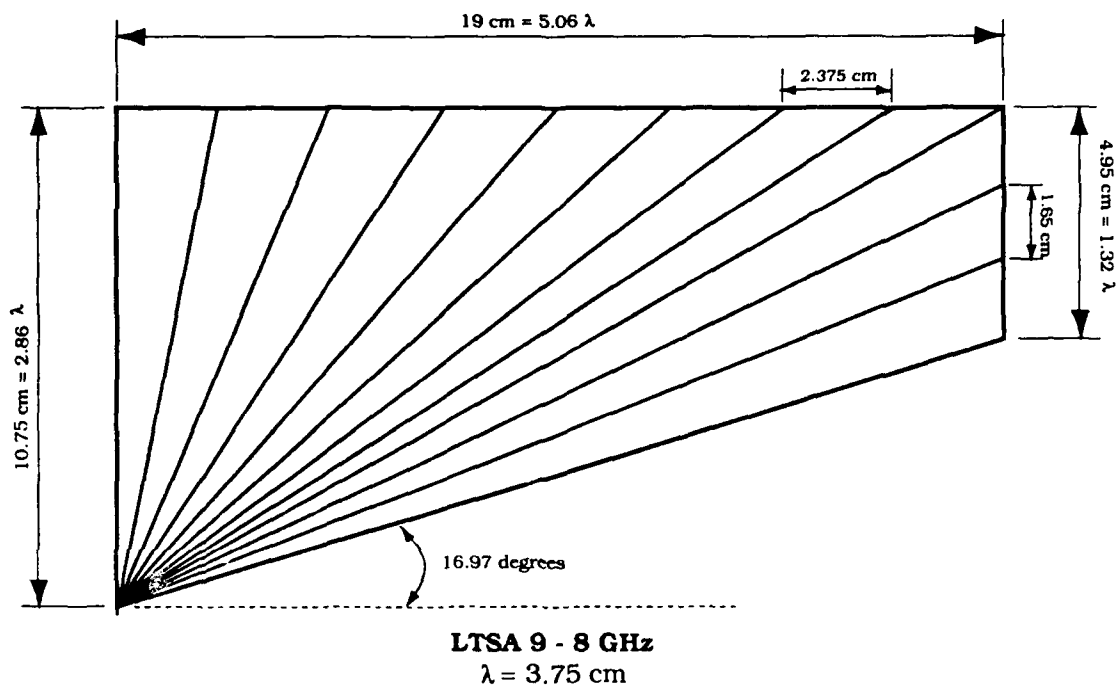
Figure A.33   LTSA Geometry with Flare Angle = 33.94 degrees - 8GHz

LTSA 9 - 8 GHz
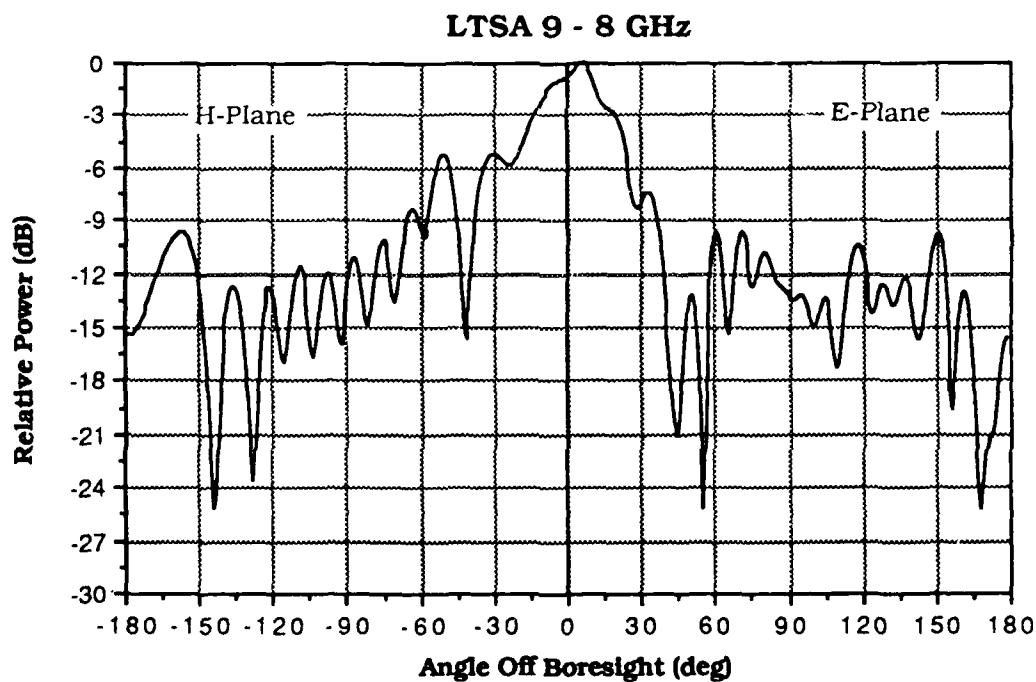
Figure A.34   Effects of Changing Flare Angle to 33.94 degrees - 8GHz

70

LTSA 9 - 10 GHz
λ = 3.00 cm
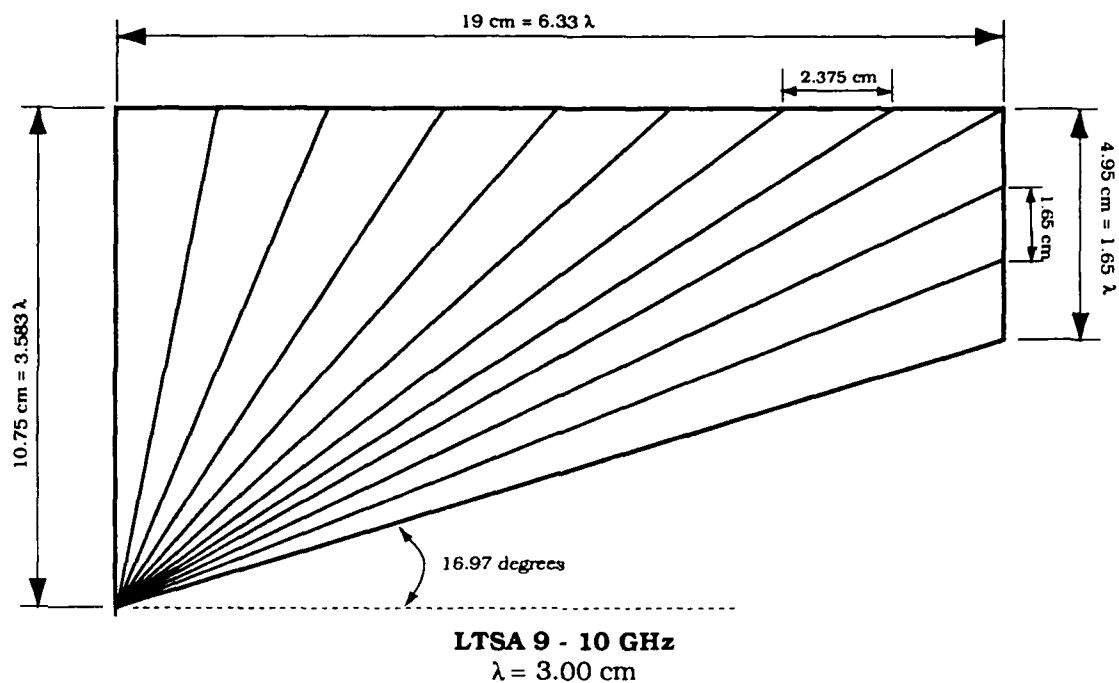
Figure A.35   LTSA Geometry with Flare Angle = 33.94 degrees - 10GHz

LTSA 9 - 10 GHz
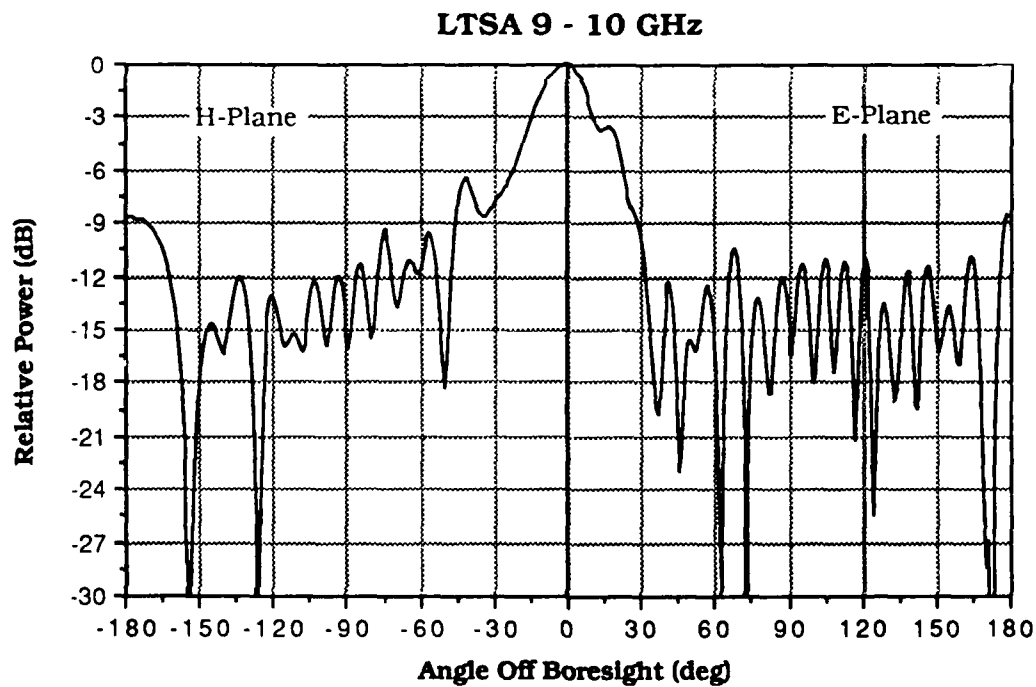
Figure A.36   Effects of Changing Flare Angle to 33.94 degrees - 10GHz

71

LTSA 10 - 8 GHz
λ = 3.75 cm
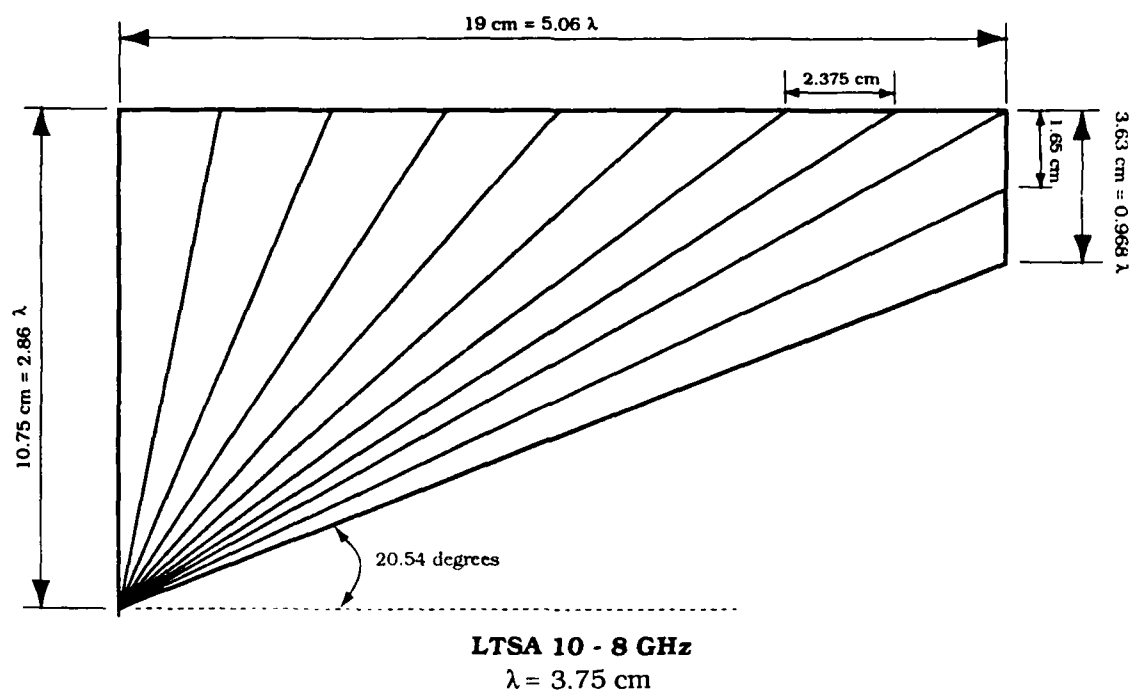
Figure A.37   LTSA Geometry with Flare Angle = 41.08 degrees - 8GHz
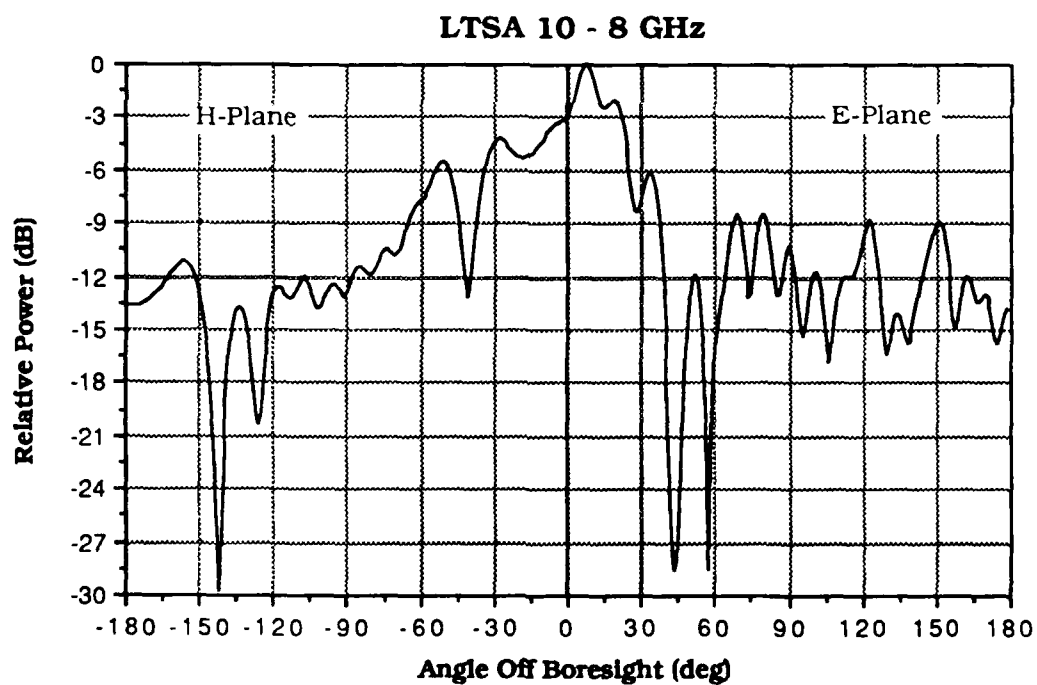
Figure A.38   Effects of Changing Flare Angle to 41.08 degrees - 8GHz

72

LTSA 10 - 10 GHz
λ = 3.00 cm
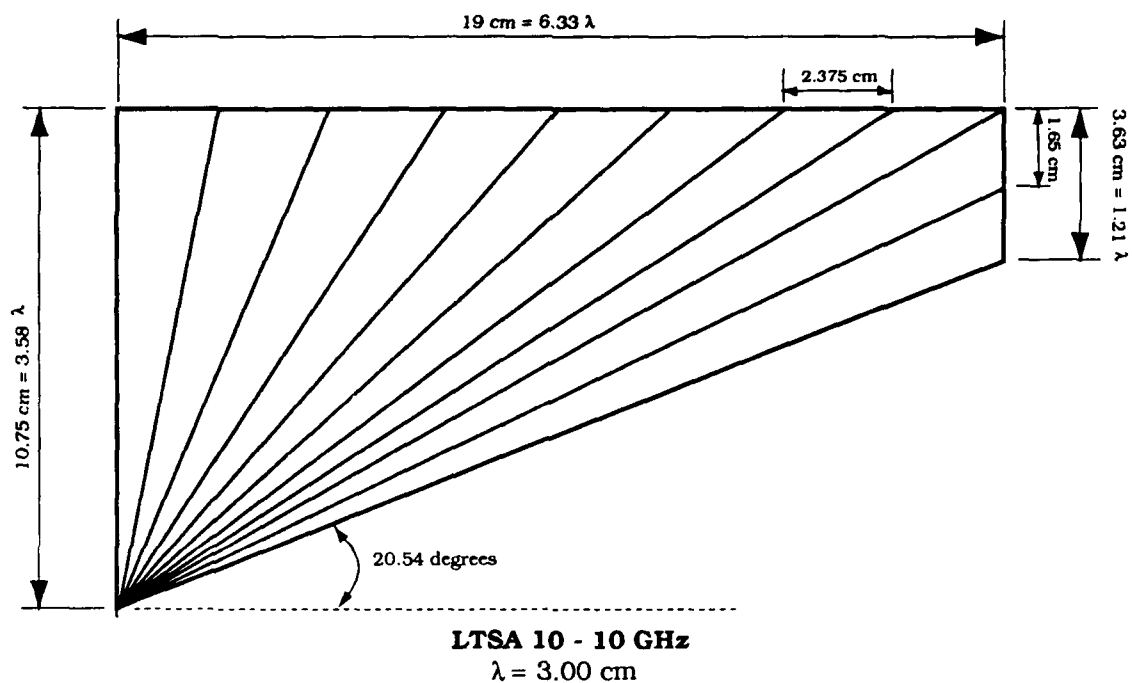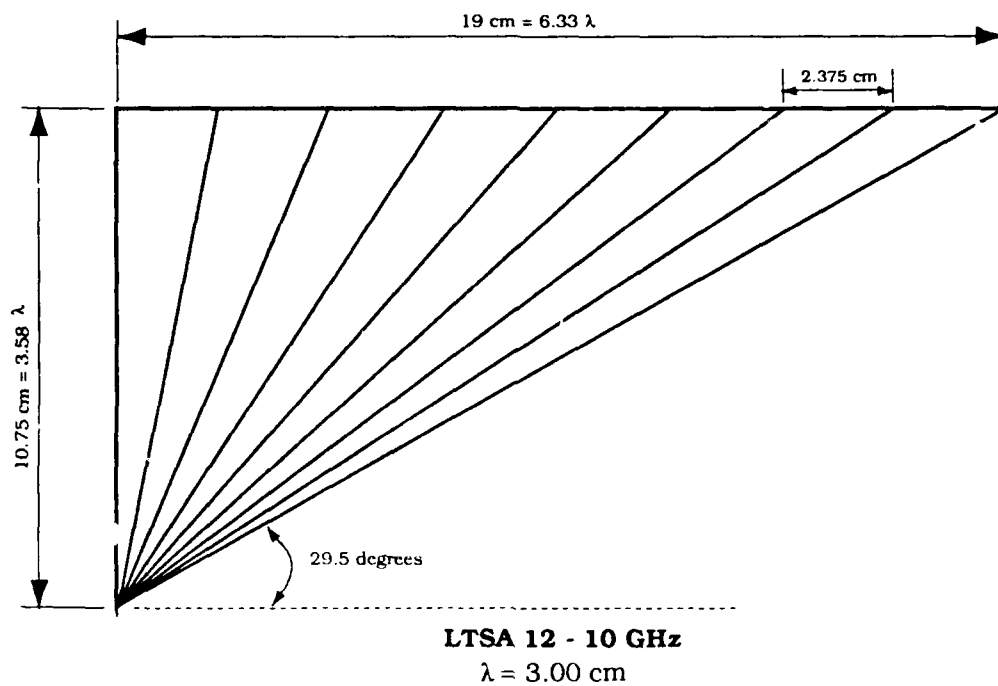
Figure A.39   LTSA Geometry with Flare Angle = 41.08 degrees - 10GHz
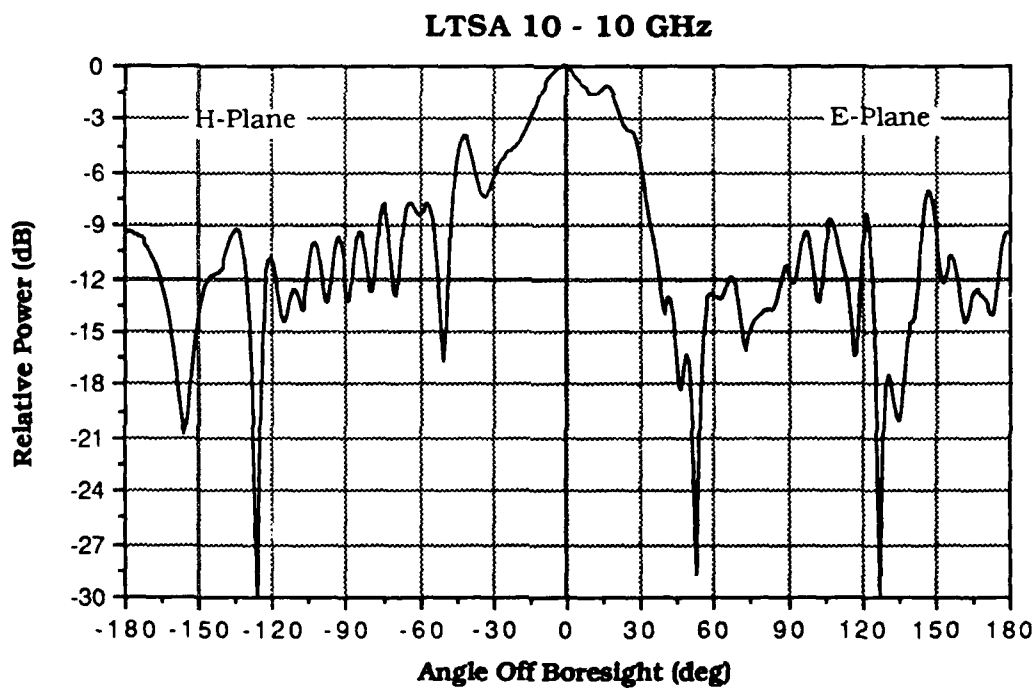
Figure A.40   Effects of Changing Flare Angle to 41.08 degrees - 10GHz

73
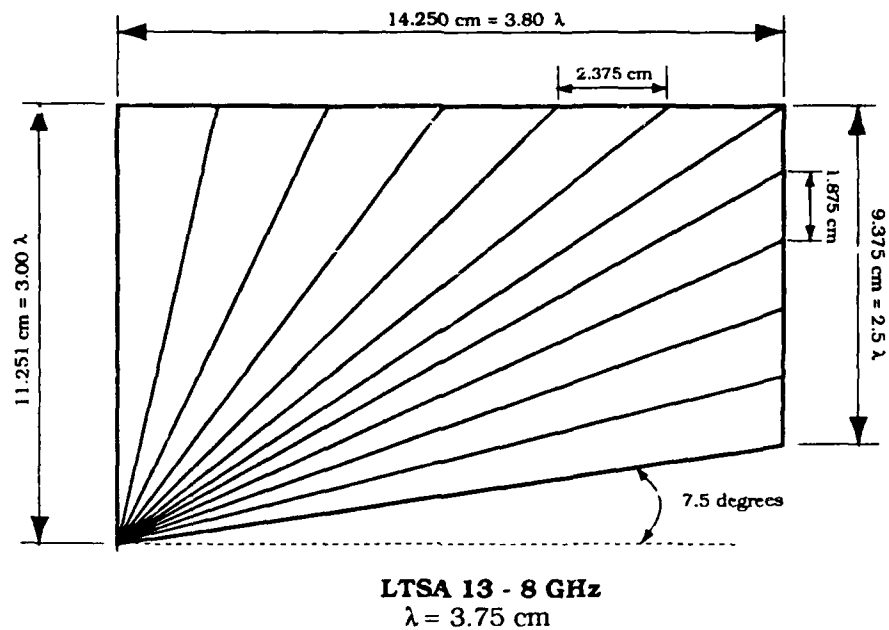
LTSA 11 - 8 GHz
λ = 3.75 cm
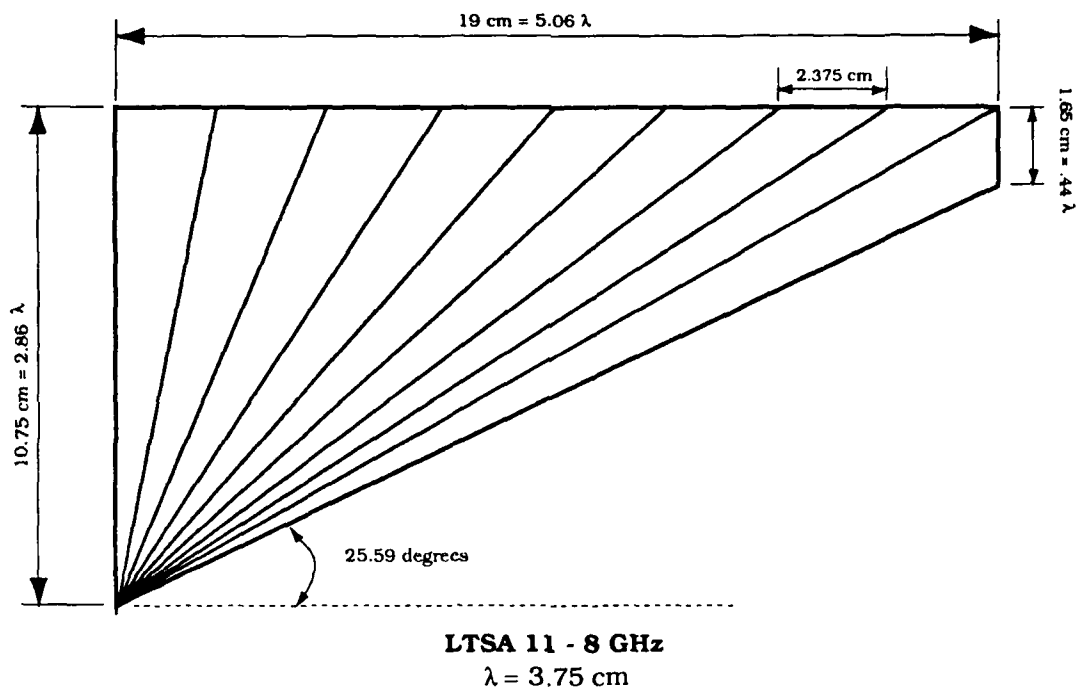
Figure A.41   LTSA Geometry with Flare Angle = 51.18 degrees - 8GHz
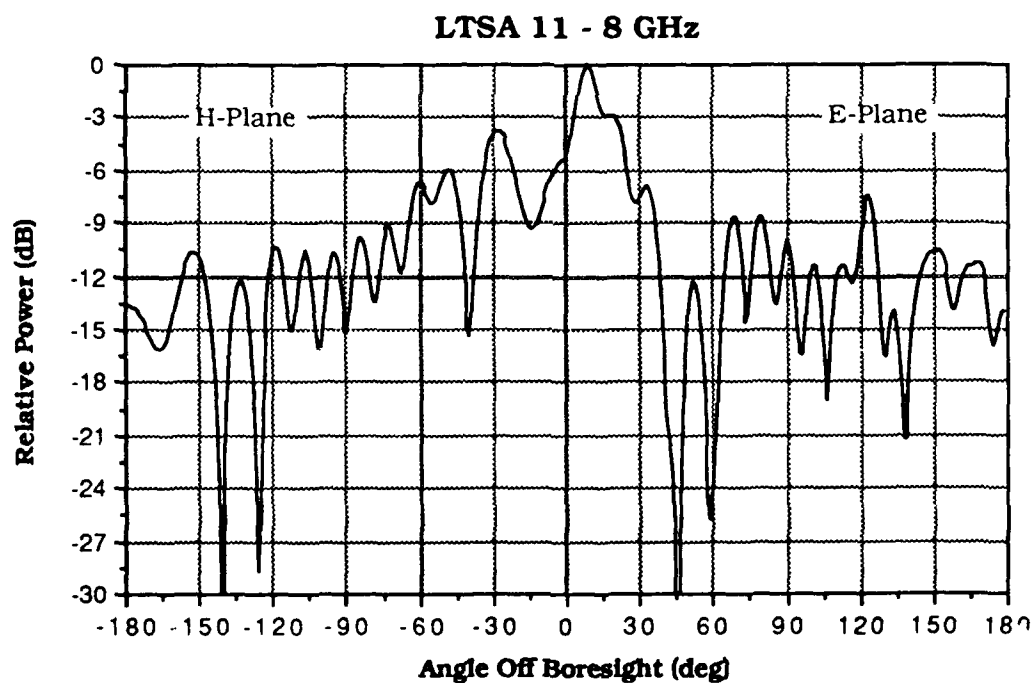
Figure A.42   Effects of Changing Flare Angle to 51.18 degrees - 8GHz

74

19 cm = 6.33 λ

2.375 cm

1.65 cm = .55 λ

10.75 cm = 3.58 λ

25.59 degrees

LTSA 11 - 10 GHz
λ = 3.00 cm

Figure A.43   LTSA Geometry with Flare Angle = 51.18 degrees - 10GHz

LTSA 11 - 10 GHz

H-Plane

E-Plane

Relative Power (dB)

Angle Off Boresight (deg)
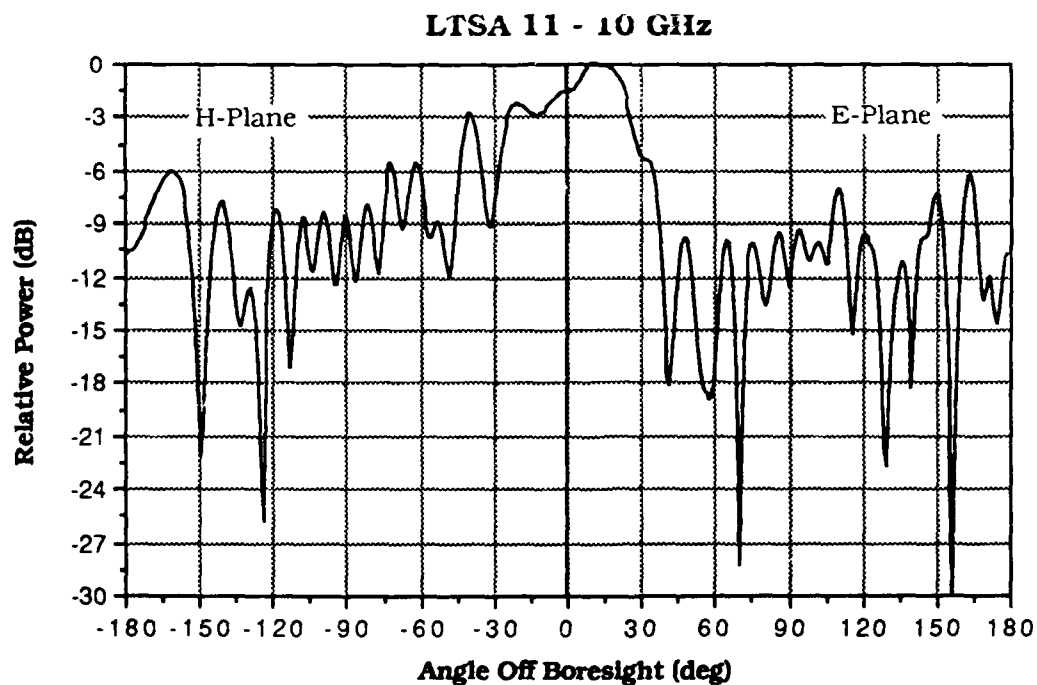
Figure A.44   Effects of Changing Flare Angle to 51.18 degrees - 10GHz

LTSA 12 - 8 GHz
λ = 3.75 cm

Figure A.45   LTSA Geometry with Flare Angle = 59 degrees - 8GHz

LTSA 12 - 8 GHz
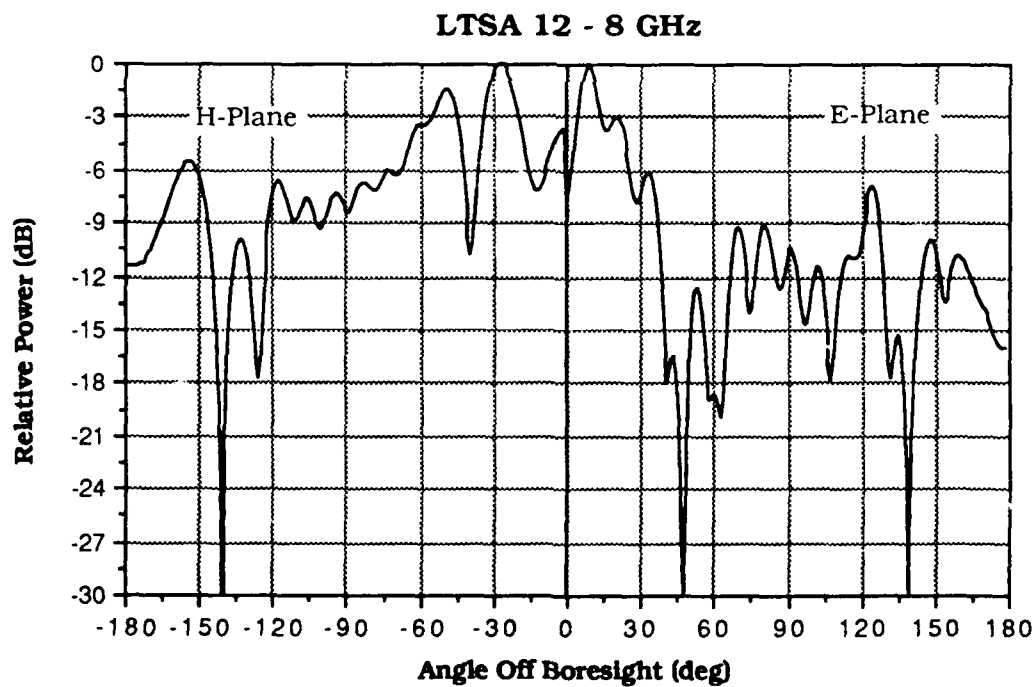
Figure A.46   Effects of Changing Flare Angle to 59 degrees - 8GHz

19 cm = 6.33 λ

2.375 cm

10.75 cm = 3.58 λ

29.5 degrees

LTSA 12 - 10 GHz

λ = 3.00 cm

Figure A.47   LTSA Geometry with Flare Angle = 59 degrees - 10GHz

LTSA 12 - 10 GHz

H-Plane

E-Plane

Relative Power (dB)

Angle Off Boresight (deg)
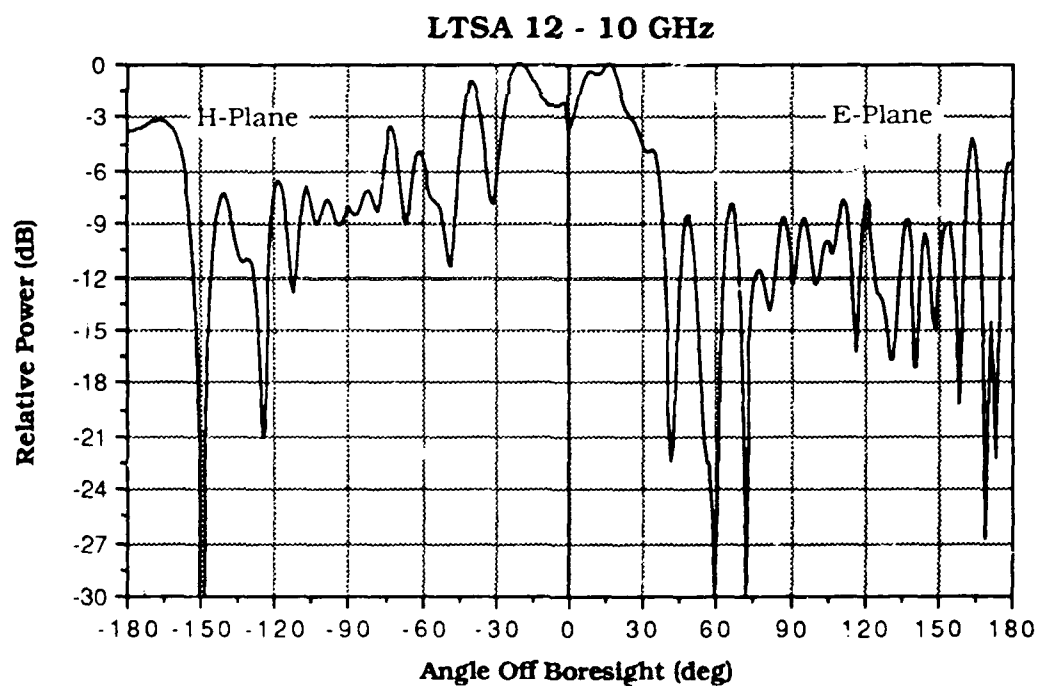
Figure A.48   Effects of Changing Flare Angle to 59 degrees - 10GHz

77

LTSA 13 - 8 GHz
λ = 3.75 cm

Figure A.49   LTSA Geometry with Length = 3.80λo z

LTSA 13 - 8 GHz
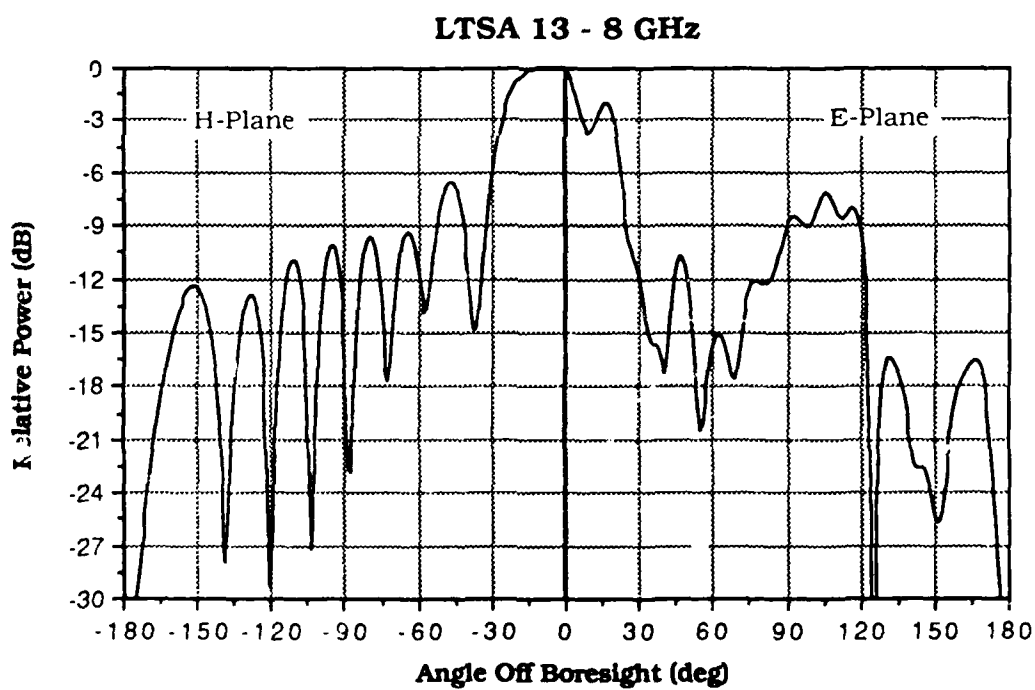
Figure A.50   Effects of Changing Length to 3.80λo

78

LTSA 13 - 10 GHz
$\lambda = 3.00$ cm
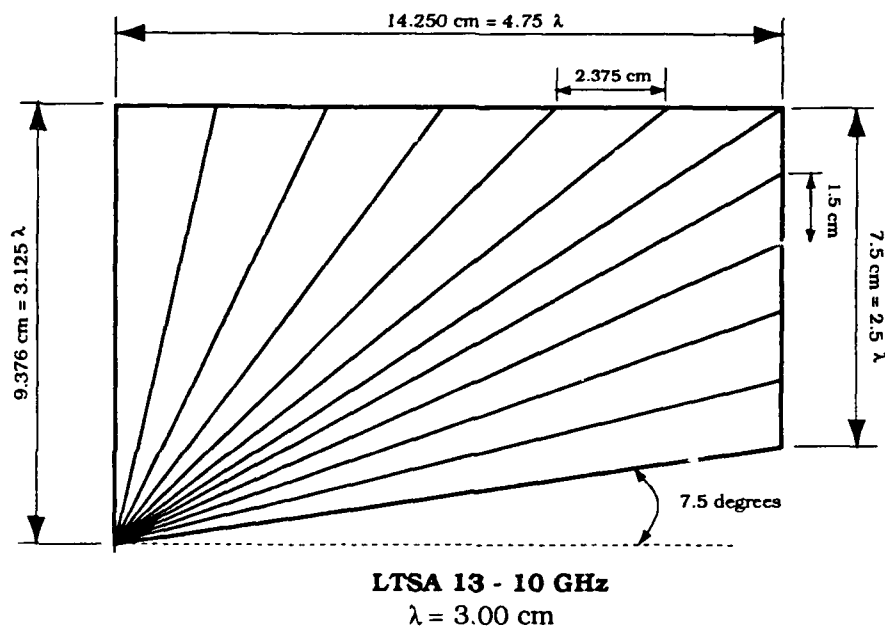
Figure A.51   LTSA Geometry with Length = 4.75λo z
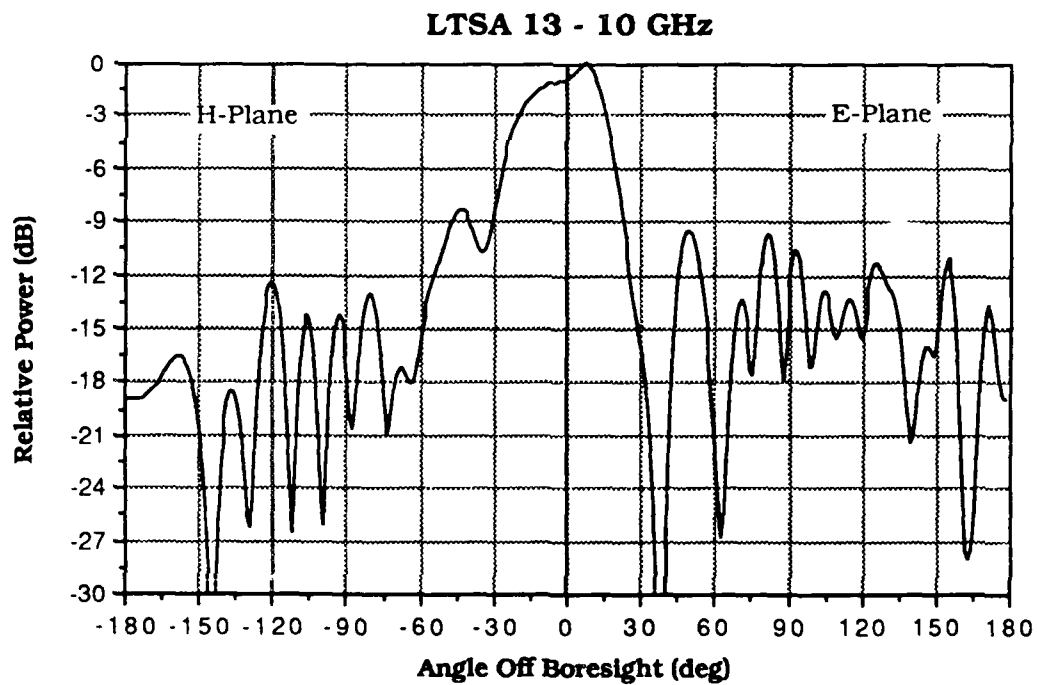
Figure A.52   Effects of Changing Length to 4.75λo

19 cm = 5.06 λ

2.375 cm

9.375 cm = 2.5 λ

1.875 cm

11.89 cm = 3.17 λ

7.5 degrees

LTSA 14 - 8 GHz
λ = 3.75 cm
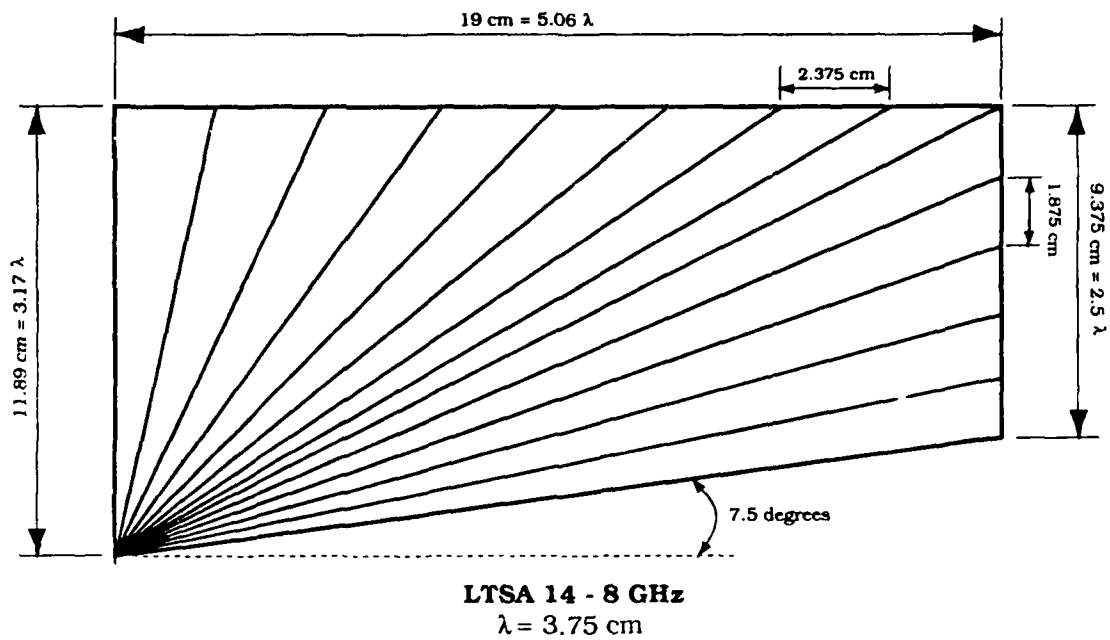
Figure A.53   LTSA Geometry with Length = 5.06λo

LTSA 14 - 8 GHz

H-Plane

E-Plane

Relative Power (dB)

Angle Off Boresight (deg)
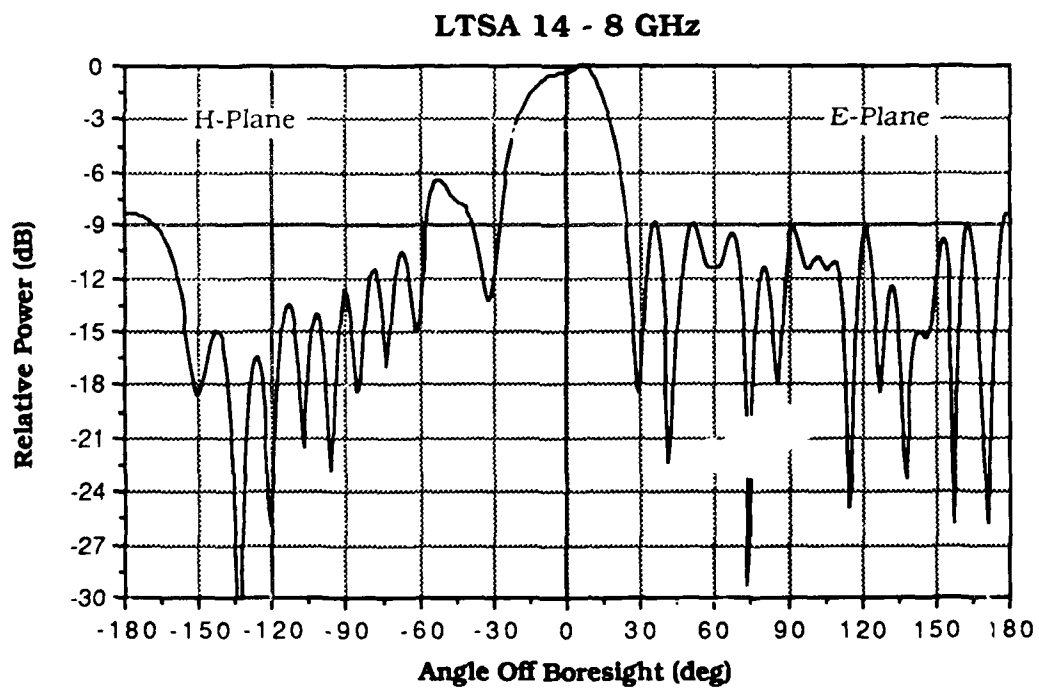
Figure A.54   Effects of Changing Length to 5.06λo

80

19 cm = 6.33 λ

2.375 cm

10.015 cm = 3.33 λ

1.5 cm

7.5 cm = 2.5 λ

7.5 degrees

LTSA 14 - 10 GHz

λ = 3.00 cm
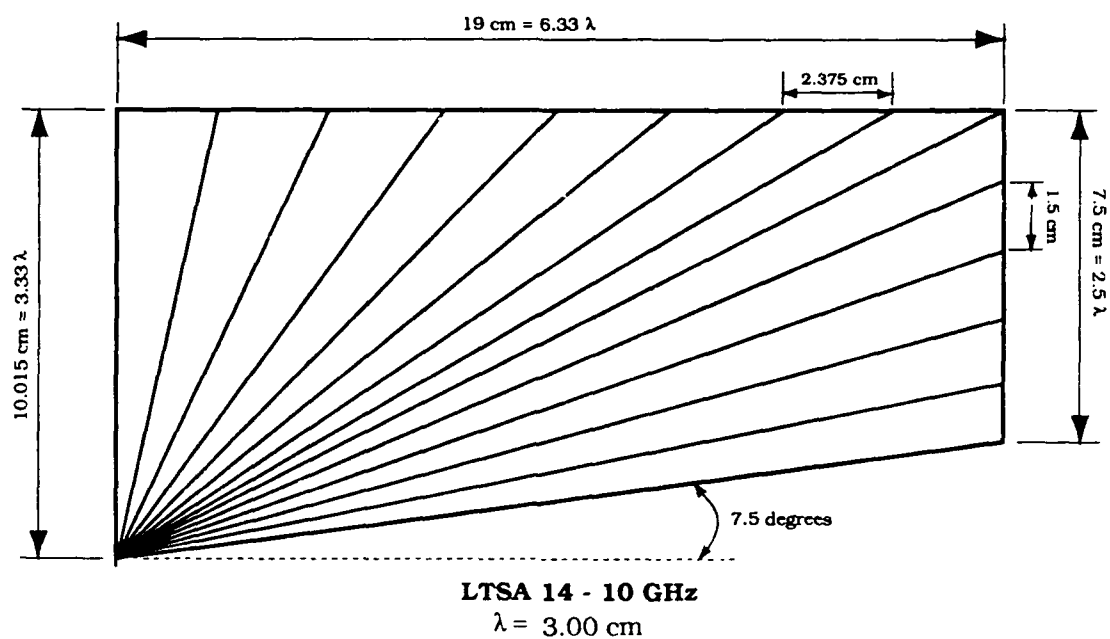
Figure A.55   LTSA Geometry with Length = 6.33λo

LTSA 14 - 10 GHz

H-Plane

E-Plane
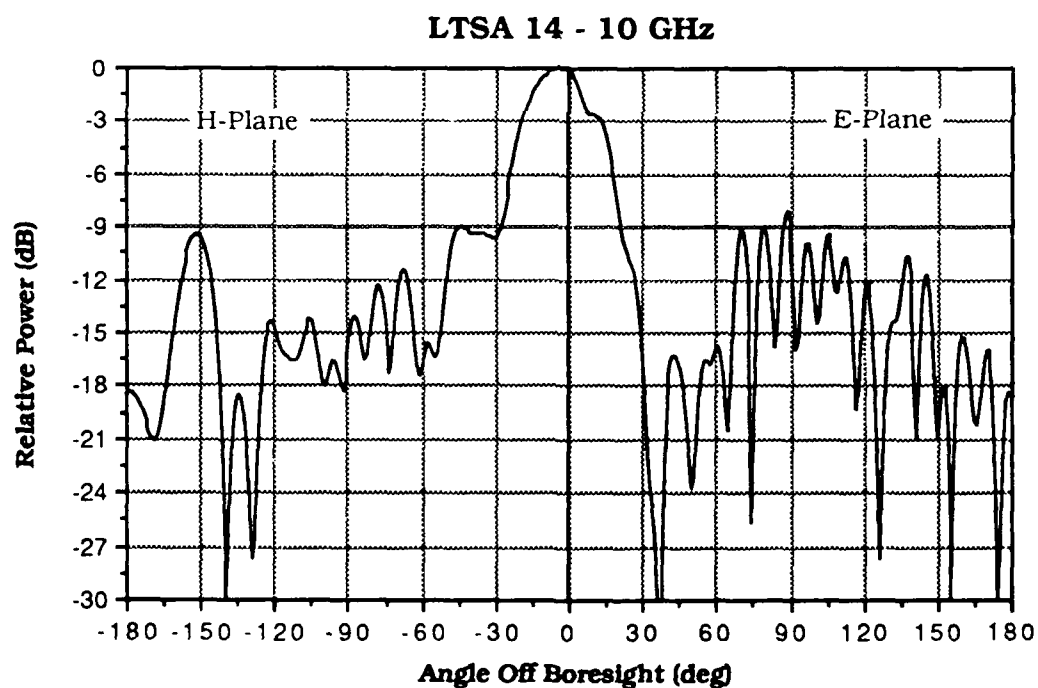
Figure A.56   Effects of Changing Length to 6.33λo

LIST OF REFERENCES

1. Yngvesson, K. S., and others, "Endfire Tapered Slot Antennas on Dielectric Substrates," IEEE Transactions on Antennas and Propagation, V. AP-33, No. 12, pp. 1392-1399, December, 1985.

2. Janaswamy, R., "An Accurate Moment Method Model for the Linear Tapered Slot Antenna," paper submitted for publication, July 1988.

3. Kelly, T. P., "Modeling the Behavior of the Linear Tapered Slot Antenna," Master's Thesis, Naval Postgraduate School, Monterey, California, December 1988.

4. Stutzman, W. L., and Thiele, G. A., Antenna Theory and Design, Chapter 7, John Wiley & Sons, Inc. 1981.

5. Burke, G. J., and Pogio, A. J., "Numerical Electromagnetics Code (NEC) - Method of Moments," NOSC Technical Document 116, Volume 2, Naval Ocean Systems Center, January 1981.

6. Janaswamy, R., Unpublished Notes

INITIAL DISTRIBUTION LIST

83